# INFORMATION TO USERS

This manuscript has been reproduced from the microfilm master. UMI films the text directly from the original or copy submitted. Thus, some thesis and dissertation copies are in typewriter face, while others may be from any type of computer printer.

**The quality of this reproduction is dependent upon the quality of the copy submitted.** Broken or indistinct print, colored or poor quality illustrations and photographs, print bleedthrough, substandard margins, and improper alignment can adversely affect reproduction.

In the unlikely event that the author did not send UMI a complete manuscript and there are missing pages, these will be noted. Also, if unauthorized copyright material had to be removed, a note will indicate the deletion.

Oversize materials (e.g., maps, drawings, charts) are reproduced by sectioning the original, beginning at the upper left-hand corner and continuing from left to right in equal sections with small overlaps.

Photographs included in the original manuscript have been reproduced xerographically in this copy. Higher quality 6" x 9" black and white photographic prints are available for any photographs or illustrations appearing in this copy for an additional charge. Contact UMI directly to order.

ProQuest Information and Learning
300 North Zeeb Road, Ann Arbor, MI 48106-1346 USA
800-521-0600

Université d'Ottawa • University of Ottawa

# Conformational Studies of Host/Guest Interactions in Calixarenes using Dynamic NMR Spectroscopy, X-ray Crystallography and Pseudo-Cavity Volume Analysis

Arvin Moser

Thesis submitted to the Faculty of Graduate and Postdoctoral Studies University of Ottawa in partial fulfillment of the requirements for the degree of Masters of Science in the Ottawa-Carleton Chemistry Institute

Ottawa, Canada
June 2001

## Acknowledgements

I would like to thank my research supervisor Dr. Christian Detellier for his patience, time, guidance and comments. In addition, I would like to thank the people from my lab group Gianni A. Caravaggio, Dr. Yael Israëli, Dr. Urs C. Meier, Dr. Marie-Josée Binette, Dr. Mark R. Weir, Sophie Quevillon, Dr. Harouna Drame and Elizabeth A. Cross for the numerous discussions, contributions and their lab assistance.

Fruitful discussions with Elizabeth A. Husk, Marcel Beaudoin, Richard LeBlanc, Nidia P. Villalva, Karol Gajewski and Dr. Alison Ingham are highly appreciated. In addition, I would like to thank Dr. Glenn A. Facey and Raj Capoor for their help in NMR, and Dr. Glenn P. A. Yap for his help in X-ray crystallography. I am grateful to Dr. David Handelman and Yoichi Kono for supplying equations 15 and 16, respectively, and to Larry Nutsch for his help in directing me to the program Rhinoceros®.

Finally, the acknowledgement for the quintessential support from my family and friends for whom all this research was worth attempting.

## Abstract

The compound 5,11,17,23-tetra-*tert*-butyl-25,26,27,28-tetrakis(*N,N*-diethylamino-carbonyl)methoxycalix[4]arene, **1**, forms a 1:1 complex with both the sodium and potassium cations in a binary mixture of chloroform-*d* and acetonitrile-$d_3$. Kinetic and mechanistic solution studies are analyzed using $^{1}H$, $^{23}Na$ and $^{39}K$ NMR in order to compare the binding modes of the guests $Na^+$ and $K^+$. Both the sodium and potassium complexes exhibit a quantitative complexation ($K_f > 10^4\ M^{-1}$) in the temperature range of 238 to 320 K. The exchange between the complexed and solvated sodium cations is very slow on the $^{23}Na$ NMR time scale at 320 K. Similarly, results for the exchange between the complexed and solvated potassium cations at 320 K were found to be slow to moderately slow on the $^{39}K$ NMR time scale.

Dynamics of the ethyl moiety are probed using $^{1}H$ NMR and EXSY techniques. Analysis of 2-D EXSY $^{1}H$ NMR data for the interconversion of the methylene protons from the $N(CH_2CH_3)_2$ moiety of the $(Na,1)^+$ and $(K,1)^+$ complexes exhibit slow exchange at 320 K.

The complexes (Na,1,MeCN),B(Ph)$_4$, (K,1,MeCN),B(*p*-PhCl)$_4$ and (MeCN,1) crystallized in the tetragonal space group *P*4*cc* with a = b = 18.128(2) Å, c = 29.457(5) Å, and $z$ = 4, in the tetragonal space group *P*4*cc* with a = b = 18.493(1) Å, c = 29.586(2) Å, and $z$ = 4, and in the monoclinic space group $P2_1$ with a = 11.380(2), b = 26.899(5), c = 11.468(2) Å, β = 96.382(3)° and $z$ = 2, respectively. A second crystallographic dataset was obtained for (K,1,MeCN),B(*p*-PhCl)$_4$ with tetragonal space group *P*4*cc* with a = b = 18.4546(11) Å, c = 29.533(3) Å, and $z$ = 4. X-ray crystallographic data of

(Na,1,MeCN),B(Ph)$_4$ and (K,1,MeCN),B(*p*-PhCl)$_4$ confirm the NMR data such that the sodium and the potassium cations are encapsulated by the hydrophilic pseudo-cavity of **1**, respectively. The crystal structures for both the sodium and potassium complexes show two diastereomorphs in the lattice differing by a twist in the $OCH_2CO$ arms. The crystal structure of (MeCN,1) shows identical preorganization of the hydrophobic pseudo-cavity to that of the sodium and potassium complexes. The methyl group of the guest acetonitrile of (MeCN,1) is oriented inside the hydrophobic pseudo-cavity as a result of the $CH_{guest}$-$\pi_{host}$ interaction.

Finally, single-crystal X-ray data points to a correlation between the ionic radius of the guests $Ni^{+2}$, $Cu^{+2}$, $Zn^{+2}$, $Fe^{+2}$, $Pb^{+2}$, $Na^+$ and $K^+$ to the volume of the hydrophilic pseudo-cavity in the host **1**. Namely, the volume calculated from the spatial arrangement of the eight oxygens of **1** is linear in respect to the ionic radius of the guest cations. The preliminary model provides a unified and reasonably good description of the interaction between a host and its guest.

# Table of Contents

## Publications

Moser, A., *Polyhedron*, **2001**, *20*, 1897-1901.

Moser, A., Yap, G. P. A., Detellier, C. *J. Chem. Soc., Dalton Trans.*, Submitted.

Moser, A., Yap, G. P. A., Detellier, C. *Supram.*, To be submitted.

The material on the following pages 4, 14, 28-29, 104-114, 116 were reprinted from Polyhedron, *20*, Moser, A., Quantitative correlation between the pseudo-cavity volume of the *p-tert*-butylcalix[4]arene tetra-acetamide and the ionic radius of cationic guests., 1897-1901, **2001**, with permission from Elsevier Science.

## List of Tables

## List of Figures

## List of Symbols and Abbreviations

| | |
|---|---|
| **1** | ***p-tert*-butylcalix[4]arene tetra-acetamide** |
| **1b** | ***p-tert*-butylcalix[4]arene 1,2-diacetamide** |
| **2** | ***p-tert*-butylcalix[4]arene tetra-oxy(2-pyridylmethyl)** |
| **3** | ***p-tert*-butylcalix[4]arene tetra-thioamide** |
| $\delta$ | **Chemical shift** |
| **DNMR** | **Dynamic NMR** |
| **EXSY (or NOESY)** | **Exchange Spectroscopy** |
| **h** | **Planck's constant** |
| $K_f$ | **Formation constant** |
| $k$ | **First-order rate constant** |
| $(L)^+_{solv}$ | **Solvated alkali metal** |
| **MeCN** | **Acetonitrile** |
| $M_0$ | **Macroscopic magnetic moment** |
| $N_0$ | **Avogadro's number** |
| $p_A$, $p_B$ | **Fractional population of nuclei in site A or B** |
| $T_1$ | **Longitudinal (spin-lattice) relaxation time** |
| $T_2$ | **Transverse (spin-spin) lattice time** |
| $\tau$ | **Lifetime** |
| $\upsilon_{1/2}$ | **Bandwidth (Hz) at half height** |
| $\upsilon_A$, $\upsilon_B$ | **Resonance frequency of site A or B** |

"Only the Whole is the Truth." G. W. F. Hegel

# 1. Introduction

## 1.1 History of Supramolecular Chemistry

Jean-Marie Lehn described the field of Supramolecular Chemistry in a Nobel lecture as "the chemistry of the intermolecular bond, covering the structures and functions of entities formed by the association of two or more chemical species".[1] Specifically speaking, the species are termed the substrate or guest and the molecular receptor or host.[2,3] The host/guest system is comparable to the notion of the lock-and-key effect, whereby, the key is linked to the shape and geometry of the lock. On a molecular scale, the guest dictates the shape and geometry of the host. Subsequently, the host can be modified to optimize recognition of the guest.

The roots of Supramolecular Chemistry can be traced back to 1811 with Sir Humphrey Davy's discovery of clathrate hydrates.[4] Moreover, the first synthesis of a possible calixarene was observed by Adolph von Baeyer in 1872 through the reaction of aldehydes with phenols.[5,6] However, due to limited characterization techniques of the time, further research into the newly-synthesized compound was not pursued. A more recent discovery in the 1960's by Charles J. Pedersen was in metallic cation complexation by crown ethers.[7,8] This research soon prompted the recognition of Supramolecular Chemistry as a new field warranting further investigation.

Further interest into calixarenes and other complexing compounds have been spawned by the realization of mimicking the natural recognition processes observed by enzymes and ionophores. Natural ionophores such as valinomycin have been observed to complex metal cations for the purpose of ion transport through lipophilic membranes.[9] With this in mind, the synthesis of new hosts serves as the backbone in mimicking the recognition process. The interaction of the host/guest system involves a detailed kinetic approach. From this analysis, research into the nature of the mechanism of molecular inclusion and recognition, and the organization of the host serves to lay the road to better hosts with specific recognition properties.

Molecular inclusion complexes fall under two categories: intramolecular and intermolecular as based on crystallographic data.[10-19] Intramolecular inclusion complexes consist of hosts encapsulating a guest within a cavity such that the guest is unexposed to the solvent molecules.[9-12] Intermolecular inclusion complexes follow a linking or clathrate-type. This is observed for the inclusion of acetone with the calix[4]arene compound.[11,13,14]

The study of Supramolecular Chemistry has led to developments in the areas of catalysis, molecular transportation and recognition.[20-22] As a result, expanding the general understanding of the flexibility of cyclic macromolecules in solution in terms of molecular recognition.[23] Current research lies in investigating the nature of the thermodynamic stability of hosts with different guests, and thus predict the factors that control the host/guest interactions.[21] The potential then lies in designing for more specific and selective molecular receptors. One such example of a versatile host system is the

calixarene compound. This thesis examines the nature of the complexation process with emphasis in predicting the molecular recognition process.

## 1.2 Calix[n]arenes: Definition, History and Chemistry

Calix[n]arenes (n = 3, 4, etc.) are a class of macrocyclic phenolic oligomers (Figure 1) where the number of repeating units in the oligomer is represented by the letter n. After the structural characterization of the calix[4]arene compound in 1978, Gutsche *et al.* suggested the name for the molecule as a representation of its shape.[6,24] The cone-shaped cyclic tetramers of the calix[4]arene show a similarity to a Greek vase known as a "Calix Crater". The "Arene" component comes from the term chalice. It is this vase- or chalice-like structure of the calix[n]arene compounds that permits the inclusion of guests such as metallic ions and neutral solvents. Other properties of calixarenes are its white colour and its high melting point (greater than 300 °C).[21] So far, only one case has been reported to melt below 300°C, namely, the *p*-methyl-*p*-*tert*-butylcalix[5]arene melts at 260 °C.[25]

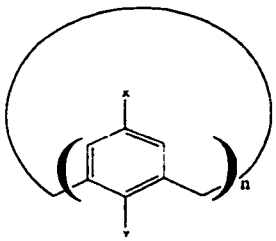


**Figure 1.** Calix[n]arene (n = 3, 4, *etc.*) consists of a cyclic phenyl ring with varying substituents for X and Y. For example, X = H, $CH_3$, *tert*-butyl, *etc.* and Y = H, OH, $OCH_3$, *etc.*.

The calix[4]arene molecule is able to interconvert between four structural isomers: cone, partial cone, 1,2-alternate, and 1,3-alternate (Figure 2). The interconversion of the calixarene has limited the complexation process for guests, and thus inhibit molecular recognition. Modifications in the hydrophilic (or lower) and hydrophobic (or upper) rim have been found to sterically inhibit the interconversion of the calixarene and enforce a single conformation such as the cone conformation.[21,26] Such modifications include bulky groups such as carbonates[27,28] and acetates[29,30].

In addition to stabilizing an isomer, modifications on the calixarene also serve to alter its solubility properties. Furthermore, calixarenes are known to exhibit different substrate complexation selectivities via the modification of their substituents.[6,31-39] These modifications have proven to be useful in exhibiting selective guests affinities such as alkali metal cations in various solvents,[40,41] thus providing insight into how molecular receptors adapt. Complex modifications provide an efficient cage or cavity that can shield the guest from the solvent molecules.[37] The key lies in balancing the flexibility/rigidity of the cavity for the purpose of designing an efficient and versatile host in molecular recognition processes.[42] This is achieved through the studies of the complexation processes of various calixarenes ranging from simple to intricate rim modifications.

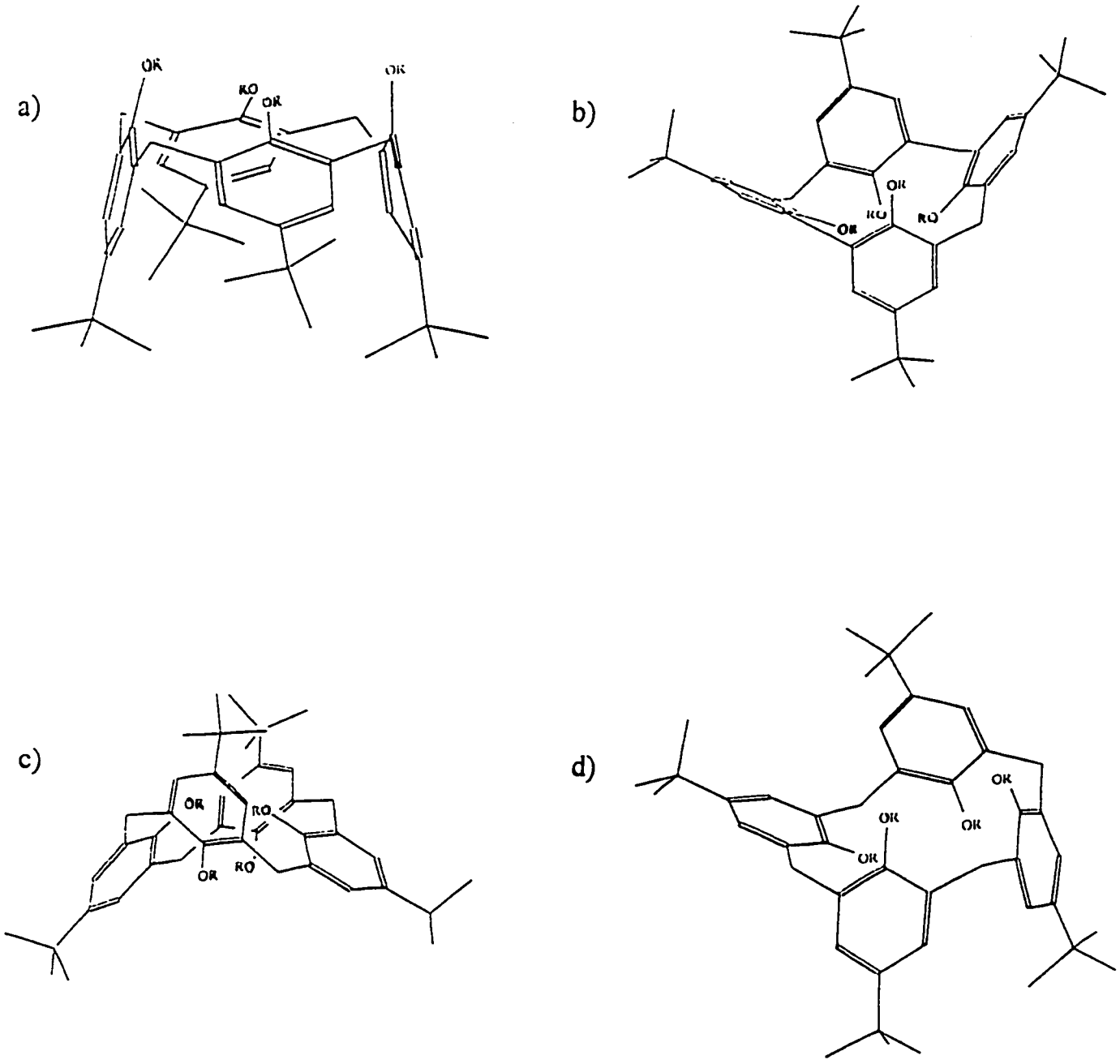


**Figure 2.** The four conformations of *p-tert*-butylcalix[4]arene varying in the interconversions about the phenyl-bridging $CH_2$. a) cone, b) partial cone, c) 1,3-alternate, d) 1,2-alternate.

## 1.3 Applications of Calixarenes

Due to the structural adaptability of calixarenes, the functionality of the calixarene may be extended to a wide range of applications.[43] And thus, is a very active topic of research today. Most applications of calixarenes are for the selective separation of specific metals. For example, the compound *p-tert*-butylcalix[8]arene is utilized for the recovery of cesium from nuclear waste solutions. The success of the cesium extraction has led to a patent.[44] A hexacid calix[6]arene is used for recovering uranium from aqueous solutions.[45] Direct separation of enantiomers such as amino acids and amines is accomplished using chiral calixarenes.[46] Attempts are underway for the extraction from the environment of the carcinogenic species Cr(VI) using calix[4]arenes.[47,48]

Other applications of calixarenes and various derivatives may serve as ion carriers[49,50] and as analytical sensors[51]. For example, calix[4]arenes complexed with radioactive guests such as $Rb^+$ are being used in organ imaging.[21,52] In the generation of microsyringes for the purpose of metal transportation, the 1,3-alternate conformation of linked calix[4]arenes serve as a nanotube.[53] A more common application is the use of calixarenes as accelerants for instant adhesives for use on paper, leather, *etc.*.[54-56]

Researchers who study the complexation of a guest to a host calixarene attempt to model and understand natural occurrences in the field of biomimetics.[57] For example, mimicking the behaviour of enzymes and in the synthesis of new catalysts[6,55] and modeling naturally occurring ionophores in ion transportation across a lipid membrane[58]. Furthermore, modified calix[4]arenes and calix[6]arenes are used in catalytic reactions such as hydrolysis reactions.[59]

## 1.4 Kinetics and Mechanisms of Complexation

Detailed kinetic and thermodynamic investigations into the complexation and decomplexation properties of the host macrocyclic molecule enable a thorough understanding in the mechanism of selectivity towards neutral, cationic, and anionic guests in solution.[6,31,32,37,39] The mechanism of the reaction is studied because the process of the reaction is just as important as the outcome of the reaction.

Techniques employed are $^{1}H$, $^{23}Na$ and $^{39}K$ NMR, 2-D $^{1}H$ EXSY (or NOESY), $T_1$ studies and dynamic NMR (DNMR). The development of DNMR follows the premise of line broadening developing into coalescence, studied under different concentrations of the reactants and different temperatures.[60-62] The program DNMR5[95] combines the use of an iterative analysis and the Taylor series in calculating NMR lineshapes for the purpose of determining the rate of exchange of a system. From the exchange rates, the entropy, enthalpy and free energy can be examined to surmise the mechanism of the reaction. Mechanistic studies serve to explain the relationship between the structure of the host to the shape and size of the accommodated guest. Several mechanistic pathways are possible when examining the complexation and decomplexation process of a host and guest system. Models of exchange between the host and the guest vary from a dissociative to an associative mechanism.

Studies in the complexation process are generally described by equation 1. This equation represents the global equation for the exchange of a single metallic guest. That is, the equation does not solely pertain to any specific mechanism for the complexation process.[63]

$$(L)^{+}_{solv} + (1)_{solv} \underset{k_d}{\overset{k_f}{\rightleftharpoons}} (L,1)^{+}_{solv} \quad (1)$$

$$A \underset{k_B}{\overset{k_A}{\rightleftharpoons}} B \quad (2)$$

In solution, the guest cation can occupy two sites (equation 2). Site A refers to the solvated or free site on $(L)^+$ and site B refers to the complexed site $(L,1)^+$.[64] Equation 2 represents the unimolecular dissociation or the dissociative exchange pathway. The constants, $k_A$ and $k_B$, are the pseudo-first order rate constants for the forward and reverse reactions, respectively.[64] The rate constant can be determined by varying the concentration of the metal cation. If the metallic guest forms quantitatively a 1:1 complex with the host ($K_f > 10^4\ M^{-1}$), then only two sites are involved in the exchange of the cationic guest.[37,64-67] NMR studies over a wide range of temperatures would show a change in the lineshape(s) if exchange occurs between two sites.[68] The rate constant for complexation, $k_A$, and the rate constant for dissociation, $k_B$, are linked to the formation constant of the complex, $K_f$, through equation 3.[9]

$$K_f = k_A / k_B \quad (3)$$

Studies in dynamic NMR show a difference in the complexed and solvated form of the cation through chemical shift and linewidth. The spectrum of a sample containing both the complexed and solvated cationic guests will depend on the rate of exchange of

the two sites.[9] At slow exchange rates, two peaks are generally observed as sharp signals whereas a single averaged peak is observed for fast exchange rate.[69] At an intermediate exchange rate, the two peaks experience broadening and thus overlap.[69]

In an exchange reaction, the chemical shift will follow equation 4 where p represents the population of the respective species and $\delta$ represents the corresponding chemical shifts. The observed chemical shift is an average of the resulting two peaks. The chemical shift is related to the width of the peak at half-height, $\upsilon_{1/2}$.

A peak is seen to broaden as the transverse relaxation rate, $T_2^{-1}$, increases (corresponding to a decrease in the relaxation time) (equation 5). This applies when no exchange is observed. For equation 6, $T_{2,inh}^{-1}$ is the field inhomogeneity contribution and $T_{2,q}^{-1}$ is the quadrupolar contribution. The equation applies for systems involved in moderately fast to fast exchange. Equation 7 illustrates the relation of the transverse relaxation rate, $T_{2,ex}^{-1}$ to the lifetime, $\tau$, of $L^+$ in the two sites A and B, $\tau = p_A / k_B = p_B / k_A = (k_A + k_B)^{-1}$, for a process at fast exchange.[60,65,70-72] The values for $\upsilon_{1/2}$, $\upsilon_A$ and $\upsilon_B$ are expressed in Hz. At slow to moderately slow exchange in a two-site system, the rate of exchange considers only one site. Therefore, only the lineshape of A is considered in equation 8 (variation of equation 5).[60] In a slow exchange model, $k_A$ is related to the dissociation rate constant ($k_{-1}$) and $k_2$ via equation 9.[60,65,73]

$$\delta_{obs} = p_A \delta_A + p_B \delta_B \quad (4)$$

$$T_2^{-1} = \pi (\upsilon_{1/2}) \quad (5)$$

$$T_{2,ex}^{-1} = T_2^{-1} - T_{2,inh}^{-1} - T_{2,q}^{-1} \quad (6)$$

$$T_{2,ex}^{-1} = 4 p_A p_B \pi^2 (\upsilon_A - \upsilon_B)^2 (k_A + k_B)^{-1} \quad (7)$$

$$(\upsilon_{1/2})_A = (1 / \pi)(k_A + T_{2,ex}^{-1}) \quad (8)$$

$$k_A = k_{-1}[(L,1)^+] / [L^+] + k_2[(L,1)^+] \quad (9)$$

In 1973, the first published results on a two site exchange using lineshape analysis were completed on sodium and cryptands.[74] At 320 K, a complete kinetic analysis from the two lineshapes of this two-site exchange shows a slow exchange rate on the $^{23}Na$ NMR chemical shift time scale.[64,65,75] The NMR spectrum of the solvated guest will appear as a narrow peak due to the highly spherical symmetry.[9]

Subsequently, the enthalpy and entropy of activation can be obtained from a linear plot using the Eyring equation (equation 10). A plot of $\ln(k / T)$ vs. $1 / T$ will have a slope of $(-\Delta H^{\ddagger} / R)$ and a y intercept of $(\Delta S^{\ddagger} / R + \ln(R / (N_0 h)))$ where $N_0$ is Avogadro's number and h is Planck's constant. From these activation parameters, we can speculate on the process of complexation. If $\Delta S^{\ddagger} > 0$, namely an increase in the freedom of motion of the product side over the reactants, then a dissociative reaction mechanism is expected.[76] Whereas a $\Delta S^{\ddagger} < 0$ implies an associative reaction mechanism. A large positive value for $\Delta H^{\ddagger}$ reflects the strength of the bond and generally implies a dissociative reaction mechanism.

$$\ln(k / T) = -\Delta H^{\ddagger} / (R T) + \Delta S^{\ddagger} / R + \ln(R / (N_0 h)) \quad (10)$$

$$(L,1)^+_{solv} \underset{k_1}{\overset{k_{-1}}{\rightleftharpoons}} (L)^+_{solv} + (1)_{solv} \quad (11a)$$

$$(L^*)^+_{solv} + (1)_{solv} \underset{k_{-1}}{\overset{k_1}{\rightleftharpoons}} (L^*,1)^+_{solv} \qquad (11b)$$

$$(L,1)^+_{solv} + (L^*)^+_{solv} \rightleftharpoons [L^+ \cdots 1 \cdots L^{*+}]_{solv} \rightleftharpoons (L^*,1)^+_{solv} + (L)^+_{solv} \qquad (12)$$

Two mechanisms that are considered for the guest cation exchange are the dissociative and the associative mechanism. The dissociative mechanism (equation 11) involves the dissociation of the guest from the host followed by a recombination of a second guest. The associative mechanism (equation 12) involves the close approach of a second guest to the complex followed by a transition state which leads to the association of the host to the second guest and the release of the first guest.[37] Subsequently, 1:2 complexes of host to guest follow the associative mechanism. Complexes in the ratio of 2:1 for host to guest follow a "sandwich-type" mechanism as seen in equation 13.[37]

$$(L,1)^+_{solv} + 1^* \rightleftharpoons (L,1^*)^+_{solv} + (1)_{solv} \qquad (13)$$

Factors such as the nature of the guest, counteranion, host and solvent dictate the mechanism of exchange. For example, large crown ethers show either a dissociative or an associative mechanism for sodium cation depending upon the conditions whereas only an associative mechanism is seen with the cesium cation.[77] Subsequently, the difference in specificity of the host for different guests is partially attributed to the ionic size of the cation.[9,78]

## 1.5 Rotation about the Amide Bond

There exists numerous studies into the barriers to rotation about the C(O)-N (amide) bond in various solutions for various compounds such as *N,N*-dimethylamide and *N,N*-diethylamide.[79-81] The amide bond is a crucial feature in proteins, and subsequently, research serves to understand the characteristics of this bond. Work generally involves the use of dynamic NMR and lineshape analysis for peaks approaching coalescence. The barrier to rotation has been found to be a result of the steric and electronic characteristics of the substituent attached to the carbonyl group.[79-81]

One approach to analyzing the rotation about the amide bond is the use of 2-D $^{1}H$ EXchange SpectroscopY or EXSY (also known as NOESY). In 1979, the technique was first applied to examine the chemical exchange process of a 1-2 methyl shift in heptamethylbenzenonium ion.[82] Basically, the 2-D NMR technique involves variations in the mixing time, $\tau_m$, such that the different frequencies of the two exchanging sites correlate. The results produce variations in the volumes of the cross-peaks in relation to the respective diagonal peaks. The rate of exchange between the two sites is a function of the variation in the volumes of the peaks as the mixing time varies.

## 1.6 Single-Crystal X-ray Diffraction Crystallography

In 1979, Andreetti *et al.* reported a crystal structure for the inclusion of the methyl group of toluene inside the compound *p-tert*-butylcalix[4]arene.[10] The conformational details reported complement previous NMR studies and conclusively proved the

formation of the cone conformation of the host. The interaction between the methyl guest and the host is seen as an attractive $CH_{guest}$-$\pi_{host}$ interaction, whereby, the methyl group of the guest is oriented and inserted inside the hydrophobic cavity.[21] The *p-tert*-butylcalix[4]arene compound contains four electron-donating substituents[83] (one hydroxyl and three alkyl substituents per phenyl ring), thus making the host π-basic.[21] Since the guest contains an electron-withdrawing substituent, the guest experiences an increase in acidity on the methyl group. This in turn strengthens the $CH_{guest}$-$\pi_{host}$ hydrogen bond interaction.[10,11,21,84-86] The CH bonds are preferred over NH or OH bonds due the hardness/softness of acids and bases.[21] The magnitude of the guest inclusion by the host system can be measured using $^{1}H$ and $^{13}C$ NMR. The change in the chemical shift is directly related to the magnitude of the inclusion interaction.[21,84,87]

Structural X-ray data reported on the complexation of an ionic guest such as sodium, iron, *etc.* by the hydrophilic (lower) rim of various calixarene hosts serve to comprehend the complexation process.[47,88-91] The process is mainly directed by the electrostatic interaction between the electron donor atom of the host and the metal cationic guest.[92] Based on these key findings, the groundwork for the calixarene systems was complete and new avenues into host/guest Supramolecular Chemistry concepts can be extended to newer and more complex calixarene systems.

## 1.7 Pseudo-Cavity Volume

Research in the field of Supramolecular Chemistry has attempted to address the molecular interactions in the host/guest systems, and thus predict the structural

recognition processes. The substituents of the calix[4]arene molecule which form the cavities can be modified to vary the recognition properties towards guests such as alkali metal cations.[33,37,40,41] Numerous examples exist of a host cavity adjusting to the ionic radius of a guest; alkali metals inside fullerenes[96] and proteins varying in cavity volumes to alter host/guest interactions[97]. Investigations into how these molecular receptors adapt allow for improved design for the efficient selectivity of a guest.

## 1.8 Goals of the Research/Thesis

It is the aim of this research to examine a calixarene system for investigating the existence and nature of the host/guest interactions. Examination of a variety of complexed metal guests will aid in establishing factors important to the selectivity of complexation.[93] NMR and kinetic studies in conjunction with molecular modeling have been done to reinforce research into the microscopic structure of the host/guest complex.

The complexation of the sodium and the potassium cations with 5,11,17,23-tetra-*tert*-butyl-25,26,27,28-tetrakis(*N*,*N*-diethylaminocarbonyl)methoxycalix[4]arene)[§], **1** (scheme 1), are studied using $^{1}H$, $^{23}Na$ and $^{39}K$ NMR spectroscopies in binary mixtures of deuterated chloroform and acetonitrile. The effects of the guest on the hydrophilic pseudo-cavity of **1** are studied and discussed. In addition, the role of a neutral guest acetonitrile on (Na,**1**),B(Ph)$_4$, (K,**1**),B(*p*-PhCl)$_4$ and free **1** are investigated via X-ray crystallography.

---

[§] (IUPAC name: $1^5,3^5,5^5,7^5$-tetra-*tert*-butyl-$1^2,3^2,5^2,7^2$-tetrakis(*N*,*N*-diethylaminocarbonylmethoxy)-1,3,5,7(1,3)-tetrabenzenacyclooctaphane)

Chapter 3 will provide insights into the complexation processes of the guest cations sodium and potassium. The investigation of single-crystal XRD is reported in Chapter 4. Finally, the hydrophilic pseudo-cavity of the host **1** is examined in terms of the relation of the volume of the host hydrophilic pseudo-cavity with respect to the cationic guest in Chapter 5. Analyzing the changes in the pseudo-cavity of the host **1**, the area, surface area and volume of the host/guest complex were calculated. Subsequently, the property that is most influential in the host/guest interactions is analyzed.

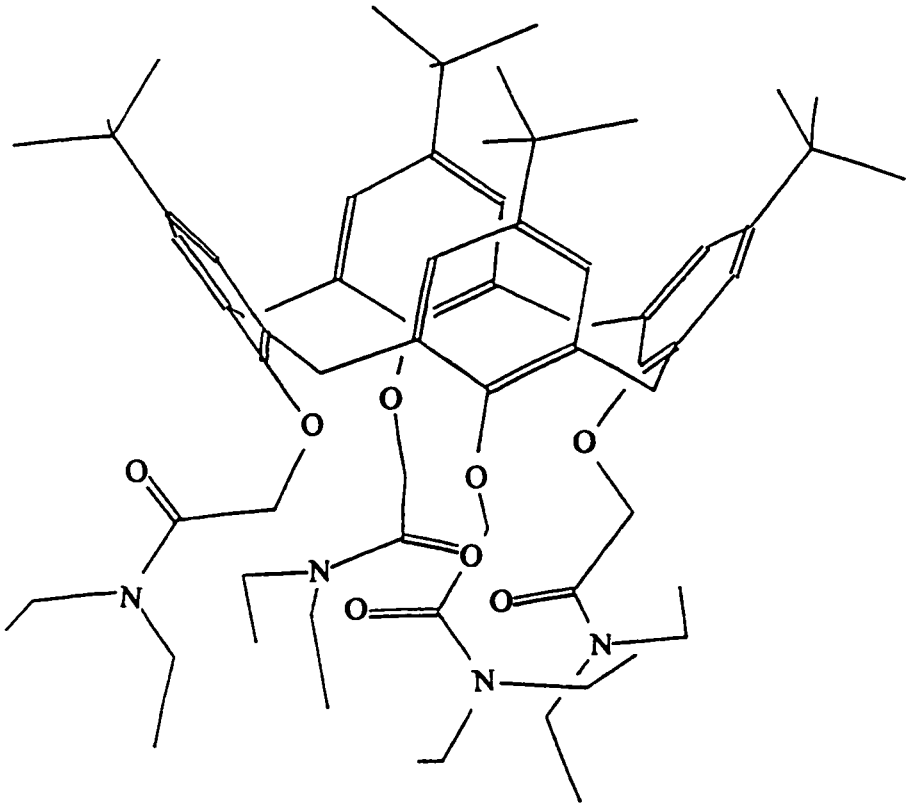

**Scheme 1.**

## References

(1) Lehn, J. M. *Angew. Chem. Int. Ed. Engl.*, **1988**, *27*, 89.

(2) Lehn, J. M. *Pure Appl. Chem.*, **1978**, *50*, 871.

(3) Cram, D. J.; Cram, J. M. *Science*, **1974**, *183*, 803.

(4) Davy, H. *Phil. Trans. Roy. Soc.*, **1811**, *101*, 1.

(5) von Baeyer, A. *Ber.*, **1872**, *5*, 1094.

(6) Gutsche, C. D. *Acc. Chem. Res.*, **1983**, *16*, 161.

(7) Pedersen, C. J. *Angew. Chem Int. Ed. Engl.*, **1988**, *27*, 1021.

(8) Pedersen, C. J. *J. Am. Chem. Soc.*, **1967**, *89*, 7017.

(9) Detellier, C.; Graves, H. P.; Brière, K. M. In *Isotopes in the Physical and Biomedical Science*, Vol. 2; Buncel, E., Jones, J. R., Eds.; Elsevier: Amsterdam, 1991; pp 159-211.

(10) Andreetti, G. D.; Ungaro, R.; Pochini, A. *J. Chem. Soc., Chem. Comm.*, **1979**, 1005.

(11) Lu, G.; Liu, F.; Liu, Y.; He, W.; Li, Q.; Zhu, L. *J. Chem. Cryst.*, **1999**, *29*, 1121.

(12) Perrin, M.; Gharnati, F.; Oehler, D.; Perrin, R.; Lecocq, S. *J. Incl. Phen. Mol. Recog.*, **1992**, *14*, 257.

(13) Ungaro, R.; Pochini, A. *J. Chem. Soc., Perkin Trans. 2*, **1984**, 1979.

(14) Zhang, P. M.; Huang, Z. T. *Acta. Chim. Sin.*, **1992**, *50*, 209.

(15) Brouwer, E.; Udachin, K. A.; Enright, G. D.; Ratcliffe, C. I.; Ripmeester, J. A. *Chem. Comm.*, **1998**, *5*, 587.

(16) Thuery, P.; Keller, N.; Lance, M.; Vigner, J.-D.; Nierlich, M. *J. Incl. Phen. Molec. Recog. Chem.*, **1995**, *20*, 373.

(17) Arduini, A.; McGregor, W. M.; Paganuzzi, D.; Pochini, A.; Secchi, A.; Ugozzoli, F.; Ungaro, R. *J. Chem. Soc., Perkin Trans. 2*, **1996**, 839.

(18) Brouwer, E.; Enright, G. D.; Ripmeester, J. A. *Supramol. Chem.*, **1996**, *7*, 7.

(19) Bohmer, V.; Ferguson, G.; Frings, M. *Acta Crystallogr. C, Cryst. Str.*, **1997**, *53*, 1293.

(20) Gutsche, C. D. *Top. Curr. Chem.* **1984**, *123*, 1.

(21) Brouwer, E. B. Structure and dynamics of *t*-butylcalix[4]arene-guest compounds. **1996**, Ph. D. Thesis.

(22) Lehn, J. M. *Angew. Chem Int. Ed. Engl.*, **1990**, *29*, 1304.

(23) Dinger, M. B.; Scott, M. J. *Eur. J. Org. Chem.*, **2000**, 2467.

(24) Gutsche, C. D.; Kung, T. C.; Hsu, M. L. *J. Org. Chem.*, **1978**, *43*, 4905.

(25) Kammerer, H.; Happel, G.; Mathiasch, B. *Makromol. Chem.*, **1981**, *182*, 1685.

(26) Gutsche, C. D.; Dhawan, B.; Levine, J. A.; No, K. H.; Bauer, L. J. *Tetrahedron*, **1983**, *39*, 409.

(27) Ferguson, G.; Kaitner, B.; McKervey, M. A.; Seward, E. M. *J. Chem. Soc., Chem. Comm.*, **1987**, 584.

(28) Arduini, A.; Pochini, A.; Reverberi, S.; Ungaro, R. *J. Chem. Soc., Chem. Comm.*, **1984**, 981.

(29) McKervey, M. A.; Seward, E. M.; Ferguson, G.; Ruhl, B. L.; Harris, S. J. *J. Chem. Soc., Chem. Comm.*, **1985**, 388.

(30) Ungaro, R.; Pochini, A.; Andreetti, G. D. *J. Incl. Phen.*, **1984**, *2*, 199.

(31) Gutsche, C. D. In *Calixarenes*; Stoddart, J. F., Ed.; Royal Society of Chemistry: Cambridge, 1989; pp. 149-185.

(32) Takeshita, M.; Shinkai, S. *Bull. Chem. Soc. Jpn.*, **1995**, *68*, 1088.

(33) Arduini, A.; Ghidini, E.; Pochini, A.; Ungaro, R.; Andreetti, G. D.; Calestani, G.; Ugozzoli, F. *J. Incl. Phen.*, **1988**, *6*, 119.

(34) Arnaud-Neu, F.; Schwing-Weill, M. J.; Ziat, K.; Cremin, S.; Harris, S. J.; McKervey, M. A. *New J. Chem.*, **1991**, *15*, 33.

(35) Arnaud-Neu, F.; Collins, E. M.; Deasy, M.; Ferguson, G.; Harris, S. J.; Kaitner, B.; Lough, A. J.; McKervey, M. A.; Marques, E.; Ruhl, B. L.; Schwing-Weill, M. J.; Seward, E. M. *J. Am. Chem. Soc.*, **1989**, *111*, 8681.

(36) Arnaud-Neu, F.; Barrett, G.; Cremin, S.; Deasy, M.; Ferguson, G.; Harris, S. J.; Lough, A. J.; Guerra, L.; Mc Kervey, M. A.; Schwing-Weill, M. J.; Schwinte, P. *J. Chem. Soc. Perkin Trans. 2*, **1992**, 1119.

(37) Detellier, C. In *Comprehensive Supramolecular Chemistry*; Gokel, G., Ed.; Elsevier Science: Oxford, 1996; Vol. 1, pp. 357-375.

(38) Arnaud-Neu, F.; Barrett, G.; Corry, D.; Cremin, S.; Ferguson, G.; Gallagher, J. F.; Harris, S. J.; Mc Kervey, M. A.; Schwing-Weill, M. J. *J. Chem. Soc., Perkin Trans. 2*, **1997**, 575.

(39) Bohmer, V. *Angew. Chem. Int. Ed. Engl.*, **1995**, *34*, 713.

(40) Arnaud-Neu, F.; Barrett, G.; Fanni, S.; Marrs, D.; Mc Gregor, W.; Mc Kervey, M. A.; Schwing-Weill, M. J.; Vetrogon, V.; Wechsler, S. *J. Chem. Soc., Perkin Trans. 2*, **1995**, 453.

(41) Arnaud-Neu, F.; Fanni, S.; Guerra, L.; Mcgregor, W.; Ziat, K.; Schwing-Weill, M. J.; Barrett, G.; McKervey, M. A.; Marrs, D.; Seward, E. M. *J. Chem. Soc., Perkin Trans 2*, **1995**, 113.

(42) Arduini, A.; Pochini, A.; Secchi, A. *Eur. J. Org. Chem.*, **2000**, 2325.

(43) Perrin, R.; Lamartine, R.; Perrin, M. *Pure Appl. Chem.*, **1993**, *65*, 1549.

(44) Izatt, R. M.; Christensen, J. J.; Hawkins, R. T. (4,477,377). 1984. U.S. Ref Type: Patent.

(45) Kondo, Y.; Yamamoto, T.; Manabe, O.; Shinkai, S. *Jpn. Kokai Tokyo Koho*, **1988**, *88*, 197544.

(46) Narumi, N.; Iki, N.; Suzuki, T.; Onodera, T.; Miyano, S. *Enantiomer*, **2000**, *5*, 83.

(47) Wolf, N. J.; Georgiev, E. M.; Yordanov, A. T.; Whittlesey, B. R.; Koch, H. F.; Roundhill, D. M. *Polyhedron*, **1999**, *18*, 885.

(48) Roundhill, D. M.; Georgiev, E. M.; Yordanov, A. T. *J. Incl. Phen. Molec. Recog. Chem.*, **1994**, *19*, 101.

(49) Visser, H. C.; Reinhoudt, D. N.; Dejong, F. *Chem. Soc. Rev.*, **1994**, *23*, 75.

(50) Espanol, M. C.; de Freitas, D. M. *Inorg. Chem.*, **1987**, *26*, 4356.

(51) Kremer, F. J. B.; Chiosis, G.; Engbersen, J. F. J.; Reinhoudt, D. N. *J. Chem. Soc., Perkin Trans. 2*, **1994**, 677.

(52) Bakker, W. I. I.; Haas, M.; Khoobeattie, C.; Ostaszewski, R.; Franken, S. M.; Denhertog, H. J.; Verboom, W.; Dezeeuw, D.; Harkema, S.; Reinhoudt, D. N. *J. Am. Chem. Soc.*, **1994**, *116*, 123.

(53) Ikeda, A.; Shinkai, S. *J. Chem. Soc., Chem. Comm.*, **1994**, 2375.

(54) Perrin, R.; Lamartine, R.; Perrin, M. *Pure Appl. Chem.*, **1993**, *65*, 1549.

(55) Harris, S. J. and MacManus, M. Eur. Patent Appl. (EP 279 521). 1998. Ref Type: Patent.

(56) Harris, S. J. (GB 2 200 909). 1988. UK Patent Appl. Ref Type: Patent.

(57) Steed, J. W.; Juneja, R. K.; Burkhalter, R. S.; Atwood, J. L. *J. Chem. Soc., Chem. Comm.*, **1994**, 2205.

(58) Grandjean, J.; Laszlo, P. *J. Am. Chem. Soc.*, **1984**, *106*, 1472.

(59) Arimura, T.; Nagasaki, T.; Shinkai, S.; Matsuda, T. *J. Org. Chem.*, **1989**, *54*, 3766.

(60) Detellier, C. In *Practical Spectroscopy*. Vol. 11; Popov, A. I., Hallenga, K., Eds.; Marcel Dekker: New York, 1990; pp. 521-566.

(61) Binsch, G. In T*opics in Spectroscopy*; Eliel, E. L., Allinger, N. L., Eds.; Wiley-Interactions: New York, 1968.

(62) Jackman, L. M.; Cotton, F. A. In *Dynamic Nuclear Magnetic Resonance Spectroscopy*; Academic Press: New York, 1975.

(63) Li, Y.; Gokel, G.; Hernandez, J.; Echegoyen, L. *J. Am. Chem. Soc.*, **1994**, *116*, 3087.

(64) Brière, K. M.; Detellier, C. *Can. J. Chem.*, **1992**, *70*, 2536.

(65) Brière, K. M.; Detellier, C. *New J. Chem.*, **1989**, *13*, 145.

(66) Gutmann, V. In *The donor-acceptor approach to molecular interactions*; Plenum Press: New York, 1978.

(67) Lin, J. D.; Popov, A. I. *J. Am. Chem. Soc.*, **1981**, *103*, 3773.

(68) Chen, Z.; Mercier, L.; Tunney, J. J.; Detellier, C. In *Physical Supramolecular Chemistry*; Echegoyen, L., Kaifer, A. E., Eds.; Kluwer Academic Publishers: Netherlands, 1996; pp 393-411.

(69) Sandström, J. In *Dynamic NMR Spectroscopy*; Academic Press: London, New York, 1982.

(70) Delville, A.; Stöver, H. D. H.; Detellier, C. *J. Am. Chem. Soc.*, **1987**, *109*, 7293.

(71) Stöver, H. D. H.; Delville, A.; Detellier, C. *J. Am. Chem. Soc.*, **1985**, *107*, 4167.

(72) Woessner, D. E. *J. Chem. Phys.*, **1961**, *35*, 41.

(73) Blixt, J.; Detellier, C. *J. Am. Chem. Soc.*, **1995**, *117*, 8536.

(74) Ceraso, J. M.; Dye, J. L. *J. Am. Chem. Soc.*, **1973**, *95*, 4432.

(75) Brière, K. M.; Detellier, C. *J. Phys. Chem.*, **1987**, *91*, 6097.

(76) Petrucci, S.; Eyring, E. M.; Konya, G. In *Comp. Supra. Chem.*; 1996; pp 483-497.

(77) Strasser, B. O.; Shamsipur, M.; Popov, A. I. *J. Phys. Chem.*, **1985**, *89*, 4822.

(78) Gertenbach, P. G.; Popov, A. I. *J. Am. Chem. Soc.*, **1975**, *97*, 4738.

(79) Siddall, T. H. I.; Stewart, W. E.; Knight F. D. *J. Phys. Chem.*, **1970**, *74*, 3580.

(80) Neuman, R. C.Jr.; Jonas, V. *J. Am. Chem. Soc.*, **1968**, *90*, 2154.

(81) Graham, L. L.; Diel, R. E. *J. Phys. Chem.*, **1969**, *73*, 2696.

(82) Jeener, J.; Meier, B. H.; Bachmann, P.; Ernst, R. R. *J. Chem. Phys.*, **1979**, *71*, 4546.

(83) Carey, F. A.; Sundberg, R. J. In *Advanced Organic Chemistry*; Plenum: New York, 1990; pp. 546-557.

(84) Fujimoto, T.; Yanagihara, R.; Kobayashi, K.; Aoyama, Y. *Bull. Chem. Soc. Jpn.*, **1995**, *68*, 2113.

(85) Andreetti, G. D.; Ori, F. O.; Ugozzoli, C.; Alfieri, A.; Pochini, A.; Ungaro, R. *J. Incl. Phen. Molec. Recog. Chem.*, **1998**, *6*, 523.

(86) Uzawa, J.; Zushi, S.; Kodama, Y.; Fukuda, Y.; Nishihata, K.; Umemura, A.; Nishio, M.; Hirota, M. *Bull. Chem. Soc. Jpn.*, **1980**, *53*, 3623.

(87) Komoto, T.; Ando, I.; Nakamoto, Y.; Ishida, S. *J. Chem. Soc., Chem. Comm.*, **1988**, 135.

(88) Lehtonen, A.; Sillanpaa, R. *Polyhedron*, **1998**, *17*, 3327.

(89) Bell, S. E. J.; Browne, J. K.; McKee, V.; Mckervey; M. A.; Malone, J. F.; Oleary, M.; Walker, A.; Arnaudneu, F.; Boulangeot, O.; Mauprivez, O.; Schwing-Weill, M. J. *J. Org. Chem.*, **1998**, *63*, 489.

(90) Lehn, J. M.; Meric, R.; Vigneron, J. P.; Cesario, M.; Guilhem, J.; Pascard, C.; Asfari, Z.; Vicens, J. *Supramol. Chem.*, **1995**, *5*, 97.

(91) Barbour, L. J.; Damon, A. K.; Orr, G. W.; Atwood, J. L. *Supramol. Chem.*, **1996**, *7*, 209.

(92) Seung Kim, J.; Ku Lee, W.; Sim, W.; Won Ko, J.; Man Cho, M.; Fung Ra, D.; An Kim, J. *J. Incl. Phen. Mol. Recog. Chem.*, **2000**, *37*, 359-370.

(93) Beer, P. D.; Drew, M. G. B.; Leeson, P. B.; Ogden, M. I. *J. Chem. Soc., Dalton Trans.*, **1995**, 1273.

(94) Danil de Namor, A. F.; Castellano, E. E.; Pulcha Salazar, L. E.; Piro, O. E.; Jafou, O. *Phys. Chem. Chem. Phys.*, **1999**, *1*, 285.

(95) Stephenson, D. S.; Binsh, G. *QCPE*, **1978**, 11, 365.

(96) Curl, R. F.; Smalley, R. E. *Science*, **1985**, *242*, 1017.

(97) Ory, J. J.; Mazhary, A.; Kuang, H.; Davies, R. R.; Distefano, M. D.; Banaszak, L. *J. Prot. Engin.*, **1998**, *11*, 253.

# 2. Experimental Section

## 2.1 Chemicals and Solutions

The 5,11,17,23-tetra-*tert*-butyl-25,26,27,28-tetrakis(*N,N*-diethylaminocarbonyl) methoxycalix[4]arene, **1**, was synthesized from *p-tert*-butylcalix[4]arene (Aldrich 99 %) as described by Arduini *et al.*[1] with an additional purification step. To ensure that all the sodium cation was removed, the newly synthesized compound (~ 0.50 g) was dissolved in 20 mL of methanol followed by 100 mL of deionized water. Subsequently, the solution was heated to evaporate the methanol leaving a white precipitate that was collected via suction filtration and dried at 110°C circa 15 minutes. The workup was performed twice. The solid was dried for approximately 12 hours at 110°C prior to use. Sodium tetraphenylborate (Aldrich 99.5 %) and potassium tetrakis(4-chlorophenyl)borate (Aldrich 98 %) were dried for about 36 hours at 110°C prior to use.

All NMR data were obtained using a binary mixture (1:1 v/v) of the solvents $CDCl_3$ and $CD_3CN$. $CDCl_3$ (99.8 %), $CD_3CN$ (99.8 %) and $D_2O$ (99.9 %) were purchased from Cambridge Isotope Laboratories. The solvents $CDCl_3$ and $CD_3CN$ were dried over 4 Å molecular sieves prior to use.

## 2.2 NMR Measurements

The $^{1}H$, $^{23}Na$ and $^{39}K$ NMR spectra were recorded on a Bruker AMX-500 spectrometer at 500.14, 132.30 and 23.34 MHz, respectively. The $^{1}H$ NMR spectra were

referenced to chloroform (7.24 ppm) and the $^{23}Na$ and $^{39}K$ NMR spectra were referenced to 0.02 M NaCl and 0.01 M KCl, respectively, in 10 % $D_2O$ in $H_2O$ (0 ppm at 300 K).[2-4] The $^{39}K$ NMR spectra were obtained using a 10 mm broadband probe. The temperature calibration was done with a thermocouple inserted in a non-spinning NMR tube containing chloroform or ethylene glycol.[2] The error on the temperature measurements was estimated to be ± 0.5 K.

The $^{1}H$ NMR spectra were recorded with a 90° pulse width of 6.3 μs. The acquisition time and delay between the two pulses were 4.65 and 1 s, respectively. A standard NOESY pulse sequence was used for the 2-D exchange spectroscopy experiments,[2,5-8] with a delay time of 300 ms, eight scans of 1024 points by 256 slices and a mixing time ranging from 50 to 400 ms for the sodium complex. The potassium samples used a delay time of 300 ms and a mixing time ranging from 10 to 600 ms.

The $^{23}Na$ and $^{39}K$ NMR spectra were recorded with a 90° pulse width of 10 and 35 μs, respectively. The acquisition times ranged from 15 to 140 ms, corresponding to sweep widths of 25 kHz for the $^{23}Na$ NMR. The acquisition time for the $^{39}K$ NMR was 0.256 ms, corresponding to sweep widths of 10 kHz. The delay time was 0.1 s (> 5 $T_1$ in all cases). The number of scans ranged from 1 to 5 k for the $^{23}Na$ NMR and 5 to 7 k for the $^{39}K$ NMR. In the case of the $^{39}K$ NMR, the correction in the dead time resulted in the removal of two points from the free induction decays (f.i.d.s) to decrease the oscillations in the baseline. The possibility exists of an obscured broad peak for the complexed potassium would be lost because of the shortening of the f.i.d.s. Potassium experiments have a low gyromagnetic ratio and thus produce a low NMR sensitivity.

The longitudinal relaxation times, $T_1$, were measured by the inversion-recovery technique.[3] A 90° pulse of 10 μs, 10 delay times (1 – 512 ms) and relaxation delays of at least 0.75 s were used for the solvated sodium sample. The solvated potassium sample was obtained using a 90° pulse of 35 μs, 13 delay times (1 – 200 ms) and relaxation delays of at least 0.10 s. The data were fitted to the equation $I(t) = M_0(1 - ke^{-t/T_1})$ and $M_0$, k, and $T_1$ determined by a nonlinear regression analysis.[3] The $T_1$ values for the solvated sodium peak were determined at 238, 274, 300, and 320 K. They were found to be respectively 8.6(1), 16.3(1), 22.7(1), and 28.2(1) ms. The $T_1$ values for the solvated potassium peak were determined at 238, 246, 255, 274, 283, 292, 300, 310 and 320 K. They were found to be respectively 9.1(1), 9.8(1), 11.5(1), 15.2(1), 17.3(1), 18.0(1), 18.7(1), 20.9(1) and 22.2(1) ms.

## 2.3 Single-Crystal X-ray Diffraction

Crystals of (Na,1,MeCN),$B(Ph)_4$, (K,1,MeCN),$B(p\text{-}PhCl)_4$ and (Li,1b),$ClO_4$ were obtained from a binary solution of deuterated chloroform and deuterated acetonitrile containing 20 mM $NaB(Ph)_4$ or $KB(p\text{-}PhCl)_4$ and 5 mM 1. The compound 1b refers to *p-tert*-butylcalix[4]arene 1,2-diacetamide. The host 1b was produced from an incomplete reaction in the synthesis of 1 with a low yield of ~1 %. The lithium crystal was obtained from a solution containing ~25 mM $LiClO_4$ and ~10 mM 1b. The sodium solution was allowed to slowly evaporate over a span of three months at ~5 °C and at room temperature for the potassium and lithium solutions. Similarly, crystals of (MeCN,1)

were obtained from the same binary mixture containing 80 mM 1 and allowed to slowly evaporate at room temperature over a span of one month.

Suitable crystals were selected, mounted on thin, glass fibers using paraffin oil and cooled to the data collection temperature. Data were collected on a Bruker AX SMART 1k CCD diffractometer using 0.3° ω-scans at 0, 90, and 180° in ϕ. Unit-cell parameters were determined from 60 data frames collected at different sections of the Ewald sphere. Semi-empirical absorption corrections based on equivalent reflections were applied.[10]

Systematic absences in the diffraction data and unit-cell parameters were consistent with *P*4*cc* and *P*4/*mcc* for (Na,1,MeCN),B(Ph)$_4$, and with $P2_1$ and $P2_1/m$ for (MeCN,1). A thorough exploration of the centric space group options yielded bizarre, unstable results. Solutions in the acentric space groups yielded computationally stable and chemically reasonable results of refinement. The structures were solved by direct methods, completed with difference Fourier syntheses and refined with full-matrix least-squares procedures based on $F^2$. Two quarter cations at four-fold rotation axes, a half anion at a two-fold rotation axis, a co-crystallized chloroform molecule at quarter occupancy, and three molecules of co-crystallized acetonitrile with half, quarter, and quarter occupancies were located for (Na,1,MeCN),B(Ph)$_4$. Two acetonitrile molecules were found co-crystallized in (MeCN,1). The calix[4]arene $OCH_2CO$ arms in (MeCN,1) were found disordered with roughly 60/40 site occupancy distributions; three arms had disordered in the $CH_2$ moiety of $OCH_2CO$ while the remaining arm had a disordered carbonyl group. Refinement of the absolute structure parameters yielded 0.6(4) for (Na,1,MeCN),B(Ph)$_4$ suggesting a 60/40 racemic twinned crystal and 1(2) for (MeCN,1),

indicating the true hand of the data set cannot be determined. Two different crystallographic datasets (named I and II) were obtained for the (K,1,MeCN),B(*p*-PhCl)$_4$ complex from two different crystals. All non-hydrogen atoms were refined with anisotropic displacement parameters. All hydrogen atoms were treated as idealized contributions. All scattering factors and anomalous dispersion factors are contained in the SHELXTL 5.10 program library.[11] Crystallographic data are given in Tables 1 and 2, and selected bond lengths and angles are given in Tables 3, 4 and 5.

## 2.4 Data Treatment

The NMR linewidths, intensities and chemical shifts were determined by fitting each peak with a Lorentzian lineshape. The integrals were calculated analytically using these linewidths and intensities.[3] Lineshape analysis was performed on $^{23}$Na and $^{39}$K NMR spectra when the concentration of the sodium and potassium are greater than the concentration of 1, using the software DNMR5[12]. The $T_2$ values of the solvated sodium, as determined from DNMR5, are within $2\sigma$ of the $T_1$ values reported above, 8.3(2), 16.0(3), 24.5(8) and 31.0(4) ms at 238, 274, 300 and 320 K, respectively. The $T_2$ values for the solvated potassium were determined using DNMR5. At 238, 246, 255, 274, 283, 292, 300, 310 and 320 K, the $T_2$ values are 7.6(2), 9.5(3), 11.0(3), 14.0(3), 15.2(3), 17.1(3), 17.6(3), 17.2(4) and 19.6(4) ms, respectively. Similarly, the $T_2$ values are comparable to the $T_1$ values mentioned earlier.

The integrated peaks for the 2-D spectra were determined using the standard Bruker software. The volumes of the cross-peaks were normalized to the total intensities

| | (Na,1,MeCN),B(Ph)$_4$ | (K,1,MeCN),B(*p*-PhCl)$_4$ | (MeCN,1) |
|---|---|---|---|
| Empirical formula | $C_{96.5}$ $H_{126.5}$ B $Cl_{1.5}$ $N_6$ Na $O_8$ | $C_{96.5}$ $H_{122.5}$ B $Cl_{5.5}$ $N_6$ K $O_8$ | $C_{72}$ $H_{104}$ $N_6$ $O_8$ |
| Formula weight | 1585.51 | 1739.39 | 1183.63 |
| Temperature (K) | 236(2) | 203(2) | 203(2) |
| Wavelength (Mo kα) (Å) | 0.71073 | 0.71073 | 0.71073 |
| Crystal color | colourless | colourless | colourless |
| Crystal system, space group | tetragonal, *P4cc* | tetragonal, *P4cc* | monoclinic, $P2_1$ |
| Cell params: a (Å) | 18.128(2) | 18.493(2) | 11.380(2) |
| b (Å) | 18.128(2) | 18.493(2) | 26.899(5) |
| c (Å) | 29.457(5) | 29.586(5) | 11.468(2) |
| ß (deg) | | | 96.382(3) |
| Volume (Å$^3$) | 9680(2) | 10118(1) | 3489(1) |
| Z | 4 | 4 | 2 |
| Density (g/cm$^3$) | 1.088 | 1.142 | 1.127 |
| Absorption coefficient (cm$^{-1}$) | 1.12 | 2.51 | 0.73 |
| *F* (000) | 3412 | 3700 | 1288 |
| $2\theta$ *max* (deg) | 41.6 | 41.6 | 46.5 |
| Reflections collected / unique | 75446 / 5085 [*R*(int) = 0.2253] | 80209 / 5305 [*R*(int) = 0.1836] | 75031 / 9863 [*R*(int) = 0.0420] |
| Data / restraints / parameters | 5085 / 13 / 525 | 5305 / 479 / 541 | 9863 / 968 / 814 |
| Goodness-of-fit on $F^2$ | 1.061 | 1.256 | 1.055 |
| Final *R* indices [I>2sigma(I)][a] | *R*1 = 0.0759, *wR*2 = 0.1901 | *R*1 = 0.1072, *wR*2 = 0.2781 | *R*1 = 0.1090, *wR*2 = 0.2855 |
| *R* indices (all data)[a] | *R*1 = 0.1062, *wR*2 = 0.2055 | *R*1 = 0.1379, *wR*2 = 0.3103 | *R*1 = 0.1258, *wR*2 = 0.2963 |
| Absolute structure parameter | 0.6(4) | -0.04(14) | 1(2) |
| Extinction coefficient | 0.0077(8) | 0.0060 | 0.017(3) |

[a] $R1 = \Sigma\,|\,|F_o| - |F_c|\,|\,/\,\Sigma|F_o|$, $wR2 = (\Sigma w(|F_o| - |F_c|)^2 / \Sigma w|F_o|^2)^{1/2}$

**Table 1.** Crystal data and structure refinement data for (Na,1,MeCN),B(Ph)$_4$, (K,1,MeCN),B(*p*-Ph)$_4$ (Dataset I) and (MeCN,1).

| | (K,1,MeCN),B(*p*-PhCl)$_4$ | (Li,1b),ClO$_4$ |
|---|---|---|
| Empirical formula | $C_{93.5}H_{120.5}BCl_{8.5}N_5KO_8$ | $C_{56}H_{78}ClN_2LiO_{10}$ |
| Formula weight | 1817.70 | 981.59 |
| Temperature (K) | 203(2) | 203(2) |
| Wavelength (Mo kα) (Å) | 0.71073 | 0.71073 |
| Crystal color | colourless | colourless |
| Crystal size (mm) | 0.2 x 0.2 x 0.2 | 0.1 x 0.1 x 0.1 |
| Crystal system, space group | tetragonal, *P4cc* | monoclinic, *P*2(1)/*c* |
| Cell params: a (Å) | 18.4546(11) | 16.284(2) |
| b (Å) | 18.4546(11) | 22.043(3) |
| c (Å) | 29.533(3) | 15.8876(19) |
| ß (deg) | | 103.917(3) |
| Volume (Å$^3$) | 10058.2(12) | 5535.3(12) |
| Z | 4 | 4 |
| Density (g/cm$^3$) | 1.200 | 1.178 |
| Absorption coefficient (cm$^{-1}$) | 3.32 | 1.26 |
| *F* (000) | 3844 | 2112 |
| $2\theta$ *max* (deg) | 49.4 | 41.6 |
| Reflections collected / unique | 78882 / 8570 [*R*(int) = 0.0522] | 43692 / 5789 [*R*(int) = 0.3644] |
| Data / restraints / parameters | 8570 / 556 / 590 | 5789 / 637 / 632 |
| Goodness-of-fit on $F^2$ | 1.045 | 1.038 |
| Final *R* indices [I>2sigma(I)][a] | *R*1 = 0.0730 *w*R2 = 0.2017 | *R*1 = 0.0703 *w*R2 = 0.1501 |
| *R* indices (all data)[a] | *R*1 = 0.0920 *w*R2 = 0.2205 | *R*1 = 0.1809 *w*R2 = 0.1920 |
| Absolute structure parameter | 0.06(7) | |

[a] $R1 = \Sigma\,||F_o| - |F_c|| \,/\, \Sigma|F_o|$, $wR2 = (\Sigma w(|F_o| - |F_c|)^2 / \Sigma w|F_o|^2)^{1/2}$

**Table 2.** Crystal data and structure refinement data for (K,1,MeCN),B(*p*-Ph)$_4$ (Dataset II) and (Li,1b),ClO$_4$.

of the diagonal peaks. The error was calculated under the assumption that the volume of the two cross-peaks should be the same. No corrections for any differences in $T_1$ were applied.[13] Exchange rates were determined by plotting the normalized volume of the cross-peak intensities for the $CH_2$ protons for the $N(CH_2CH_3)_2$ moiety of the sodium complexed species against the mixing times. A slow exchange rate would fit the equation $I_{i\rightarrow j} = k_{i\rightarrow j}p_i\tau_m$, and a fast exchange rate would follow the equations $I_{i\rightarrow j} = a(1 - e^{-b\tau m})$ and $k_{i\rightarrow j} = ab/p_i$ where $I_{i\rightarrow j}$ refers to the volume of the cross-peak and $p_i$ refers to the equilibrium percentage of conformer i (in this case, $p_i = 0.5$).[5,7,8]

## References

(1) Arduini, A.; Ghidini, E.; Pochini, A.; Ungaro, R.; Andretti, G. D.; Calestani, G.; Ugozzoli, F. *J. Incl. Phen.*, **1988**, *6*, 119.

(2) Israëli, Y.; Detellier, C. *J. Phys. Chem. B*, **1997**, *101*, 1897.

(3) Meier, U. C.; Detellier, C. *J. Phys. Chem. A*, **1999**, *103*, 3825.

(4) Meier, U. C.; Detellier, C. *J. Phys. Chem. A*, **1999**, *103*, 9204.

(5) Blixt, J.; Detellier, C. *J. Am. Chem. Soc.*, **1994**, *116*, 11957.

(6) Blixt, J.; Detellier, C. *J. Am. Chem. Soc.*, **1995**, *117*, 8536.

(7) Perrin, C. L.; Dwyer, T. *J. Chem. Rev.*, **1990**, *90*, 935.

(8) Jeener, J.; Meier, B. H.; Bachmann, P.; Ernst, R. R. *J. Chem. Phys.*, **1979**, *71*, 4546.

(9) Ernst, R. R.; Bodenhausen, G.; Wokaun, A. In *Principles of Nuclear Magnetic Resonance in One and Two Dimensions*; Clarendon Press: Oxford, 1987.

(10) Blessing, R. *Acta Cryst.*, **1995**, *A51*, 33.

(11) Sheldrick, G. M. *Bruker AXS*, Madison, WI, 1997.

(12) Stephenson, D. S.; Binsh, G. *QCPE*, **1978**, *11*, 365.

(13) Meier, U. C.; Detellier, C. *J. Phys. Chem. A*, **1998**, *102*, 1888.

# 3. Sodium and Potassium Complexation Studies

## 3.1 $^1$H NMR Analysis

Typical $^1$H NMR titration experiments, involving variations in the amount of $NaB(Ph)_4$ in a 1:1 (v/v) $CDCl_3$:$CD_3CN$ solution of 20 mM of compound **1**, produced new peaks resulting from the complexation of the sodium cation to **1** (Figure 3). Namely, the singlet for the $OCH_2CO$ methylene protons (4.75 ppm) and the pair of doublets of the bridging $CH_2$ protons (4.97 and 2.92 ppm) of the uncomplexed **1** diminished as new peaks for the $OCH_2CO$ methylene protons and the bridging $CH_2$ protons evolved at a higher field (4.29 ppm, and 4.23 and 3.12 ppm, respectively). The $CH_2$ protons from the $N(CH_2CH_3)_2$ moiety exhibited two quartets, one at 2.91 and 3.19 ppm, upon addition of $NaB(Ph)_4$ signifying a difference of environment between the two $CH_2$ sites. The peaks for the aromatic and the methyl protons are not shown on the NMR spectra due to obstruction by the proton peaks of the tetraphenylborate anion or because of a lack of change in the chemical shift of the peaks. An excess amount of $NaB(Ph)_4$ did not produce any additional peaks in addition to the ones associated with the $(Na,1)^+$ complex (Figure 3e, f, g).

Figure 4 illustrates a linear relationship between the ratio of $[NaB(Ph)_4]/[1]$ and the area of the $\alpha$ methylene protons peaks from the $OCH_2CO$ moiety as analyzed by $^1$H NMR. The intersection point for the lines when $[NaB(Ph)_4] < [1]$ and $[NaB(Ph)_4] > [1]$ is at (1,1) for 320 K (identical results were also recorded at temperatures 238 and 274 K), therefore, indicating a quantitative complexation ($K_f > 10^4\ M^{-1}$) at a 1:1 stoichiometry of

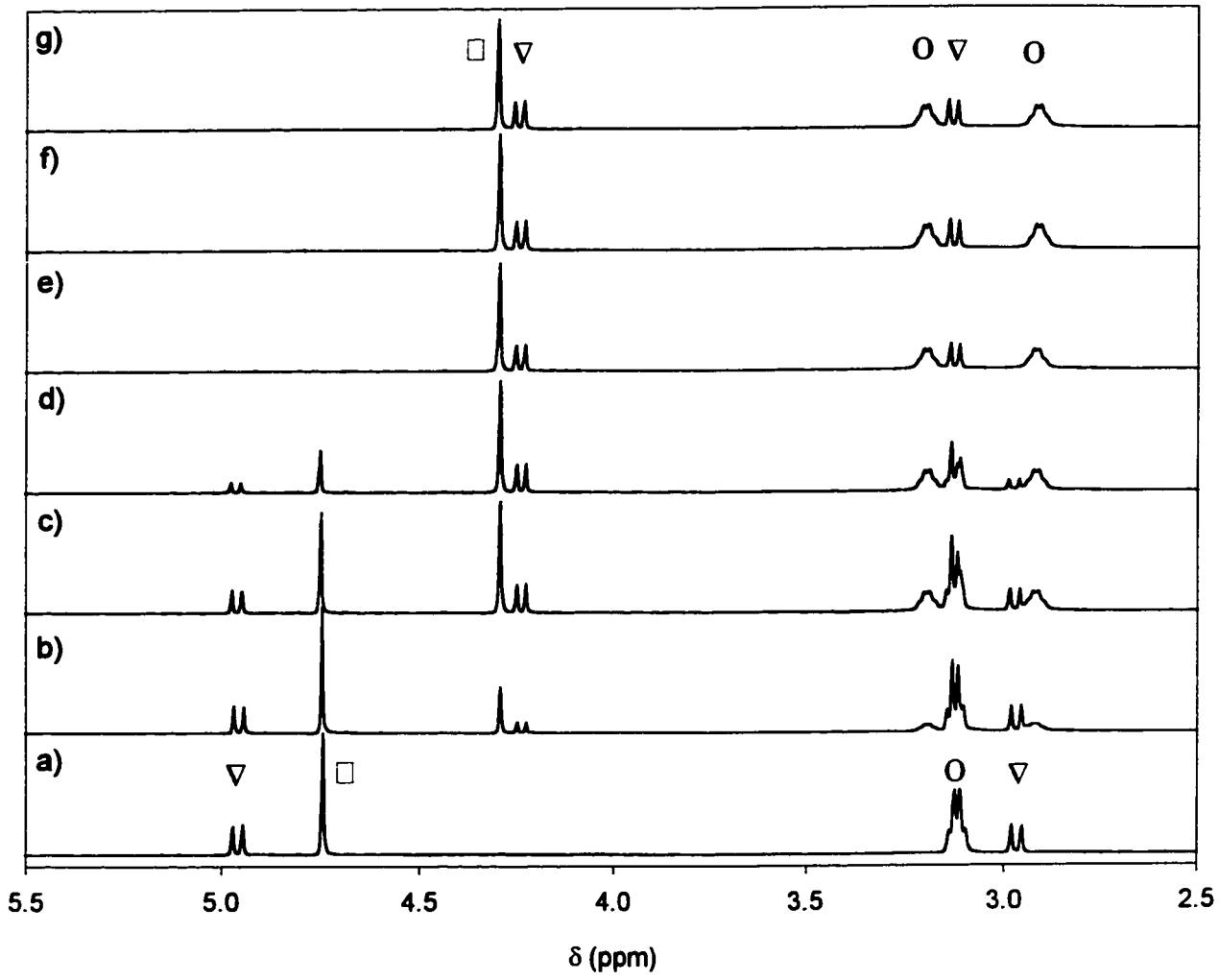


**Figure 3.** Sections of the $^1$H NMR spectra (500 MHz, 1:1 (v/v) $CDCl_3$:$CD_3CN$) of 20 mM **1** in the absence (a) and in the presence (b-g) of various amounts of $NaB(Ph)_4$ at 320 K. b) 5, c) 10, d) 15, e) 20, f) 45, g) 50 mM. (∇) phenyl-bridging $C\underline{H}_2$; (□) $OC\underline{H}_2CO$; (O) $NC\underline{H}_2$.

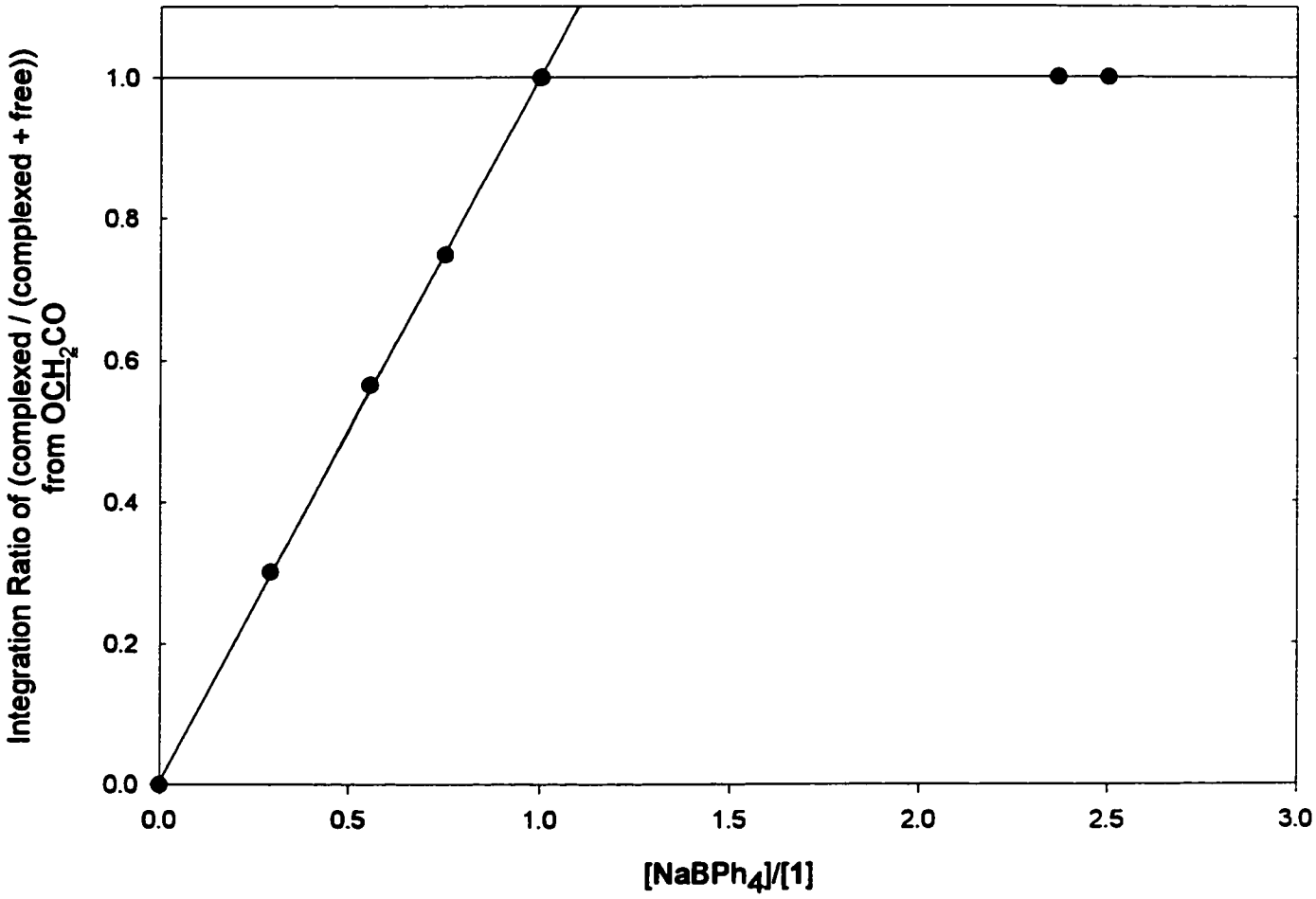


**Figure 4.** Integration ratio (complexed / (complexed + free)) for $^1$H NMR peak of $O\underline{CH_2}CO$ as a function of ($[NaB(Ph)_4]_{tot}/[1]_{tot}$) at 320 K. $[1]_{tot}$ = 20 mM.

1 with the sodium guest. Figure 5 gives the $^1$H NMR spectra of a 20 mM solution of 1 in the presence of 15 mM $NaB(Ph)_4$ at 238, 274 and 320 K. The complexation is quantitative at all temperatures. At 320 K, the linewidths of the $NCH_2$ moiety in the sodium complex broadens, showing a faster interconversion between the two methylene sites.

Similarly, Figure 6 shows the $^1$H NMR spectra of samples containing 20 mM 1 and varying amounts of $KB(p\text{-}PhCl)_4$. As the concentration of the potassium cation increases, the signals corresponding to the uncomplexed 1 diminish as new signals for the $(K,1)^+$ complex intensify. As the concentration of $KB(p\text{-}PhCl)_4$ equals or exceeds the concentration of 1, the peaks corresponding to uncomplexed 1 are no longer observed. At 320 K, the methylene protons of the $OCH_2CO$ arm (4.75 ppm) and the doublet pair of the linking $CH_2$ protons (4.98 and 2.95 ppm) of the uncomplexed 1 diminish as new peaks for the methylene protons and the linking $CH_2$ protons evolve at a higher field (4.36, and 4.39 and 3.12 ppm, respectively). The $CH_2$ protons from the $N(CH_2CH_3)_2$ moiety exhibited two quartets at 2.93 and 3.21 ppm upon addition of $KB(p\text{-}PhCl)_4$ signifying a difference of environment between the two $CH_2$ sites.

Comparison of the integration of the singlets for the complexed and uncomplexed 1 as a function of the concentration ratio of the potassium salt to 1 (Figure 7), shows two linear plots intersecting at (1,1). The results point to a 1:1 complexation ratio between the guest potassium and the host 1. In addition, signals are not observed for other ratios, specifically, the complexation of a second potassium cation to $(K,1)^+$ species. Figure 8 illustrates the changes in the $^1$H NMR spectra of the potassium complex as the temperature is varied. The 1:1 complexation ratio is quantitatively observed for the

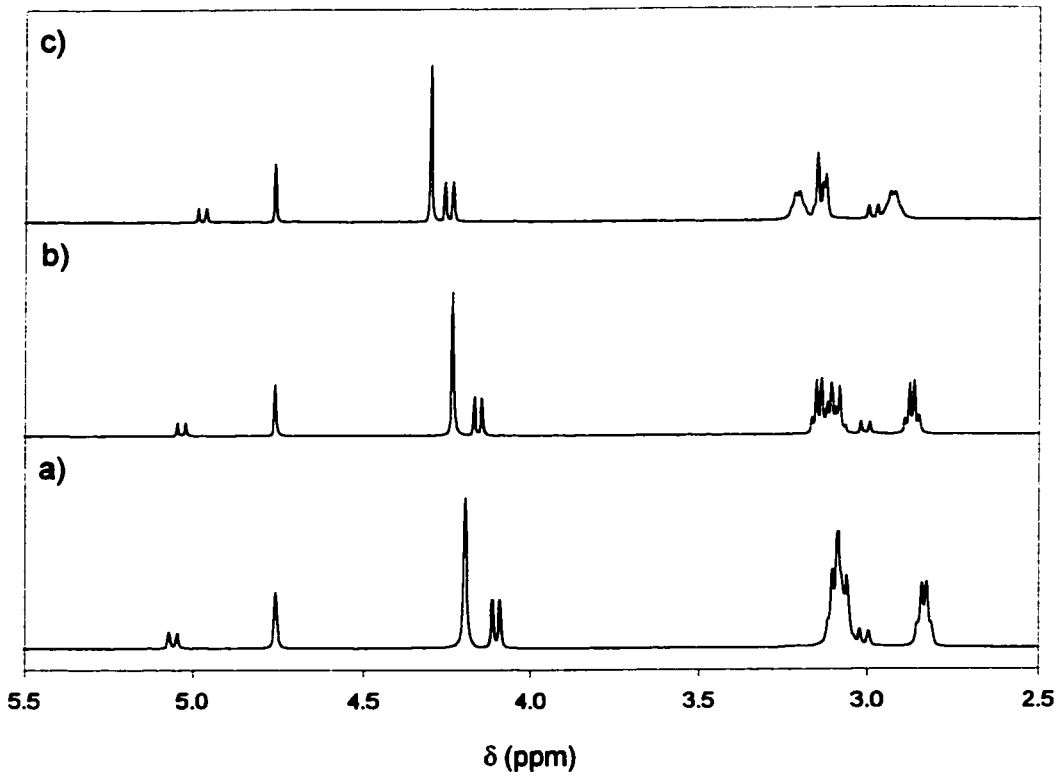


**Figure 5.** Section of the $^{1}H$ NMR spectra of 20 mM 1 and 15 mM $NaB(Ph)_4$ at various temperatures a) 238, b) 274, and c) 320 K.

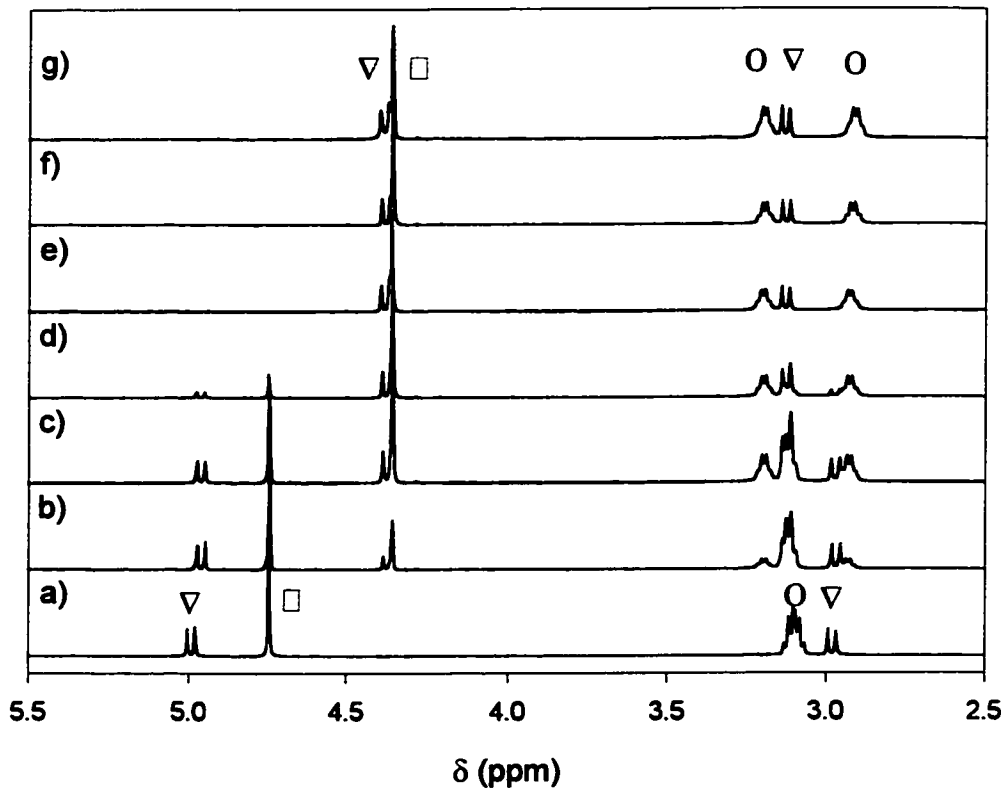


**Figure 6.** Sections of the $^1$H NMR spectra of 20 mM **1** in the absence (a) and in the presence (b-g) of various amounts of KB(*p*-PhCl)$_4$ at 320 K. b) 5, c) 10, d) 15, e) 20, f) 30, g) 50 mM. (∇) phenyl-bridging C$\underline{H_2}$; (□) OC$\underline{H_2}$CO; (O) NC$\underline{H_2}$.

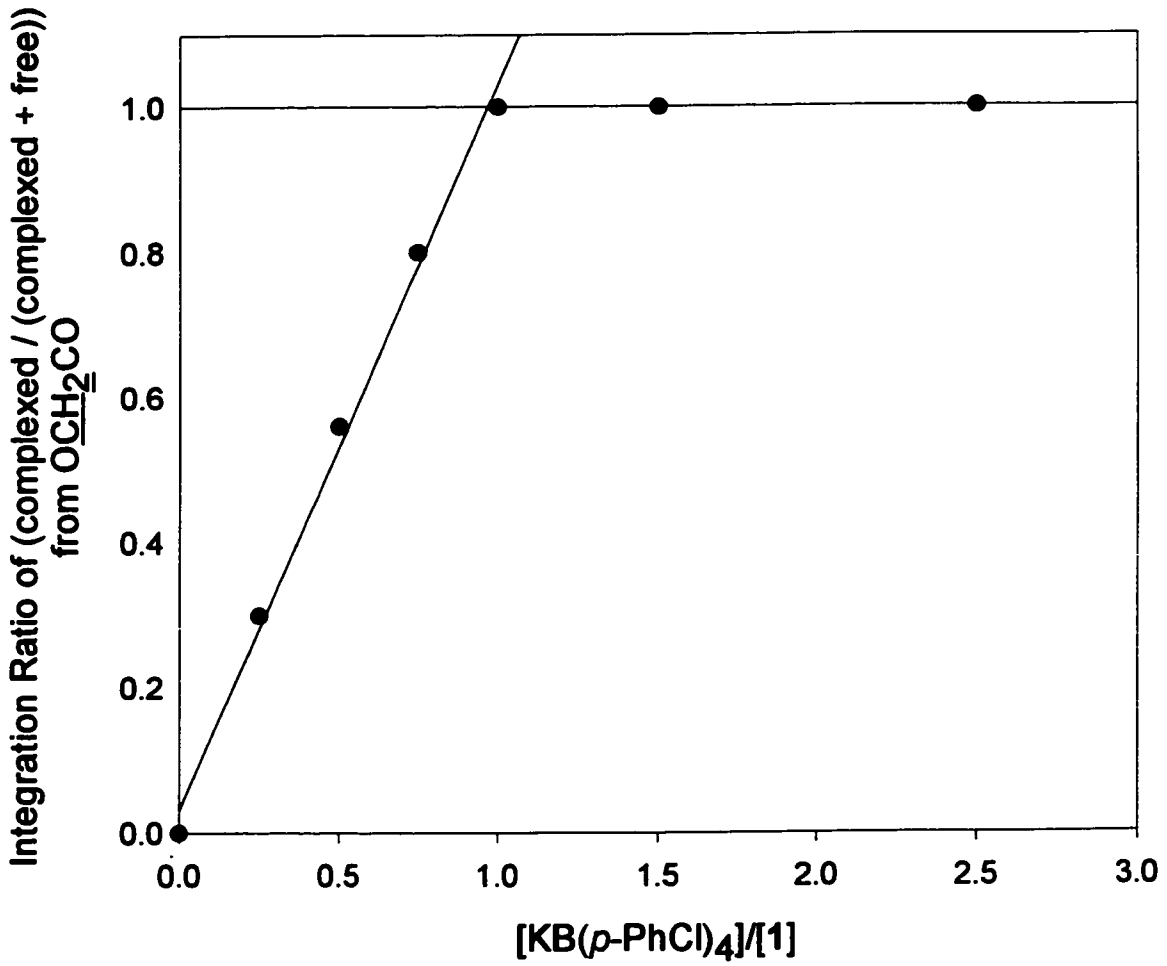


**Figure 7.** Integration ratio (complexed / (complexed + free)) for $^1$H NMR peak of $O\underline{CH_2}CO$ as a function of ($[KB(p\text{-}PhCl)_4]_{tot}/[1]_{tot}$) at 320 K. $[1]_{tot}$ = 20 mM.

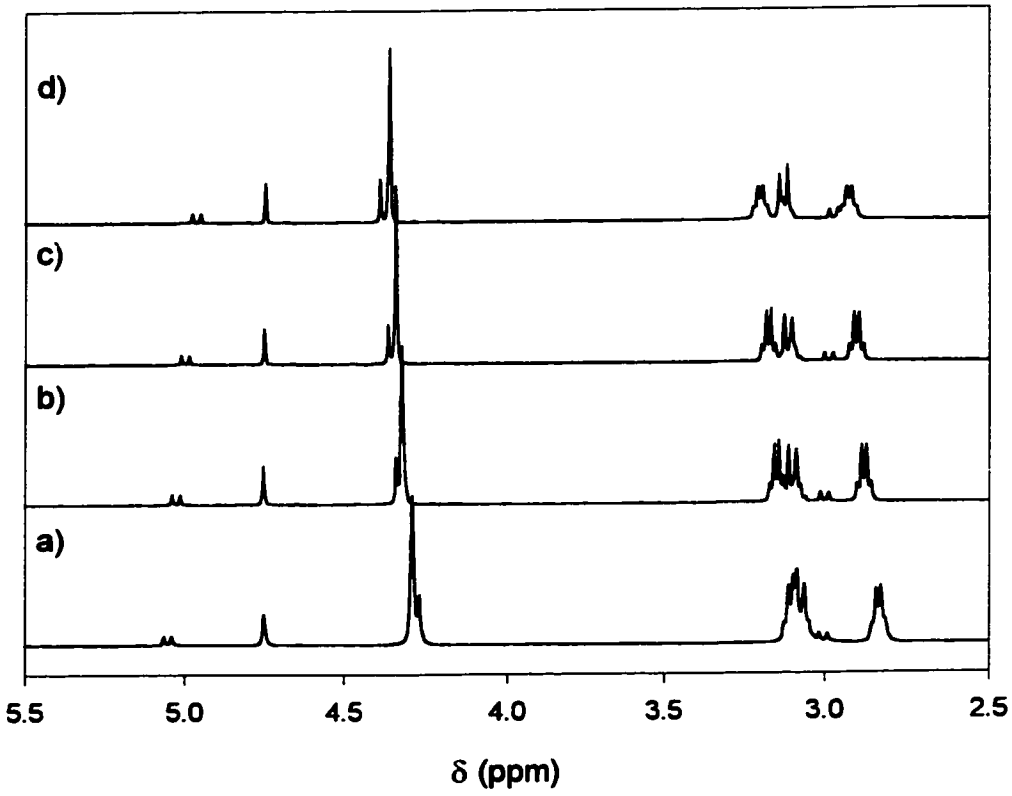


**Figure 8.** Section of the $^{1}$H NMR spectra of 20 mM **1** and 15 mM KB(*p*-PhCl)$_4$ at various temperatures a) 238, b) 274, c) 300 and c) 320 K.

temperature range of 238 to 320 K. Figure 9 compares the $^1H$ NMR spectra at 320 K of sodium and potassium in the presence of 5 mM 1. The chemical shift for the uncomplexed 1 are identical whereas the peaks corresponding to the complexed species differ by 0.07 and 0.02 ppm for the methylene protons of the $OCH_2CO$ arm and the doublet pair of the linking $CH_2$ protons, respectively. As for the $(Cs,1)^+$ complex,[1] the methylene protons of the $OCH_2CO$ arm and the doublet pair of the bridging $CH_2$ protons appear at 4.54, and 4.58 and 3.10 ppm at 328 K. The general trend appears to demonstrate that the larger the ionic radius of the guest cation, the more the methylene and the bridging $CH_2$ protons are shifted downfield.

### 3.2 2-D EXSY Analysis

Analysis of the 2-D EXSY $^1H$ NMR data for the interconversion of the two methylene sites from the $N(CH_2CH_3)_2$ moiety of the $(Na,1)^+$ complex is characterized by rate constants 0.09(2) and 1.22(2) $s^{-1}$ at 300 K and 320 K, respectively. A plot of the cross-peak volumes as a function of the mixing time at 320 K is given in Figure 10. No cross-peaks could be observed at 274 K. Figure 10b provides an Eyring plot for the temperatures 300, 310 and 320 K.

At 320 K, the linewidths of the $NCH_2$ moiety in the potassium complex broadens, showing a faster interconversion between the two methylene sites. As for the case of the potassium complex, the methylene interconversion is characterized by rate constants 0.11(2) and 1.24(2) $s^{-1}$ at 300 K and 320 K, respectively. A plot of the cross-peak volumes as a function of the mixing times at 300 to 320 K is given in Figure 11. No

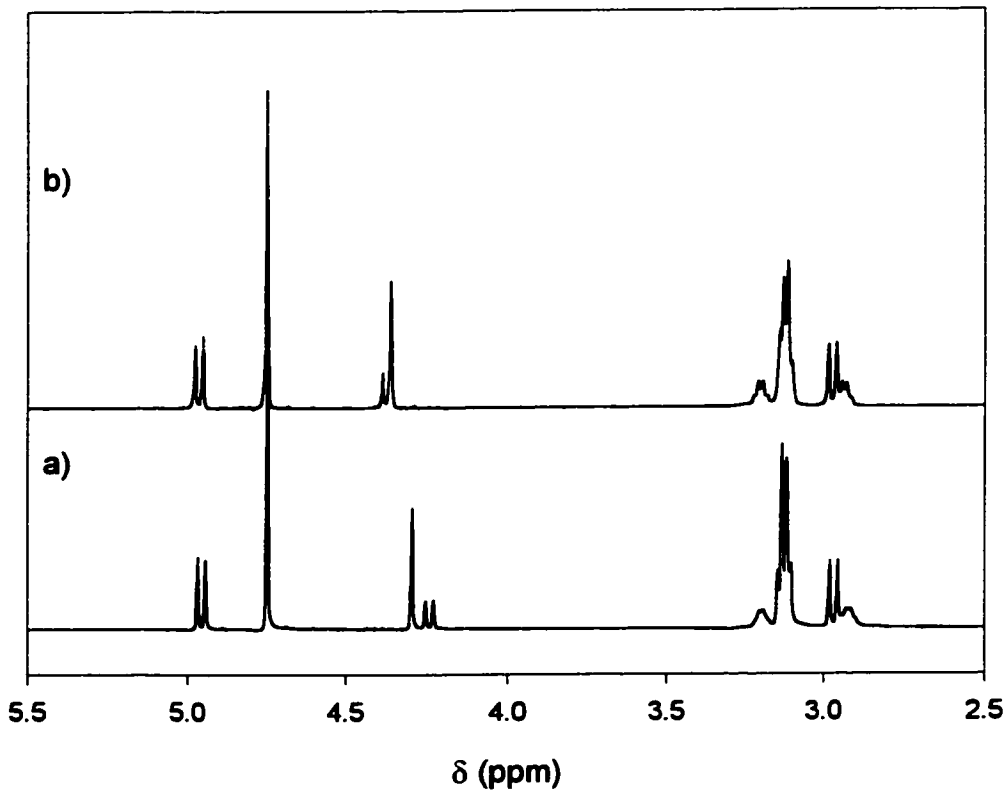


**Figure 9.** Comparison of the $^{1}H$ NMR spectra for a) sodium and b) potassium at 320 K containing 20 mM 1 and 5 mM of the respective salt.

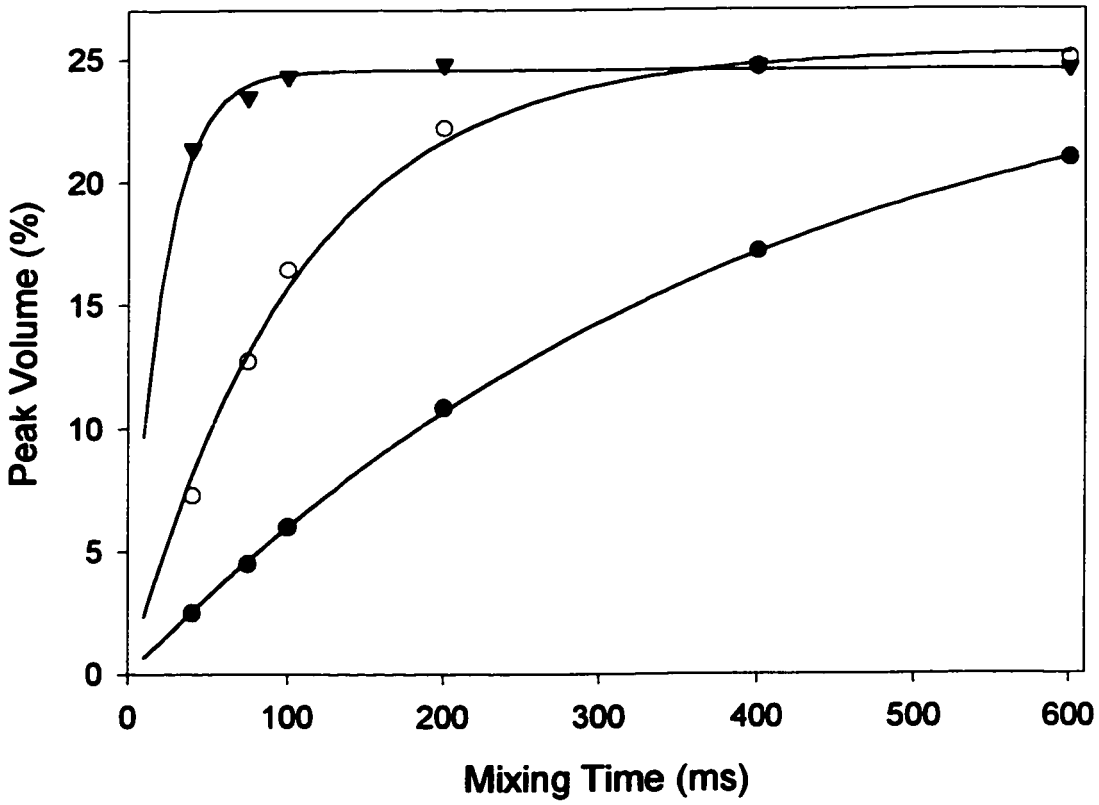


**Figure 10a.** Cross peak volumes as a function of mixing times (ms) obtained at various temperatures. The exchange between the $CH_2$ sites on the $N(CH_2CH_3)_2$ moiety (see Figure 1d) corresponds to a sample containing 15 mM 1 and 20 mM $NaB(Ph)_4$. • 300, o 310 and ▼ 320.

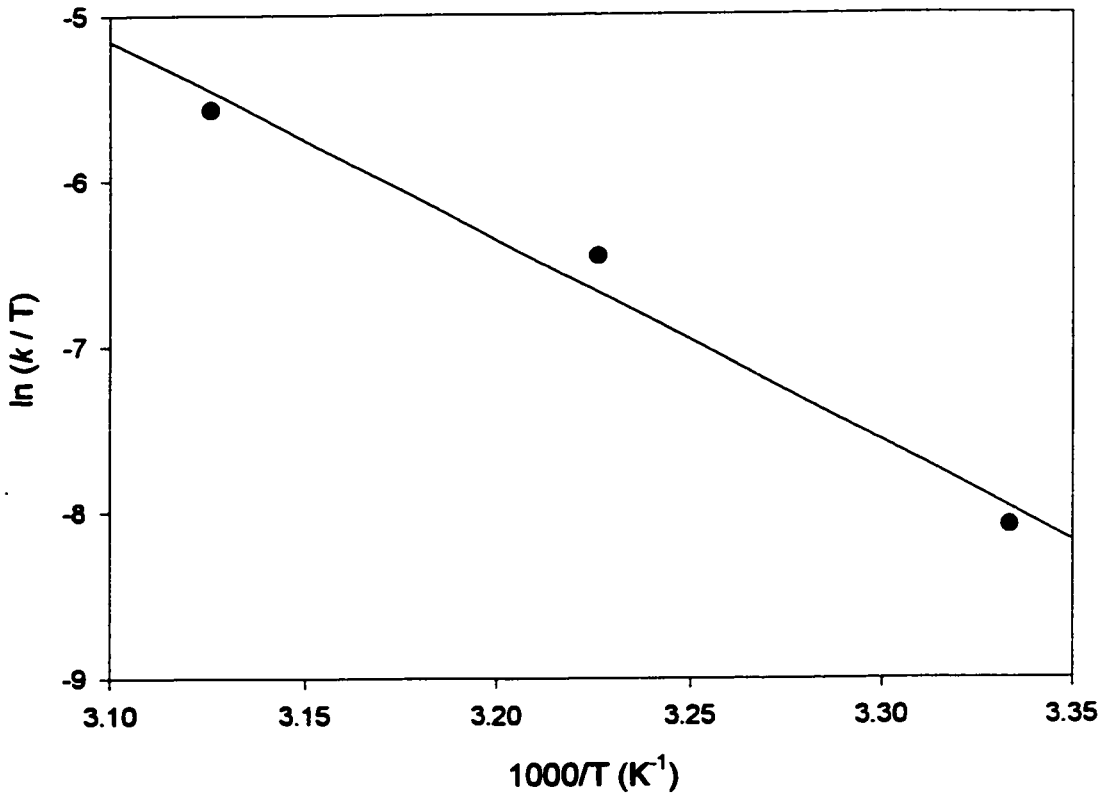


**Figure 10b.** Eyring plot for the interconversion of the $NCH_2$ moieties of $(Na,1)^+$ over a temperature range of 300 to 320 K.

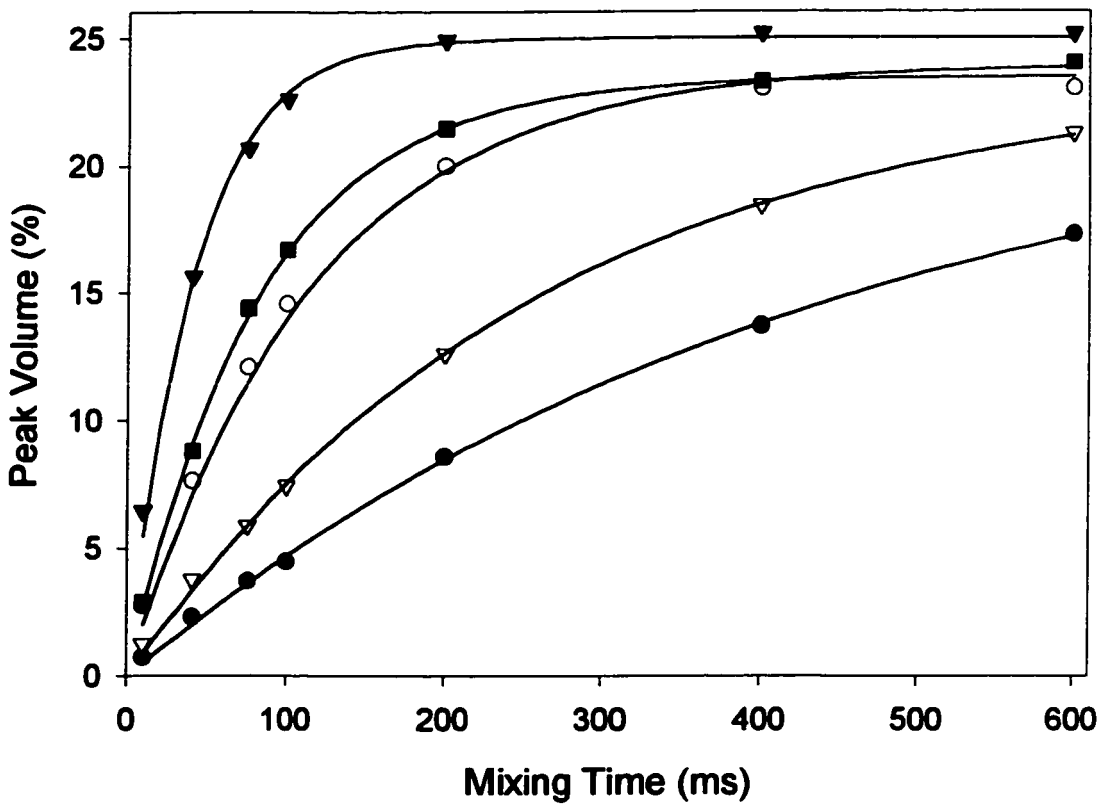


**Figure 11.** Cross peak volumes as a function of mixing times (ms) obtained at various temperatures. The exchange between the $CH_2$ sites on the $N(CH_2CH_3)_2$ moiety (see Figure 6d) corresponds to a sample containing 15 mM 1 and 20 mM KB(*p*-PhCl)$_4$. • 300, ▿ 305, o 310, ■ 315 and ▼ 320 K.

cross-peaks could be observed at 283 K. Figure 12 provides an Eyring plot over the temperature range of 300 to 320 K.

At 320 K, the $^1$H NMR resonances (Figure 13) of the two methylene sites of uncomplexed **1** appears as a single quartet showing a fast exchange. The rates of exchange were determined for the temperature range of 290 to 310 K. A linear regression over five temperatures in that range afforded values for $\Delta H^{\ddagger}$ and $\Delta S^{\ddagger}$ of 105(2) kJ/mol and 112(2) J/mol·K, respectively (Figure 14). The free energy of activation for the two methylene sites of uncomplexed **1** was calculated to be 71(3) kJ/mol at the coalescence temperature of 305 K. The result is comparable to $\Delta G^{\ddagger}$ literature values of 74.3(1.5) kJ/mol for *N,N*-diethylacetamide[2] at 331 K.

The barrier to rotation about the C(O)-N (amide) bonds for **1** increases after complexation of the cation. For example, at 300 K, the $\Delta G^{\ddagger}$ for the interconversion is 80(2), 79(2) and 72(3) kJ/mol, respectively for the complexed sodium and potassium, and the uncomplexed **1**.

### 3.3 $^{23}$Na NMR Analysis

Figure 15 shows the $^{23}$Na NMR spectra of solutions of 20 mM $NaB(Ph)_4$ in the presence of increasing concentration of **1**. The exchange of free sodium with complexed sodium is sensitive to the cavity's geometry and symmetry.[3] A broad line, characterized by a linewidth at half height of approximately 1.0(1) kHz, grows in at –2.11 ppm. It is attributed to a 1:1 complex $(Na,1)^+$. The solvated sodium peak at –3.77 ppm disappears when $[1] \geq [NaB(Ph)_4]$ (Figure 15f, g). The relative intensity of the solvated sodium peak

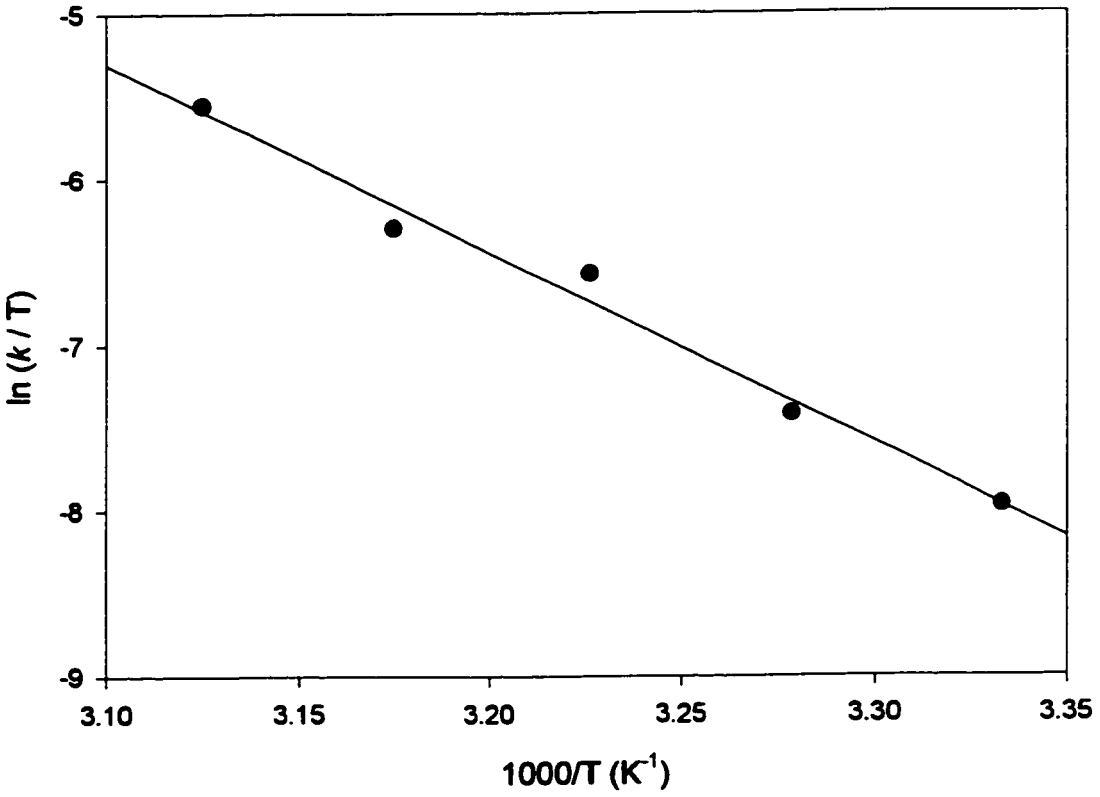


**Figure 12.** Eyring plot for the interconversion of the $NCH_2$ moieties of $(K,1)^+$ over a temperature range of 300 to 320 K.

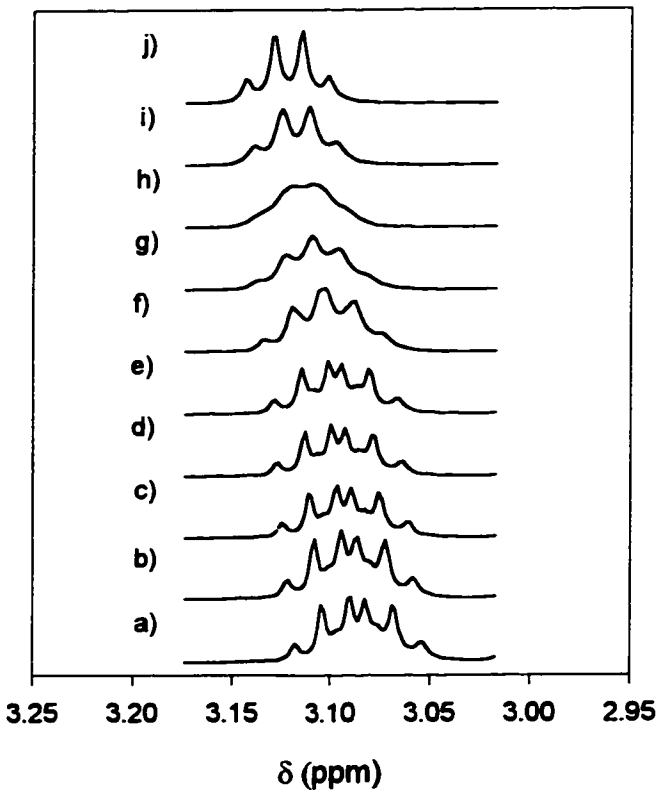


**Figure 13.** Section of the $^1$H NMR of 20 mM **1** illustrating the interconversion between the $NCH_2$ moieties over various temperatures. a) 275, b) 280, c) 285, d) 290, e) 295, f) 300, g) 305, h) 310, i) 315 and j) 320 K.

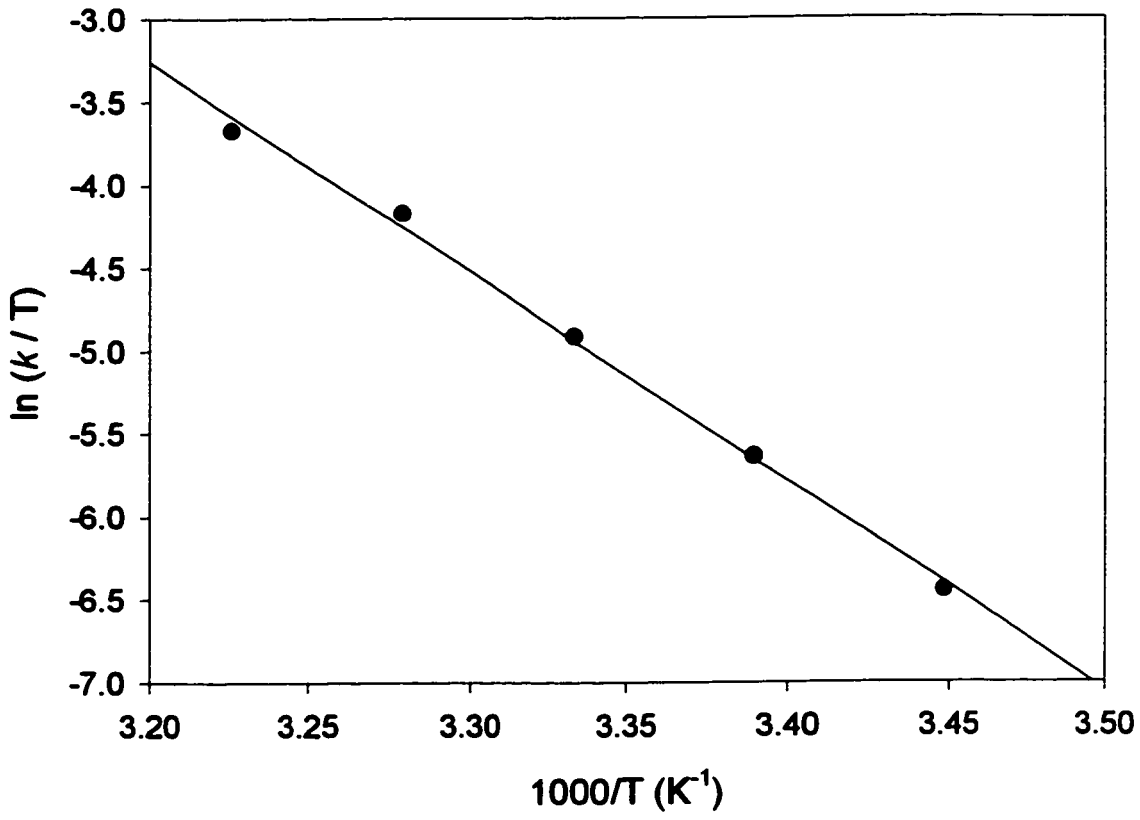


**Figure 14.** Eyring plot for the interconversion of the $NCH_2$ moieties of 20 mM **1** over a temperature range of 290 to 310 K.

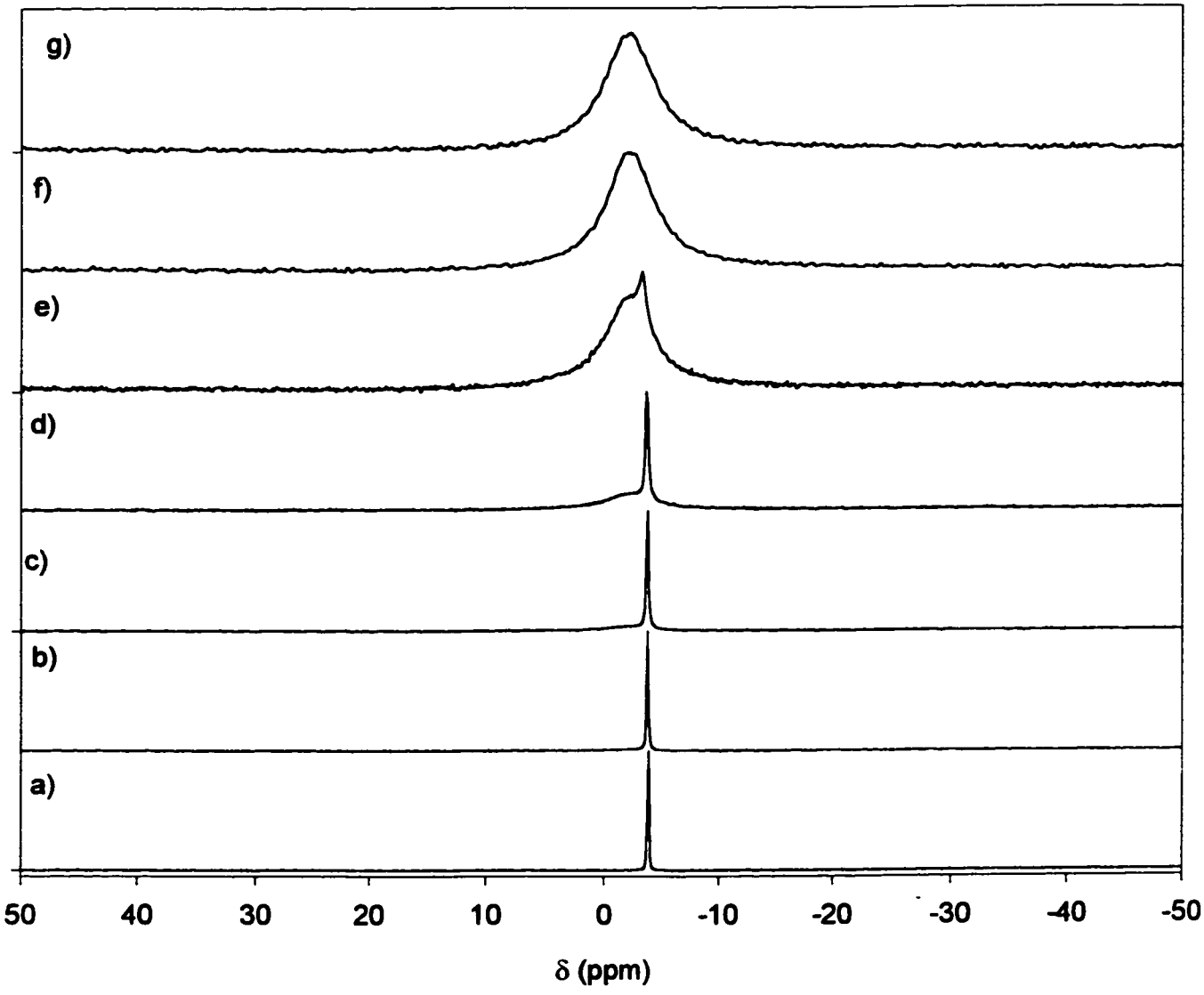


**Figure 15.** $^{23}Na$ NMR spectra (132 MHz, 1:1 (v/v) $CDCl_3$:$CD_3CN$) of 20 mM $NaB(Ph)_4$ in the absence (a) and in the presence (b-f) of various amounts of 1 at 320 K. b) 5, c) 10, d) 15, e) 18, f) 25, g) 45 mM. The intensities for the various spectra are not on the same scale.

decreases as [1] increases while maintaining the total sodium concentration, thus verifying the 1:1 complexation stoichiometry observed by data from $^{1}H$ NMR. $^{23}Na$ NMR spectra in Figure 16 illustrate a small change (~ 0.12 ppm) in the chemical shifts of the peaks as the temperature changes from 238 to 320 K.

Figure 17 shows an excellent agreement between the experimental and calculated spectra for fits using DNMR5[5] at 320 K. Additional $^{23}Na$ NMR spectra were recorded at temperatures 238, 255, 274 and 300 K. They show excellent fits between the experimental and calculated spectra as analyzed by DNMR5, confirming no observable exchange between the complexed sodium and solvated sodium on the $^{23}Na$ NMR time scale. The $^{23}Na$ NMR data point to a strong affinity of 1 for the sodium cation. Conformational flexing of the hydrophilic pseudo-cavity appears to be small considering the lack of exchange of the sodium guest. Theoretical work via molecular dynamics simulation[4] supports the notion of rigidity in the hydrophilic pseudo-cavity due to the encapsulation of the cation.

### 3.4 $^{39}K$ NMR Analysis

Upon inspection of the $^{39}K$ NMR spectra (Figure 18), a single peak at 13.4 Hz at 320 K is present when the $[K^+] > [1]$. As the concentration of 1 increases, the peak diminishes in intensity. Therefore, the peak can be assigned to the solvated potassium under the premise of a two-site case. This is evident from $^{1}H$ NMR where peaks for the 2:1 complex of $(K_2 1)^+$ are not observed. When the $[K^+] \leq [1]$, no peaks are observed for the complexed potassium. This trend is observed for the temperature range of 238 to 320

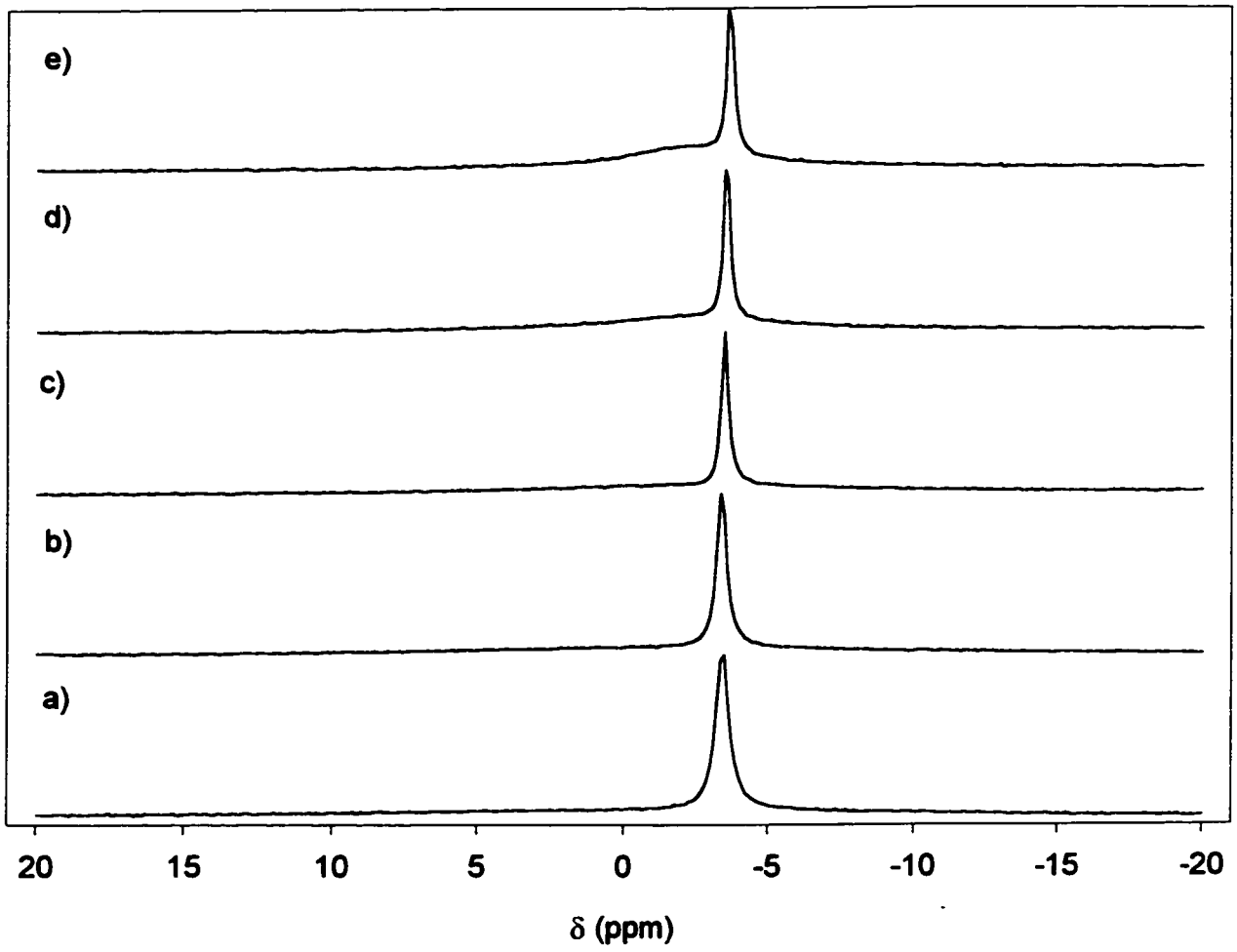


**Figure 16.** $^{23}$Na NMR spectra of 10 mM 1 and 20 mM $NaB(Ph)_4$ at various temperatures.

a) 238, b) 255, c) 274, d) 300 and e) 320 K.

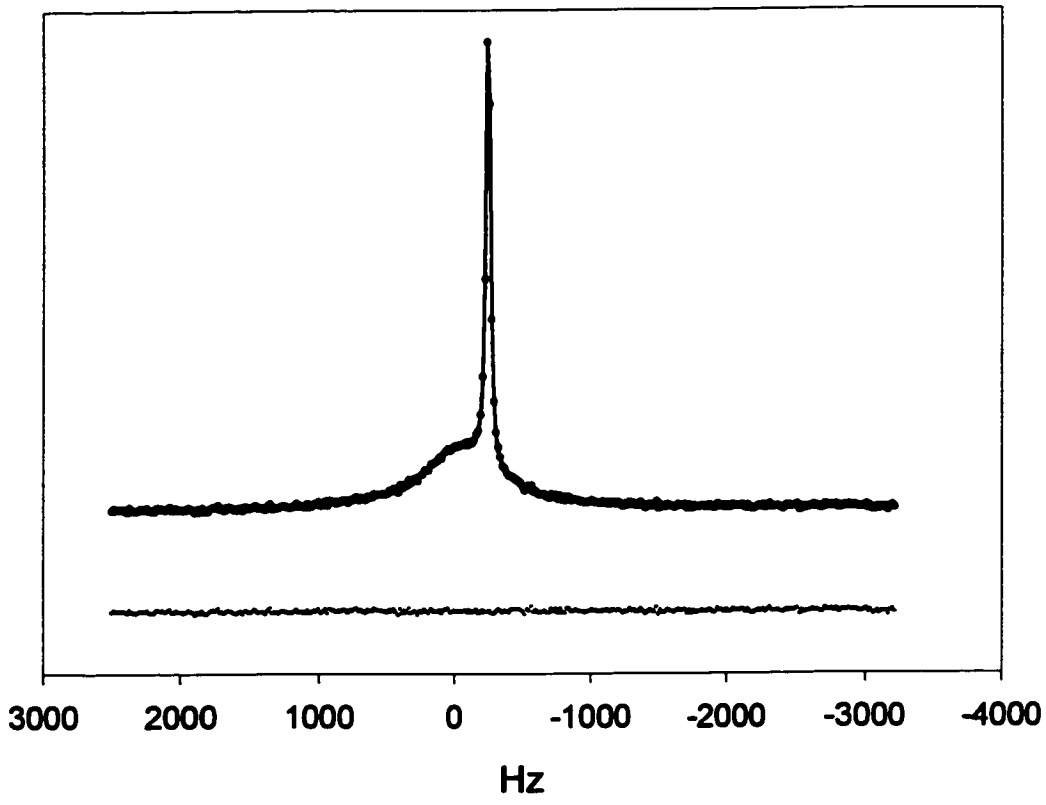


**Figure 17.** $^{23}$Na NMR spectra of 15 mM 1 and 20 mM $NaB(Ph)_4$ at 320 K ($k = 0\ s^{-1}$). • measured spectrum, — fit with DNMR5, and --- difference.

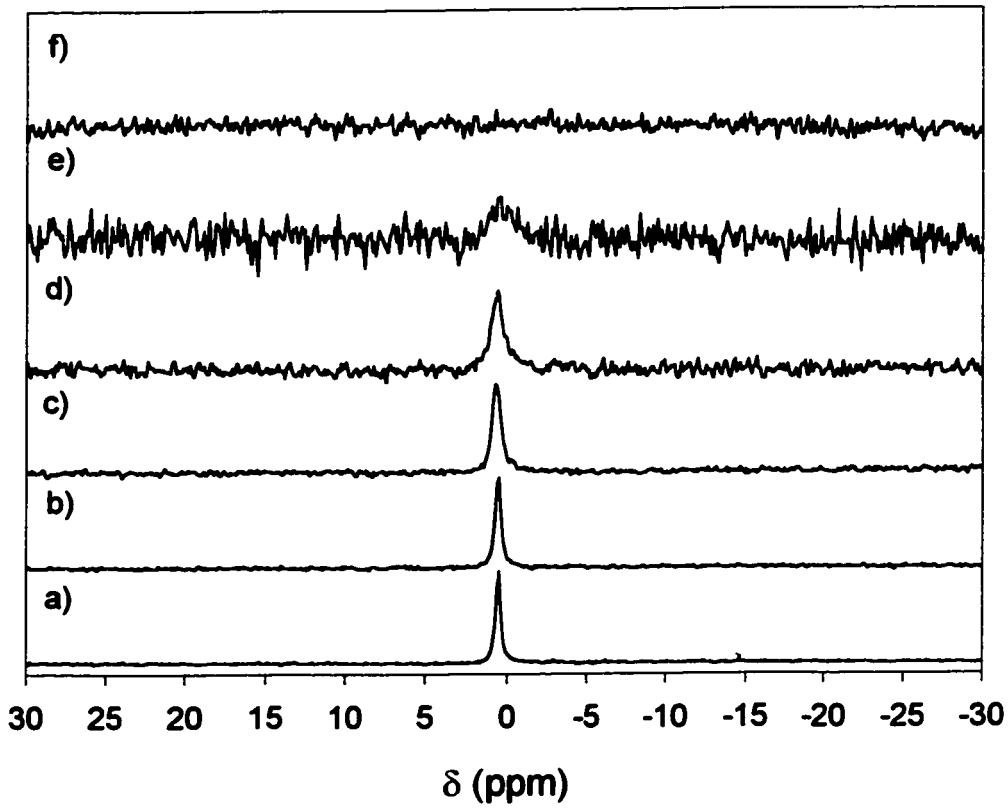


**Figure 18.** $^{39}$K NMR spectra (23 MHz, 1:1 (v/v) $CDCl_3$:$CD_3CN$) of 40 mM KB(*p*-PhCl)$_4$ in the absence (a) and in the presence (b-f) of various amounts of 1 at 320 K. b) 10, c) 20, d) 30, e) 35, f) 80 mM. The intensities for the various spectra are not on the same scale.

K. Analysis to determine the rate of exchange between the solvated and complexed potassium was performed using the program DNMR5[5] on the single potassium peak. To prove the validity of DNMR5 in the determining the rate constant for a single peak, the program was first applied to $^{23}$Na NMR spectra of known rate constants. $^{23}$Na NMR spectra containing 0 mM 1 and 20 mM $NaB(Ph)_4$ at 300 and 320 K show an excellent fit when the rate constant was set between zero and five, and when a broad or narrow peak was added to simulate the complexed sodium (Figure 19). When DNMR5 was applied to the $^{39}$K NMR spectra, the results show a slow to moderately slow exchange. The exchange was determined using a broad or narrow peak to simulate the complexed potassium (Figure 20). This trend was observed for the 238, 246, 255, 265, 274, 283, 292, 300, 310 and 320 K, and at the concentrations of 10, 20, 30 and 35 mM of 1 with KB(*p*-$PhCl)_4$ at a fixed concentration of 40 mM.

$$(L)^+_{solv} + (1)_{solv} \underset{k_d}{\overset{k_f}{\rightleftharpoons}} (L,1)^+_{solv} \qquad (1)$$

$$A \underset{k_B}{\overset{k_A}{\rightleftharpoons}} B \qquad (2)$$

$$k_A = 1 / T_2 - 1 / T_{2,free} \qquad (8)$$

$$k_A = k_{-1} [(L,1)^+] / [L^+] + k_2 [(L,1)^+] \qquad (9)$$

$$(L,1)^+_{solv} + (L^*)^+_{solv} \overset{k_2}{\rightleftharpoons} (L^*,1)^+_{solv} + (L)^+_{solv} \qquad (12)$$

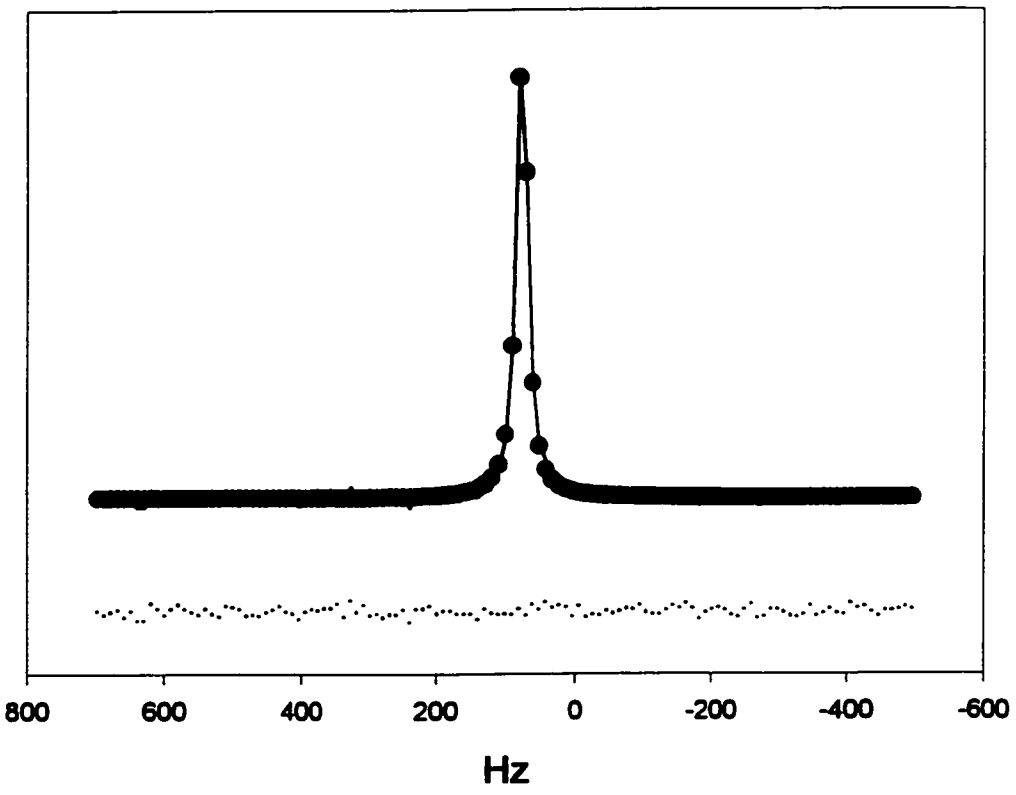


**Figure 19.** $^{39}K$ NMR spectra of 10 mM **1** and 40 mM KB(*p*-PhCl)$_4$ at 320 K ($k = 0\ s^{-1}$).

• measured spectrum, — fit with DNMR5, and --- difference.

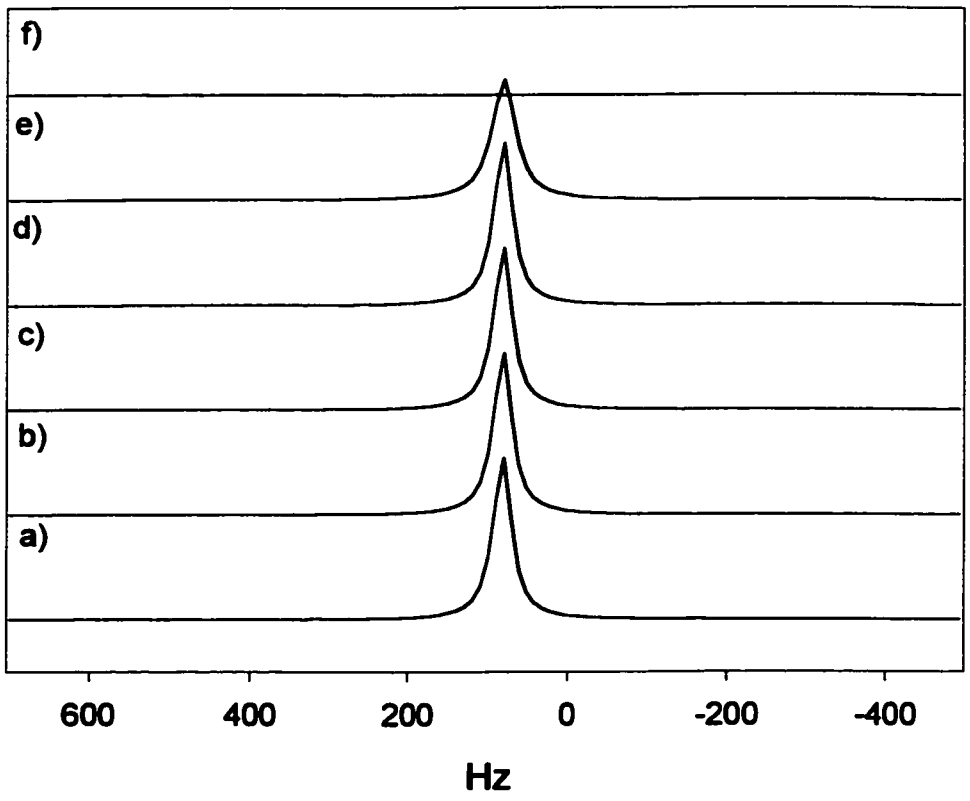


**Figure 20.** Simulated $^{39}K$ NMR spectra of 20 mM **1** and 40 mM KB(*p*-PhCl)$_4$ for various rates of exchange and $T_2$ values at 320 K. a) $k = 0\ s^{-1}$, $T_2 = 0.0115(3)$ s, b) 1, 0.0116(3), c) 10, 0.0129(4), d) 50, 0.027(2), e) 100, 0.074(23), f) 1000, >0.1.

Figure 21 was linearized according to equation 9. Equation 9 was derived from equation 8 where both $T_2$ and $T_{2,free}$ are related to the solvated sodium peak but $T_{2,free}$ is obtained from a sample in the absence of 1.[6,7d] The concentration of the species $(L,1)^+$ is assumed be equal to the concentration of 1 since the reaction has been found to be quantitative. The y-intercept is related to the $k_2$ and has been found to be approximately zero, thus confirming a lack of exchange as seen with $^{23}Na$ and $^{39}K$ NMR experiments. The unimolecular dissociation model does not address the association effect of the anion or the solvent, thereby accounting for the discrepancy in the y intercept. The slope for the solvated sodium peak shows a decrease in the rate of dissociation ($k_{-1}$) as temperature increases. Therefore, the complexation of sodium is favoured as temperature decreases. However, at temperatures below 285 K, the broadening of the peak is a result of the quadrupolar and inhomogeneity contributions to the relaxation exchange.[7] The dissociation rate constant is relatively small for both the sodium and potassium complexes, thus in accordance with the results of DNMR5. A linear regression over five temperatures afforded values for $\Delta H^{\ddagger}$ and $\Delta S^{\ddagger}$ of –5.4(19) J/mol and -208(9) J/mol·K, respectively (Figure 22a). For the potassium sample, the ten temperatures analyzed afforded values for $\Delta H^{\ddagger}$ and $\Delta S^{\ddagger}$ of 2(7) J/mol and -185(22) J/mol·K, respectively (Figure 22b). The results indicate that the reaction is dictated solely by entropic conditions. The two cations exhibit identical dissociation rates. The results indicate that the host 1 can accommodate two guests equally well, and as such, would seemingly not be able to distinguish or prefer one cation over another.

The ethyl groups form a barrier for the interactions of the complexed cations with the external environment. This prevents a second cation from interacting with the

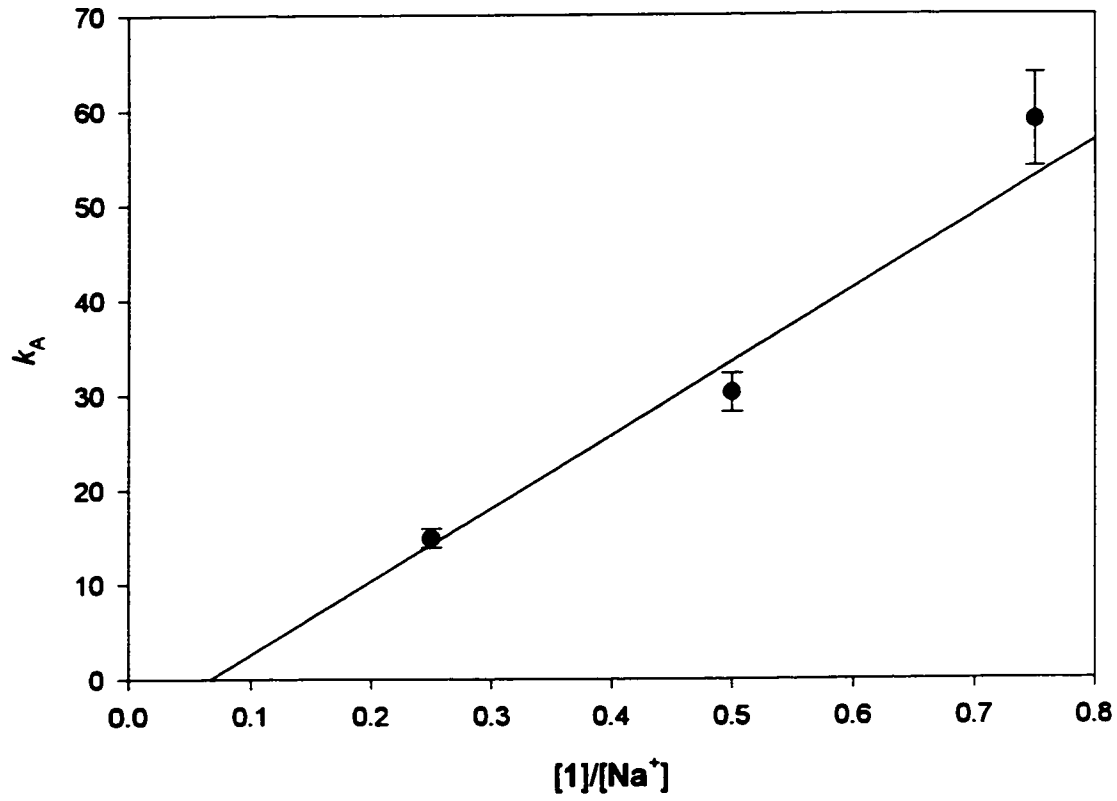


**Figure 21a.** Plot of $k_A$ as a function of [1] / [$L^+$] (see equation 9) for sodium at 274 K.

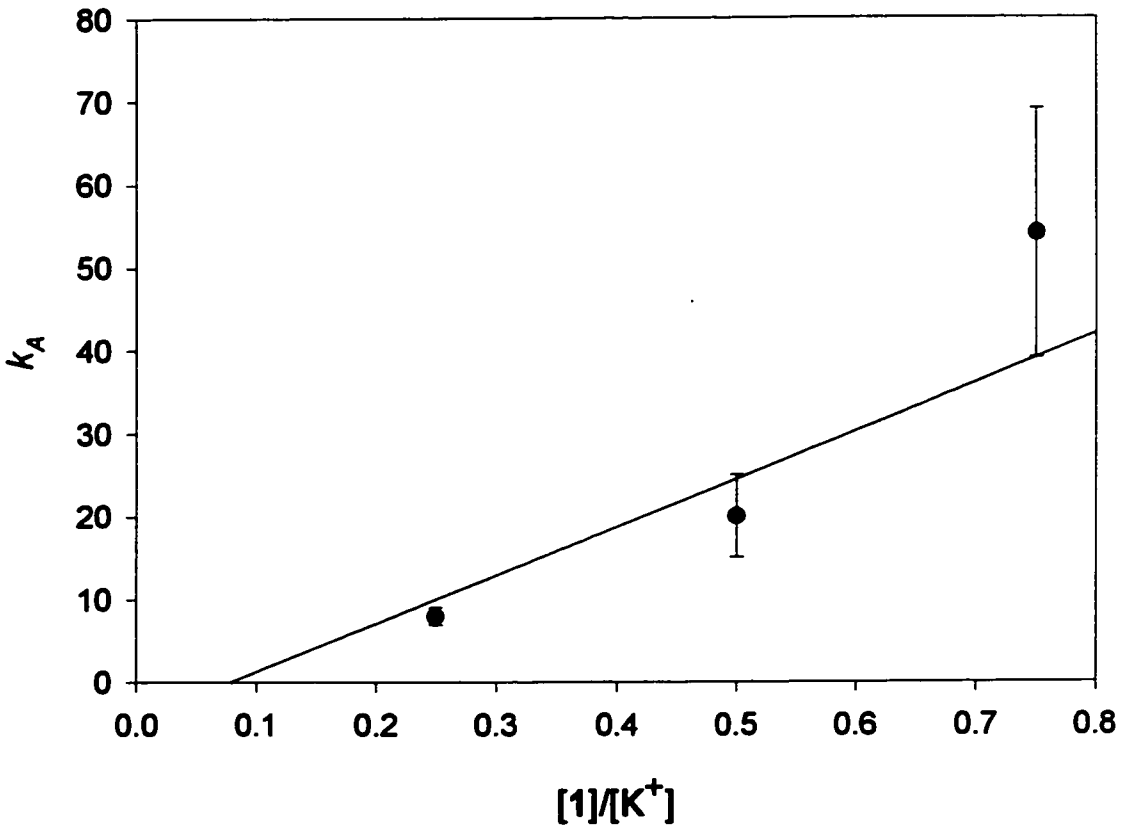


**Figure 21b.** Plot of $k_A$ as a function of [1] / [$L^+$] (see equation 9) for potassium at 274 K.

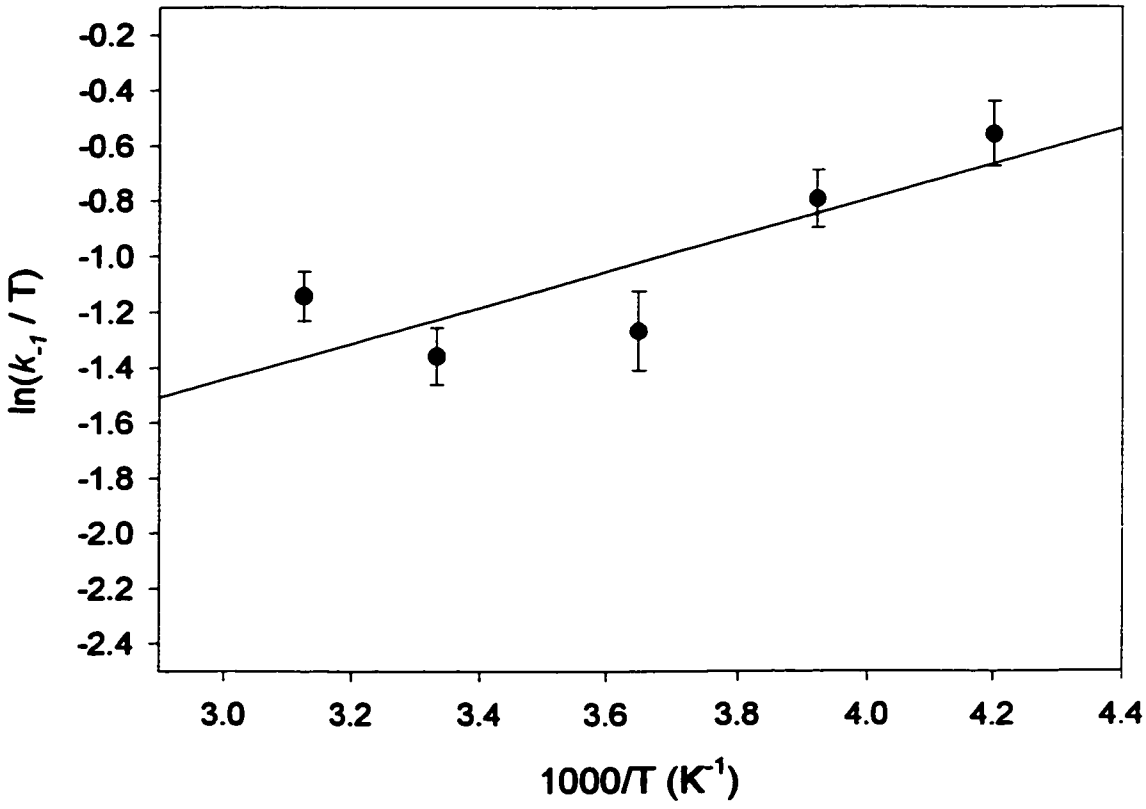


**Figure 22a.** Eyring plot for the change in the linewidth of the free sodium peak in the presence of various amounts of 1 for $^{23}Na$ NMR over a temperature range of 238 to 320 K.

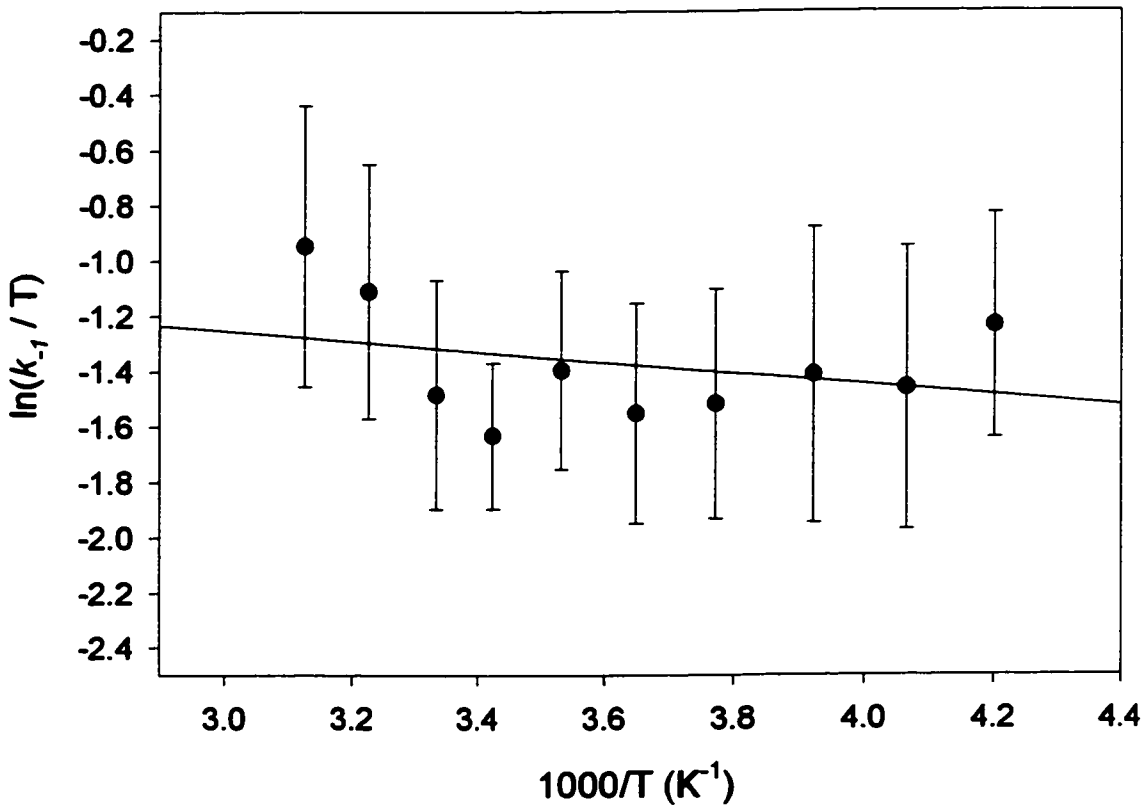


**Figure 22b.** Eyring plot for the change in the linewidth of the free potassium peak in the presence of various amounts of 1 for $^{39}K$ NMR over a temperature range of 238 to 320 K.

carbonyl groups. Previous work on the compound *p-tert*-butylcalix[4]arene tetra-{$OCH_2COOCH_2CH_3$} and $NaB(Ph)_4$,[8] showed similar slow exchange of solvated and complexed sodium on the $^{23}Na$ NMR time scale. However, the calix[4]arene appears to allow the sharing of the sodium guest with a second calix[4]arene molecule forming a 2:1 host/guest complex, whereas, the compound **1** forms only a 1:1 host/guest complex. The presence of an additional ethyl group on the nitrogen adds to the steric bulk at the entrance site of the hydrophilic pseudo-cavity. If a larger guest such as a cesium cation is used, then we expect the compound **1** to reorganize first to compensate for the large cesium cation such that the ethyl groups are pushed away from the cavity's opening. The larger the hydrophilic pseudo-cavity is, the more likely the guest will dissociate from **1** as is seen for the cesium cation.[1] The larger pseudo-cavity also exposes the carbonyl groups for a possible weak complexation with a second cesium cation. This is not observed with the solvated sodium and potassium cations.

Molecular dynamic studies by Varnek *et al.*[4,9] suggested an interaction of acetonitrile with the hydrophobic pseudo-cavity of **1** and its involvement in complexation of alkali metal cations. Smirnov *et al.*[10] have reported a weak complex of **1** with acetonitrile in $CCl_4$ with a stability constant of $K = 1.8\ M^{-1}$. They also suggested that the methyl group fits best in the hydrophobic pseudo-cavity of **1**. It also has been reported that the primary solvation shell is made exclusively of acetonitrile molecules.[11]

Extraction comparisons[12] from water to $CH_2Cl_2$ show sodium (95.5 %) and calcium (98 %) being highly favoured followed by potassium (73.7 %), strontium (86.3 %) and barium (74 %) over lithium, rubidium, and cesium cations. Changing the ethyl groups to propyl and butyl groups showed similar results. In addition, amides were found

to be better at extracting alkali metals than esters, but were less selective.[12b] Extraction experiments from water to chloroform show a selectivity order of $Na^+ >> K^+ > Cs^+ > Li^+$.[3] Although the sodium cation is favoured in this solvent system, the binary acetonitrile/chloroform system shows little distinction between the sodium and potassium cations.

## References

(1) Meier, U. C.; Detellier, C. *J. Phys. Chem. A*, **1999**, *103*, 3825.

(2) (a) Siddall, T. M.; Stewart, W. E.; Knight, F. C. *J. Phys. Chem.*, **1970**, *74*, 3580. (b) Gryff-Keller, A.; Terpinski, J.; Zajaczkowska-Terpinska, E. *J. Chem. Research (S)*, **1984**, 330.

(3) Brouwer, E. B., Structure and dynamics of *t*-butylcalix[4]arene-guest compounds. **1996**, Ph.D. Thesis.

(4) Guilbaud, P.; Varnek, A.; Wipff, G. *J. Am. Chem. Soc.*, **1993**, *115*, 8298.

(5) Stephenson, D. S.; Binsh, G. *QCPE*, **1978**, *11*, 365.

(6) (a) Detellier, C. In *Practical Spectroscopy*; Popov, A. I., Hallenga, K., Eds.; Marcel Dekker: New York. 1990; Vol. 11. pp 521-566. (b) Sandström, J. In *Dynamic NMR Spectroscopy*; Academic Press: New York, 1982.

(7) (a) Blixt, J.; Detellier, C. *J. Am. Chem. Soc.* **1994**, *116*, 11957. (b) Blixt, J.; Detellier, C. *J. Am. Chem. Soc.*, **1995**, *117*, 8536. (c) Delville, A.; Stöver, H. D. H.; Detellier, C. *J. Am. Chem. Soc.*, **1987**, *109*, 7293. (d) Brière, K. M.; Detellier, C. *New J. Chem.*, **1989**, *13*, 145. (e) Graves, H. P.; Detellier, C. *J. Am. Chem. Soc.*, **1988**, *110*, 6019. (f) Brière, K. M.; Detellier, C. *J. Phys. Chem.*, **1992**, *96*, 2185.

(8) Israëli, Y.; Detellier, C. *J. Phys. Chem. B*, **1997**, *101*, 1897.

(9) Varnek, A.; Wipff, G. *J. Phys. Chem.*, **1993**, *97*, 10840.

(10) Smirnov, S.; Sodorov, V.; Pinkhassik, E.; *Havlíček, J.;* Stibor, I. *Supram. Chem.*, **1997**, *8*, 187.

(11) Meier, U. C.; Detellier, C. *J. Phys. Chem. A*, **1998**, *102*, 1888.

(12) (a) Arnaud-Neu, F.; Schwing-Weill, M. J.; Ziat, K.; Cremin, S.; Harris, S. J.; McKervey, M. A. *New J. Chem.*, **1991**, *15*, 33. (b) Arnaud-Neu, F.; Barrett, G.; Fanni, S.; Marrs, D.; McGregor, W.; McKervey, M. A.; Schwing-Weill, M. J.; Vetrogon, V.; Wechsler, S. *J. Chem. Soc. Perkin Trans 2*, **1995**, 453.

# 4. Single-Crystal X-ray Analysis

## 4.1 Single-Crystal X-ray Analysis of (Na,1,MeCN),B(Ph)$_4$

The synthetic procedure used in this work leads to compound 1 with only the cone conformation that is kinetically stable.[1] A crystallographic investigation confirms the presence of a 1:1 complex of $(Na,1)^+$ (Figure 23), whereby the sodium cation is encapsulated into the hydrophilic pseudo-cavity of 1. The phenolic and amide oxygens surround the sodium cation in a four-fold symmetrical environment The bond lengths, bond angles and torsion angles are presented in Table 3. The counteranion tetraphenylborate fits the space in between the two diastereomorphs A and B, with no inclusion of the phenyl rings within the hydrophobic pseudo-cavity (Figure 24). The crystal structure for (Na,1),I was previously reported by Wolf *et al.*,[2] however, it lacks the co-complexation of a solvent molecule and possesses a high degree of disorder.

The complexes $(Na,1,MeCN)^+$ and $(Na,1)^+$ exhibit almost identical distances in the $Na^+$-$O_{amide}$, 2.464(5) and 2.477(5) Å, respectively, but vary slightly in the $Na^+$-$O_{phenolic}$ distances, 2.584(5) and 2.524(5) Å, respectively. The inclusion of an acetonitrile molecule into the hydrophobic pseudo-cavity forces the sodium from maintaining optimal interaction with the four phenolic oxygens as seen with $(Na,1)^+$.

As mentioned above, the lack of accessibility of a second sodium cation to the $(Na,1)^+$ complex may be accounted for by the positions of the terminal ethyl groups. This is evidenced in Figure 24. The optimal bond lengths for $Na^+$-O creates an oxygen

| $(Na,1,MeCN)^+$ | | $(Na,1)^+$ | | (MeCN,1) | |
|---|---|---|---|---|---|
| Na(1) -O(2) | 2.464(5) | Na(2) -O(4) | 2.477(5) | C(71) -O(1), C(71) - O(5) | 3.447(15) |
| Na(1) -O(1) | 2.584(5) | Na(2) -O(3) | 2.524(5) | C(71) -O(3) | 3.432(15) |
| O(1) -O(1)A | 3.213(5) | O(3) -O(3)A | 3.185(5) | C(71) -O(7) | 3.498(15) |
| O(1) -O(2) | 2.650(5) | O(3) -O(4) | 2.636(5) | C(71) -O(2) | 3.840(15) |
| O(2) -O(2)A | 3.081(5) | O(4) -O(4)A | 3.090(5) | C(71) -O(4) | 3.947(15) |
| N(1) -C(13) | 1.341(9) | N(2) -C(30) | 1.330(9) | C(71) -O(6) | 3.596(15) |
| C(1) -C(53) | 4.473(8) | | | C(71) -O(8) | 4.003(15) |
| O(2) -Na(1) -O(2)A | 77.4(2) | O(4) -Na(2) -O(4)A | 77.2(2) | N(1) -C(12) | 1.498(15) |
| O(2) -Na(1) -O(2)B | 124.3(3) | O(4) -Na(2) -O(4)B | 123.8(3) | N(2) -C(29) | 1.452(14) |
| O(1) -Na(1) -O(2)A | 127.8(2) | O(3) -Na(2) -O(4)A | 130.3(2) | N(3) -C(46) | 1.375(13) |
| O(1) -Na (1) -O(2)B | 153.5(2) | O(3) -Na(2) -O(4)B | 150.4(2) | N(4) -C(63) | 1.510(15) |
| O(2) -Na(1) -O(1) | 63.3(2) | O(4) -Na(2) -O(3) | 63.6(2) | C(69) -C(17) | 4.463(12) |
| O(2) -Na(1) -O(1)A | 80.3(2) | O(4) -Na(2) -O(3)A | 77.2(2) | C(69) -C(34) | 4.513(12) |
| O(1) -Na(1) -O(1)A | 76.9(2) | O(3) -Na(2) -O(3)A | 78.3(2) | C(69) -C(51) | 4.557(12) |
| O(1) -Na(1) -O(1)B | 123.1(3) | O(3) -Na(2) -O(3)B | 126.3(3) | C(69) -C(68) | 4.542(12) |
| C(7) -O(1) -C(12) | 111.3(5) | C(24) -O(3) -C(29) | 112.0(5) | C(6) -O(1) -C(11) | 119.8(5) |
| O(1)-C(12)-C(13)-O(2) | -3.0(7) | O(3)-C(29)-C(30)-O(4) | 6.0(7) | O(1)-C(11)-C(12)-O(2) | 14.0(11) |
| | | | | O(3)-C(28)-C(29)-O(4) | 19.7(9) |
| | | | | O(5)-C(45)-C(46)-O(6) | 6.8(10) |
| | | | | O(7)-C(62)-C(63)-O(8) | -3.2(11) |

**Table 3.** Relevant bond distances (Å) and angles (°) for $(Na,1,MeCN),B(Ph)_4$, $(Na,1),B(Ph)_4$ and (MeCN,1) (only the major-contributing disorder form of (MeCN,1) is considered). The letter A refers to an adjacent monomer and B refers to the opposite monomer within 1.

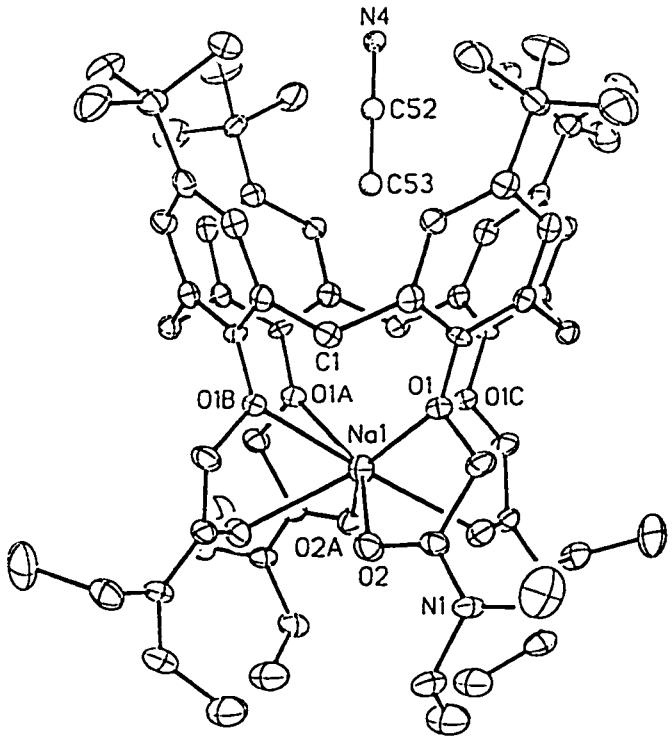


**Figure 23a.** Molecular diagram of 1:1:1 $(Na,1,MeCN)^+$. Hydrogen atoms are omitted for clarity.

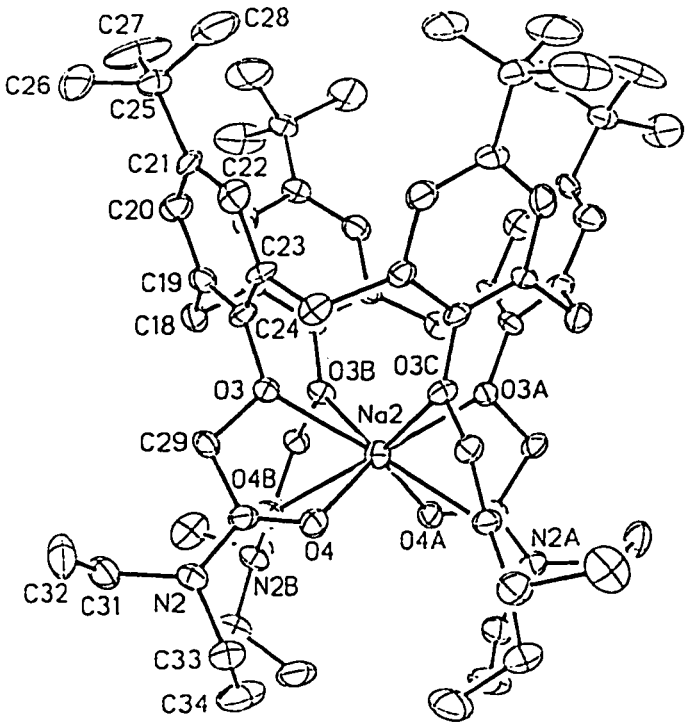


**Figure 23b.** Molecular diagram of 1:1 $(Na,1)^+$. Hydrogen atoms are omitted for clarity.

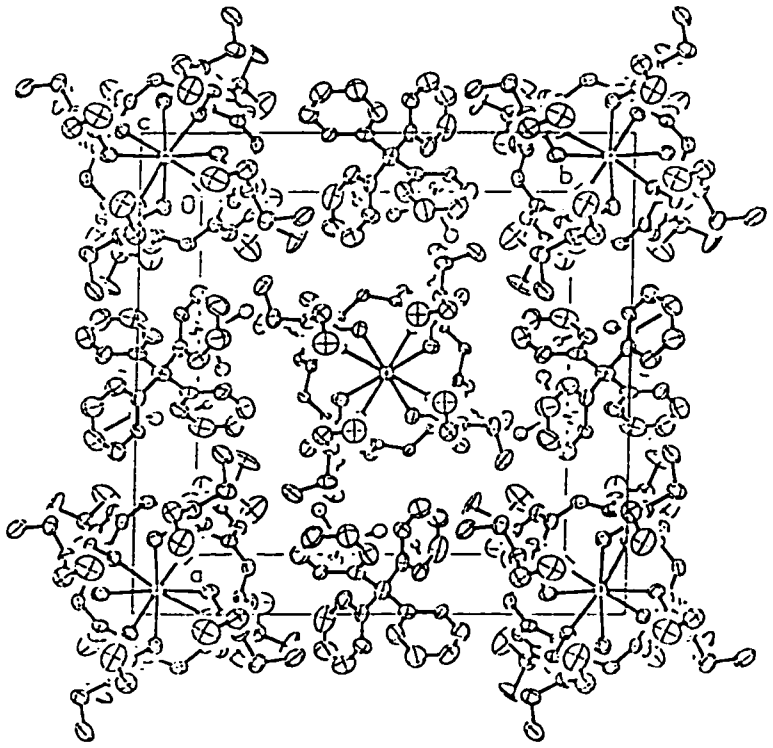

**Figure 24.** Molecular packing diagram from the perspective of the amide groups for $(Na,1),B(Ph)_4$ (the complex $(Na,1,MeCN)^+$ is located at the centre of the diagram with the four $(Na,1)^+$ complexes located at the corners). Hydrogen atoms are omitted for clarity.

pseudo-cavity, which in turn forces the ethyl groups to shield the pseudo-cavity's opening for access of the amide oxygen by a second sodium cation. A larger guest such as a cesium cation may expand the oxygen pseudo-cavity, and thus remove the shielding from the terminal ethyl groups allowing access of a second cesium cation, as previously shown.

The crystallographic data exhibit two alternating diastereomorphs, A and B, that differ in the twist of the $OCH_2CO$ arms (Figure 24). That is, diastereomorph A exhibits torsion angles in the $OCH_2CO$ arms of 6° and diastereomorph B, including acetonitrile in the hydrophobic pseudo-cavity, exhibits –3° torsion angles. We speculate that on the approach to crystallization, B crystallizes with acetonitrile included in the hydrophobic pseudo-cavity. When a second complex molecule crystallizes adjacent to B, acetonitrile is excluded as a result of high energy packing effects and the diastereomorph A is obtained. The process continues, alternating A and B sites. The crystallographic data obtained were 60/40 racemically twinned such that the twin components are mirror images.

The X-ray data for 1 complexed with a strontium cation[3] shows a 1:1 complex with nearly identical oxygen-to-guest bond lengths as (Na,1,MeCN),$B(Ph)_4$ ($Sr^{+2}$-$O_{phenolic}$ 2.577(5) avg. and $Sr^{+2}$-$O_{amide}$ 2.501(6) avg.). This can be attributed to the similar ionic radius of the strontium cation (1.26 Å)[4] with the sodium cation (1.18 Å)[4]. However, in relation to a potassium cation (1.51 Å)[4], the bond lengths ($K^+$-$O_{phenolic}$ 2.708(7) Å and $K^+$-$O_{amide}$ 2.739(13) Å)[1] differ significantly due to the increase of the ionic radius. In addition, the positions of the terminal ethyl groups are directed away from the pseudo-cavity for the cations strontium and potassium, as is predicted for larger cations.

## 4.2 Single-Crystal X-ray Analysis of (K,1,MeCN),B(*p*-PhCl)$_4$

The bond lengths, bond angles and torsion angles for the (K,1,MeCN),B(*p*-PhCl)$_4$ crystals are presented in Tables 4 and 5. The data consists of two different crystallographic datasets for the complex (K,1,MeCN),B(*p*-PhCl)$_4$, named datasets I and II for brevity purposes. Both datasets I (Figure 25) and II (Figure 26) exhibit characteristics identical to that observed with (Na,1,MeCN),B(Ph)$_4$, that is, the presence of two diastereomorphs. But differ, in that, both the potassium complexes contain a co-complexed acetonitrile molecule in the *tert*-butyl region.

Both datasets exhibit a 1:1 $(K,1)^+$ complexation with similar $K^+$-$O_{phenolic}$ and $K^+$-$O_{amide}$ bond lengths. From dataset I, the $K^+$-$O_{phenolic}$ and $K^+$-$O_{amide}$ bond lengths for $(K(1),1,MeCN)^+$ are 2.671(7) and 2.626(9) Å, and for $(K(2),1,MeCN)^+$ are 2.682(6) and 2.708(7) Å, respectively. From dataset II, the $K^+$-$O_{phenolic}$ and $K^+$-$O_{amide}$ bond lengths for $(K(1),1,MeCN)^+$ are 2.685(3) and 2.704(3) Å, and for $(K(2),1,MeCN)^+$ are 2.669(3) and 2.639(5) Å, respectively. The complexes $(K(2),1,MeCN)^+$ (I) and the $(K(1),1,MeCN)^+$ (II) and the potassium complex (K,1,MeOH),SCN, reported by Arduini *et al.*[1], possess identical $K^+$-O bond lengths. In addition, the three complexes exhibit the identical "S" twisting of the terminal ethyl groups (Figure 27 and 28). Similarly, the complexes $(K,1,MeCN)^+$ (I) and $(K(2),1,MeCN)^+$ (II) have identical bond lengths and show the identical "C" twisting of the terminal ethyl groups.

| $(K(1),1,MeCN)^+$ | | $(K(2),1,MeCN)^+$ | | $(Li,1b)^+$ | |
|---|---|---|---|---|---|
| K(1) -O(2) | 2.626(9) | K(2) -O(4) | 2.708(7) | Li -O(2) | 1.873(12) |
| K(1) -O(1) | 2.671(7) | K(2) -O(3) | 2.682(6) | Li -O(3) | 1.963(12) |
| O(1) -O(1)A | 3.308(9) | O(3) -O(3)A | 3.350(8) | Li -O(4) | 1.899(12) |
| O(1) -O(2) | 2.749(8) | O(3) -O(4) | 2.637(8) | Li -O(5) | 1.988(12) |
| O(2) -O(2)A | 3.400(9) | O(4) -O(4)A | 3.536(8) | O(1) -O(3) | 3.162(12) |
| N(1) -C(13) | 1.328(17) | N(2) -C(30) | 1.315(13) | O(2) -O(4) | 3.068(12) |
| C(1) -C(53) | 4.427(10) | C(18) –C(51) | 4.463(10) | N(1) -C(13) | 1.308(8) |
| O(2) -K(1) -O(2)A | 80.68(17) | O(4) -K(2) -O(4)A | 81.54(13) | N(2) -C(30) | 1.336(8) |
| O(2) -K(1) -O(2)B | 132.5(5) | O(4) -K(2) -O(4)B | 134.9(4) | Li -Cl | 5.573(12) |
| O(1) -K(1) -O(2)A | 130.9(3) | O(3) -K(2) -O(4)A | 126.6(2) | O(2) -Li -O(4) | 108.8(6) |
| O(1) -K (1) -O(2)B | 148.2(3) | O(3) -K(2) -O(4)B | 151.8(2) | O(3) -Li -O(4) | 83.2(5) |
| O(2) -K(1) -O(1) | 62.5(3) | O(4) -K(2) -O(3) | 58.6(2) | O(2) -Li -O(3) | 120.7(6) |
| O(2) -K(1) -O(1)A | 74.5(3) | O(4) -K(2) -O(3)A | 76.3(2) | O(1) -Li -O(3) | 76.4(6) |
| O(1) -K(1) -O(1)A | 76.53(14) | O(3) -K(2) -O(3)A | 77.30(13) | O(3) -Li -O(5) | 106.1(5) |
| O(1) -K(1) -O(1)B | 122.3(3) | O(3) -K(2) -O(3)B | 124.1(3) | C(7) -O(1) -C(12) | 110.4(4) |
| C(7) -O(1) -C(12) | 112.5(7) | C(24) -O(3) -C(29) | 111.8(7) | C(24) -O(3) -C(29) | 113.9(5) |
| O(1)-C(12)-C(13)-O(2) | 14.6(9) | O(3)-C(29)-C(30)-O(4) | 9.6(9) | O(1)-C(12)-C(13)-O(2) | 0.1(9) |
| | | | | O(3)-C(29)-C(30)-O(4) | 4.9(9) |

**Table 4. Relevant bond distances (Å) and angles (°) for (K,1,MeCN),B($p$-PhCl)$_4$ (Dataset I) and (Li,1b),ClO$_4$. The letter A refers to an adjacent monomer and the B refers to the opposite monomer within 1.**

| $(K(1),1,MeCN)^+$ | | $(K(2),1,MeCN)^+$ | |
|---|---|---|---|
| K(1) -O(2) | 2.704(3) | K(2) -O(4) | 2.639(5) |
| K(1) -O(1) | 2.685(3) | K(2) -O(3) | 2.669(3) |
| O(1) -O(1)A | 3.348(4) | O(3) -O(3)A | 3.305(6) |
| O(1) -O(2) | 2.643(4) | O(3) -O(4) | 2.710(6) |
| O(2) -O(2)A | 3.528(4) | O(4) -O(4)A | 3.428(6) |
| N(1) -C(13) | 1.338(6) | N(2) -C(30) | 1.361(8) |
| C(1) -C(36) | 4.439(5) | C(18) -C(38) | 4.454(6) |
| O(2) -K(1) -O(2)A | 81.45(6) | O(4) -K(2) -O(4)A | 81.01(8) |
| O(2) -K(1) -O(2)B | 134.64(16) | O(4) -K(2) -O(4)B | 133.4(2) |
| O(1) -K(1) -O(2)A | 126.55(10) | O(3) -K(2) -O(4)A | 129.48(13) |
| O(1) -K (1) -O(2)B | 151.94(11) | O(3) -K(2) -O(4)B | 149.43(13) |
| O(2) -K(1) -O(1) | 58.74(10) | O(4) -K(2) -O(3) | 61.38(13) |
| O(2) -K(1) -O(1)A | 76.59(10) | O(4) -K(2) -O(3)A | 75.30(12) |
| O(1) -K(1) -O(1)A | 77.16(6) | O(3) -K(2) -O(3)A | 76.50(6) |
| O(1) -K(1) -O(1)B | 123.74(14) | O(3) -K(2) -O(3)B | 122.22(15) |
| C(7) -O(1) -C(12) | 112.9(3) | C(24) -O(3) -C(29) | 111.6(3) |
| O(1)-C(12)-C(13)-O(2) | -12.7(6) | O(3)-C(29)-C(30)-O(4) | 13.0(6) |

**Table 5.** Relevant bond distances (Å) and angles (°) for (K,1,MeCN),B(*p*-PhCl)$_4$ (Dataset II). The letter A refers to an adjacent monomer and the B refers to the opposite monomer within **1**.

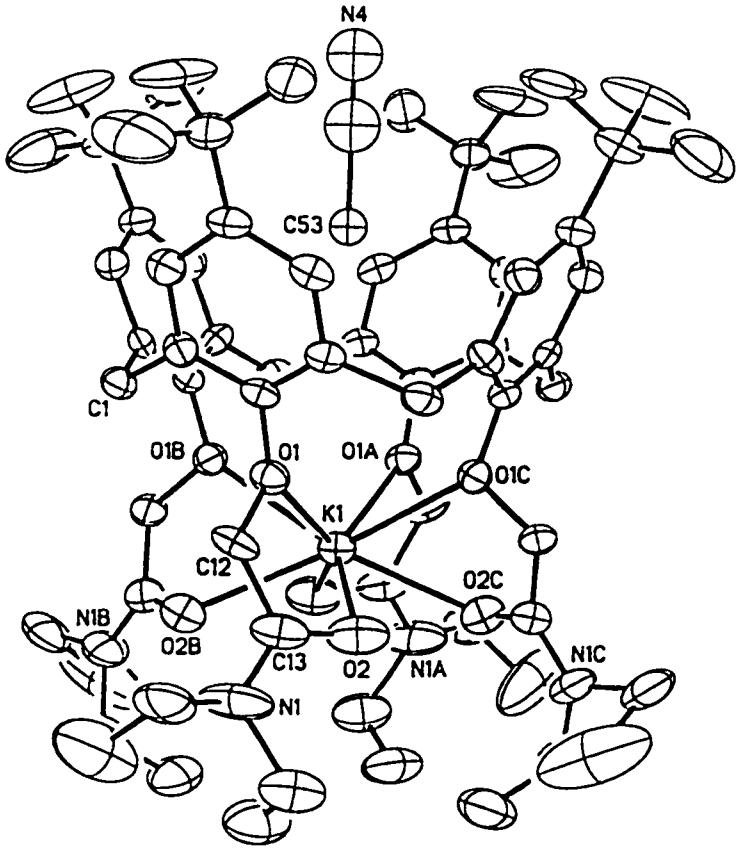


**Figure 25a.** Molecular diagram of 1:1:1 $(K(1),1,MeCN)^+$ (Dataset I). Hydrogen atoms are omitted for clarity.

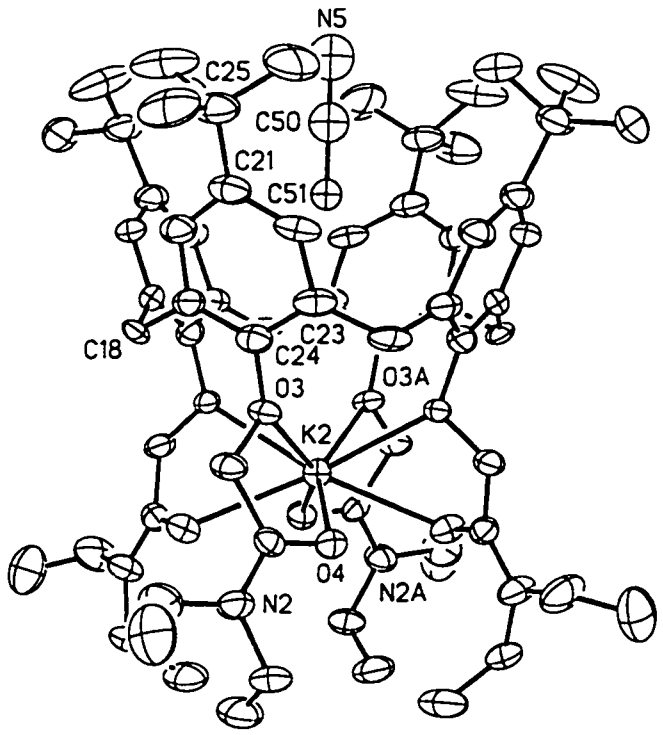


**Figure 25b.** Molecular diagram of 1:1:1 $(K(2),1,MeCN)^+$ (Dataset I). Hydrogen atoms are omitted for clarity.

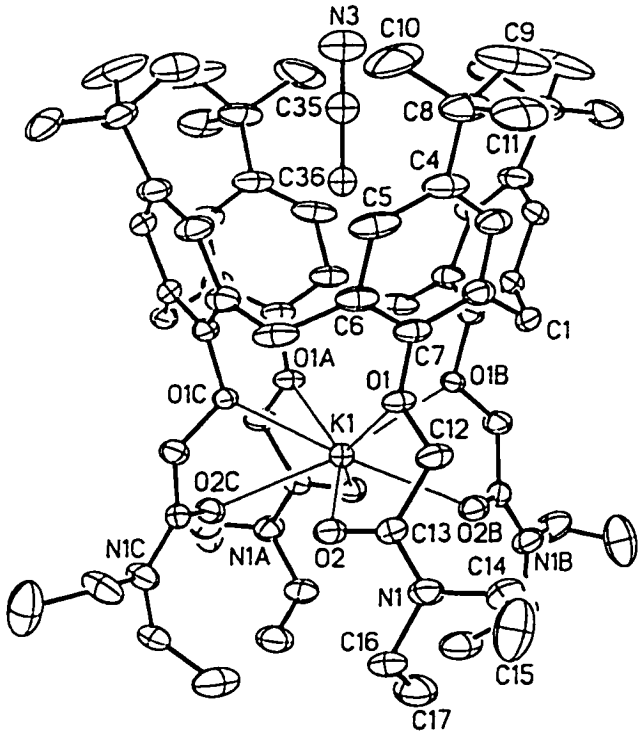


**Figure 26a.** Molecular diagram of 1:1:1 $(K(1),1,MeCN)^+$ (Dataset II). Hydrogen atoms are omitted for clarity.

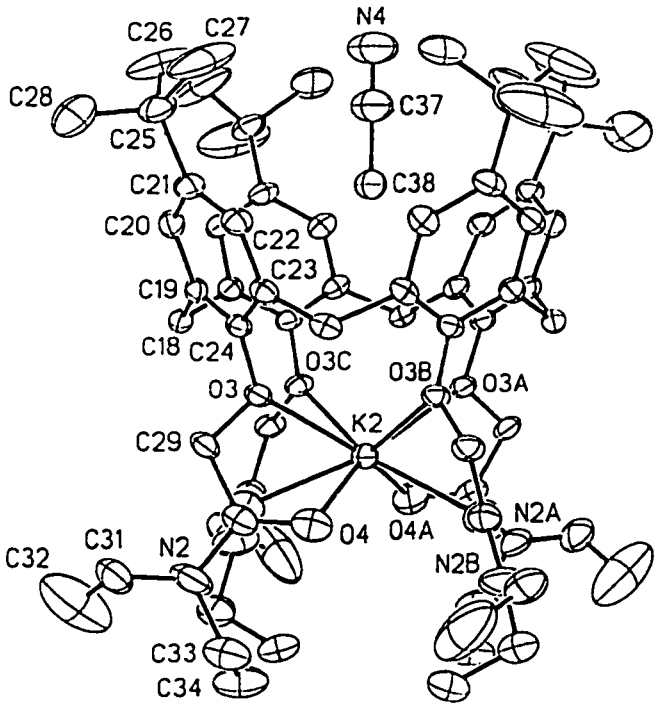


**Figure 26b.** Molecular diagram of 1:1:1 $(K(2),1,MeCN)^+$ (Dataset II). Hydrogen atoms are omitted for clarity.

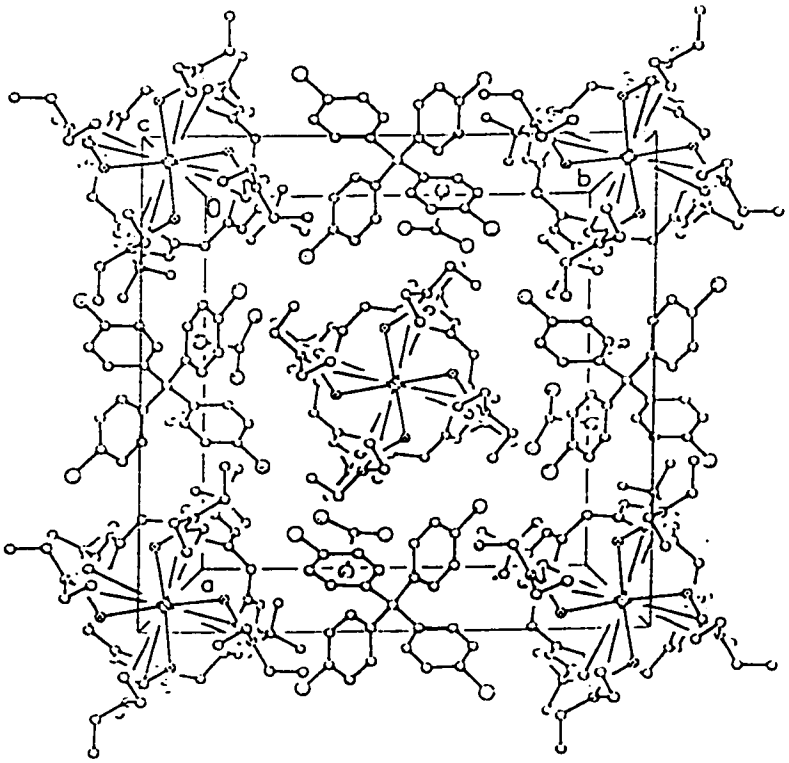


**Figure 27.** Molecular packing diagram from the perspective of the amide groups for (K,1,MeCN),B(*p*-PhCl)$_4$ (Dataset I) (the complex (K(1),1,MeCN)$^+$ is located at the centre of the diagram with the four (K(2),1,MeCN)$^+$ complexes located at the corners). Hydrogen atoms are omitted for clarity.

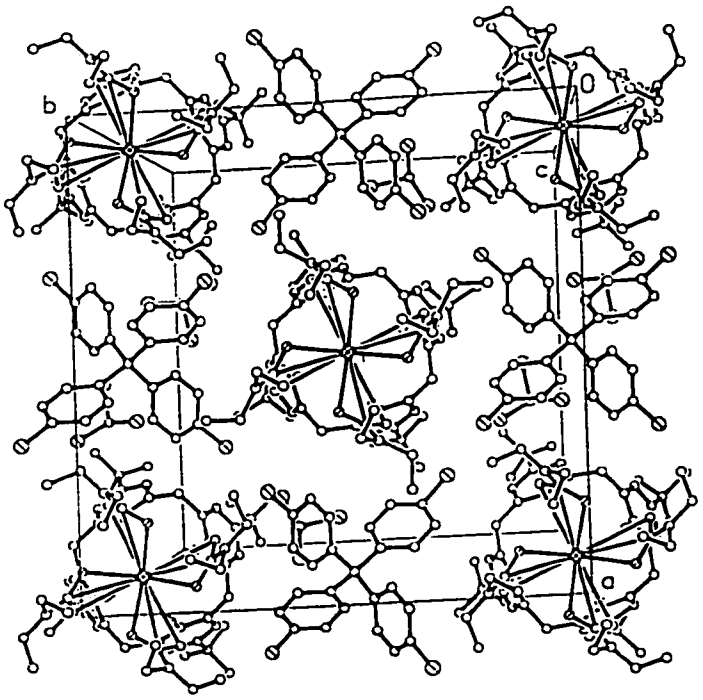


**Figure 28.** Molecular packing diagram from the perspective of the amide groups for (K,1,MeCN),B(*p*-PhCl)$_4$ (Dataset II) (the complex (K(1),1,MeCN)$^+$ is located at the centre of the diagram with the four (K(2),1,MeCN)$^+$ complexes located at the corners). Hydrogen atoms are omitted for clarity.

The difference in the two datasets lies in the torsion angles. From dataset I, the torsion angles for $(K(1),1,MeCN)^+$ and $(K(2),1,MeCN)^+$ are 14.6(9) and 9.6(9)°, respectively. Torsion angles for $(K(1),1,MeCN)^+$ and $(K(2),1,MeCN)^+$ (II) are -12.7(5) and 13.0(5)°, respectively. The torsion angle for (K,1,MeOH),SCN (-12.2(2.0)°)[1] is identical to that of $(K(1),1,MeCN)^+$ (II).

## 4.3 Single-Crystal X-ray Analysis of (MeCN,1)

The bond lengths, bond angles and torsion angles for the (MeCN,1) crystal are presented in Table 3. The single-crystal structure of (MeCN,1) shows two acetonitriles per 1 (Figure 29). The high R value may be attributed to the poorly-packed crystal as a result of disorder in the hydrophilic pseudo-cavity of 1 and in the solvent chloroform. The bridging methylene bond angles (110.4(8)° avg.) are within experimental range to the complex $(Na,1)^+$ (109.2(5) and 107.7(6)° for $(Na,1)^+$ and $(Na,1,MeCN)^+$, respectively, exhibiting a preorganization by acetonitrile in the hydrophobic pseudo-cavity of 1. Arduini *et al.*[1] reported the crystal structure of 1 with no guest in the hydrophobic pseudo-cavity such that the arrangement of the four phenyl rings lacks the four-fold rotation. The distance of the methyl carbon of the acetonitrile molecule to the bridging methylene carbons is 4.52(2) Å (avg.) The distance between the methyl carbon of the acetonitrile and bridging methylene carbons for $(Na,1,MeCN)^+$, $(K(1),1,MeCN)^+$ (I), $(K(2),1,MeCN)^+$ (I), $(K(1),1,MeCN)^+$ (II) and $(K(2),1,MeCN)^+$ (II) are 4.473(8), 4.427(10), 4.463(10), 4.439(4) and 4.454(4) Å, respectively. The values are within

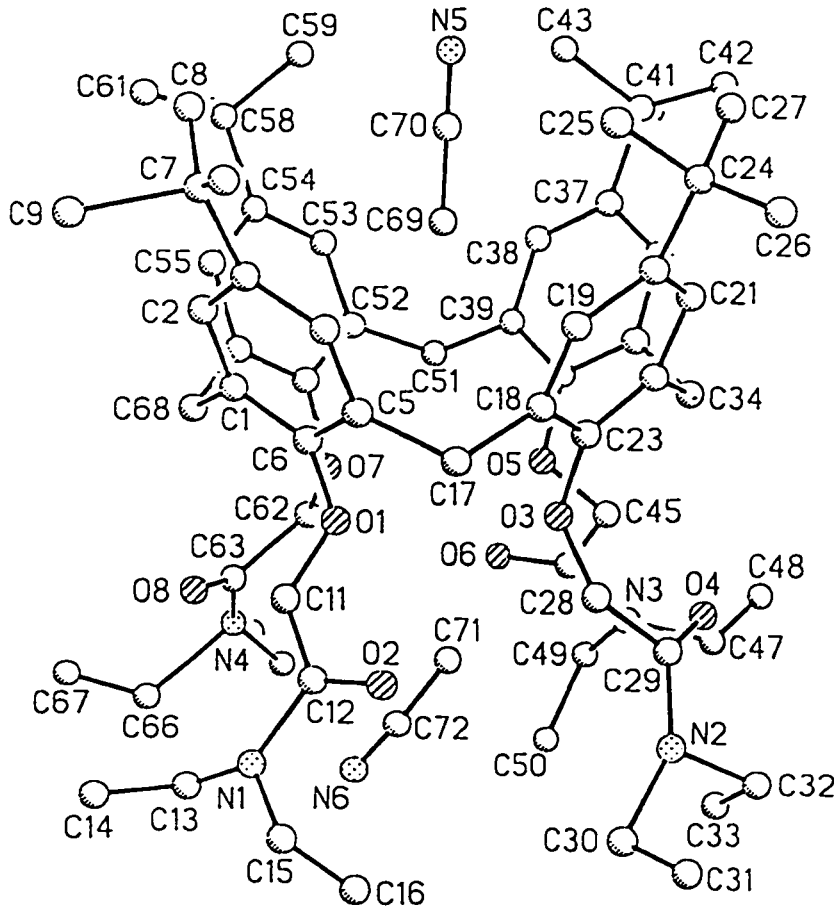


**Figure 29. Molecular diagram of 2:1 (MeCN,1) (the minor contributing disorder form is not shown). Hydrogen atoms are omitted for clarity.**

experimental range of each other, thus indicating the formation of an identical hydrophobic pseudo-cavity.

The C(O)-N (amide) bonds are significantly longer than those seen with the sodium and potassium complexes. The shorter bond length supports the dynamic $^1H$ NMR data obtained from the exchange rate of the methylene moieties. The complexation of a cationic guest generates an increased double bond character on the C-N bonds.

The positioning of the acetonitrile in the hydrophilic pseudo-cavity is a result of a polarity effect. The slightly positive methyl group in acetonitrile is oriented inside the pseudo-cavity as predicted by molecular dynamic studies.[5] The methyl carbon in acetonitrile is closer to the phenolic oxygens than the amide oxygens, 3.45(2) (avg.) and 3.85(2) (avg.) Å, respectively. The nitrogen is directed towards one of the monomers forcing both ethyl groups of the $N(CH_2CH_3)_2$ moiety to point away from the pseudo-cavity (Figure 30). The torsion angles for the $OCH_2CO$ arms differ significantly. The acetonitrile is directed towards one of the arms, O(7)-C(62)-C(63)-O(8), forcing it into a counterclockwise torsion angle of -3(1)°.

## 4.4 Single-Crystal X-ray Analysis of (Li,1b),$ClO_4$

The bond lengths, bond angles and torsion angles for the (Li,1b),$ClO_4$ complex are presented in Table 2. The single-crystal structure of $(Li,1b)^+$ shows **1b** in the cone conformation and complexed to lithium in a 1:1 ratio (Figure 31).

The $Li^+$-O bond lengths are significantly smaller than the bond lengths for the sodium and potassium complexes by approximately 0.5 Å. The lithium cation is located

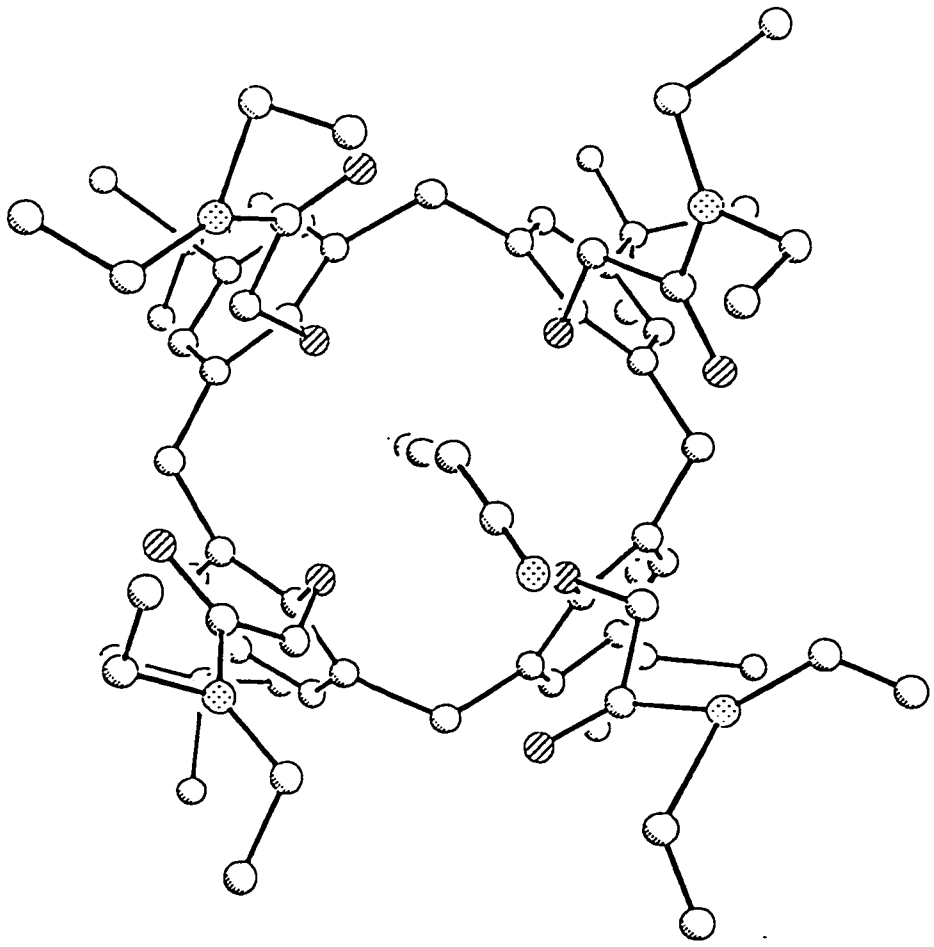

**Figure 30. Molecular diagram from the perspective of the amide groups of 2:1 (MeCN,1) (the minor contributing disorder form is not shown). Hydrogen atoms are omitted for clarity.**

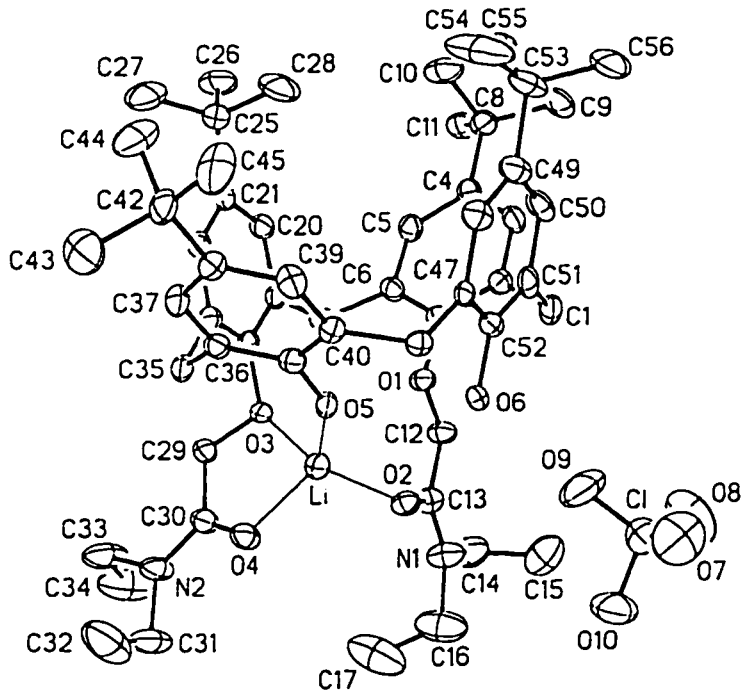


**Figure 31.** Molecular diagram of 1:1 $(Li,1b)^{+}$. Hydrogen atoms are omitted for clarity.

closer to the amide oxygens than the phenolic oxygens. In addition, the C(O)-N bond length shows a double bond character. In contrast to the sodium and potassium complexes, the counteranion is located within the layers of the lithium complexes in close proximity to the lithium cation (Figure 32). The ethyl groups on the amide show the "S" twist.

Although attempts to crystallize the complex $(Li,\mathbf{1})^+$ were unsuccessful, the existence of the nickel(II) and copper(II) complexes with $\mathbf{1}^6$, *i.e.* with smaller ionic radii than that of the lithium cation, demonstrates that there is a high probability to obtain the lithium complex. Molecular dynamic simulations have shown that three arms are sufficient for binding lithium.[7] The lithium complex leads to the fact that two arms may be sufficient for binding lithium. However, lithium binding modes may differ due to different hardness and coordination numbers with respect to sodium and potassium[7], such that lithium complexes generally achieve four to five coordination[8]. Hence, three arms are sufficient for complexation.

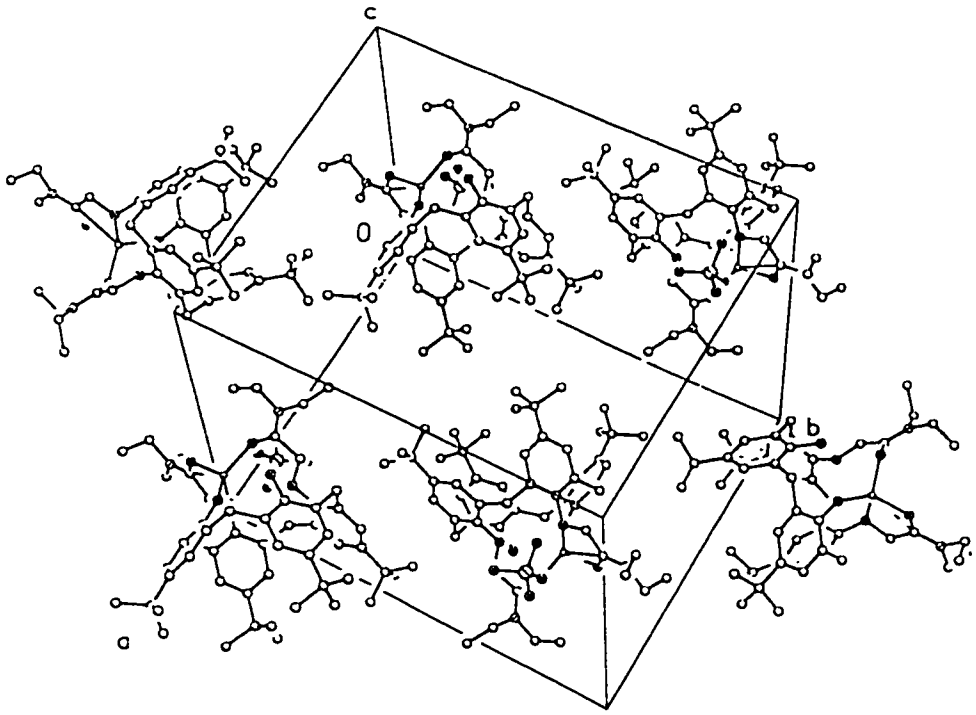


**Figure 32.** Molecular packing diagram from the perspective of the amide groups for (Li,**1b**),$ClO_4$. Hydrogen atoms are omitted for clarity.

## References

(1) Arduini, A.; Ghidini, E.; Pochini, A.; Ungaro, R.; Andretti, G. D.; Calestani, G.; Ugozzoli, F. *J. Incl. Phen.*, **1988**, *6*, 119.

(2) Wolf, N. J.; Georgiev, E. M.; Yordanov, A. T.; Whittlesey, B. R.; Koch, H. F.; Roundhill, D. M. *Polyhedron*, **1999**, *18*, 885.

(3) Muzet, N.; Wipff, G.; Casnati, A.; Domiano, L.; Ungaro, R.; Ugozzoli, F. *J. Chem. Soc. Perkin Trans. 2*, **1996**, 1065.

(4) *CRC Handbook of Chemistry and Physics*; Lide, D. R., Ed.; CRC Press LLC: Boca Raton, 1998; Chap. 12, pp 14-16.

(5) Guilbaud, P.; Varnek, A.; Wipff, G. *J. Am. Chem. Soc.*, **1993**, *115*, 8298.

(6) Beer, P. D.; Drew, M. G. B.; Leeson, P. B.; Ogden, M. I. *J. Chem. Soc. Dalton Trans.*, **1995**, 1273.

(7) Baaden, M.; Wipff, G.; Yaftian M. R.; Burgard, M.; Matt, D. *J. Chem. Soc. Perkin Trans. 2*, **2000**, 1315.

(8) Cornell, W. D.; Cieplak, P.; Bayly, C. I.; Gould, I. R.; Merz, K. M.; Ferguson, D. M.; Spellmeyer, D. C.; Fox, T.; Caldwell, J. W.; Kollman, P. A. *J. Am. Chem. Soc.*, **1995**, *117*, 5179.

# 5. 3-D Pseudo-Cavity Volume Analysis

## 5.1 Computational Background

The coordinates of the eight oxygens in **1**, are comparable to the vertices of a polyhedron varying between a rectangular parallelepiped and a distorted Archimedean anti-prism. The vertices were utilized for calculating the areas and the volumes of the hydrophilic pseudo-cavity.

All areas and volumes plotted employ the program Rhinoceros® NURBS (Non-Uniform Rational B-Splines).[1] Rhinoceros® NURBS is a numerical algorithm that subdivides a larger shape into smaller shapes of a known volume and area. The volumes calculated by the program Rhinoceros® are under-calculated in comparison to equations 14 and 15 by a difference of 0.89 to 1.60 $Å^3$, except for the nickel complex (Table 6). In addition, the volumes calculated using equation 16 show a difference between 0.01 and 0.18 $Å^3$ to the values obtained from equations 14 and 15. Therefore, the volumes obtained from the program are under-calculated by 1.25(35) $Å^3$ to the volumes calculated using equations 14, 15 and 16. The crystallographic data sets for the complexes $(Na,1)^+$, $(Na,2)^+$ and $(K,1)^+$ contain a $C_4$ axis, thus simplifying the calculations to equations 14 and 15. Equations 14 and 15 were determined using integration and ratio ($side/side_1$ = $height/height_1$) techniques, respectively. Errors between equations 14 and 15 were estimated to be ± 0.10 $Å^3$. The areas calculated by Rhinoceros® for the complexes $(Na,1)^+$, $(Na,2)^+$ and $(K,1)^+$ were found to follow the equation area = length * width. Therefore, the areas calculated for the other complexes were presumed to be small using

Rhinoceros®. The values for the ionic radius of the metals were obtained from reference 8. Although the ionic radius of the metal varies in relation to the number of coordination sites, only the eight-coordinated ionic radius was utilized. The choice is based on the premise that the vicinity of the cationic guest will influence the positions of the eight oxygens and thus alter the structural encapsulation of the guest. Values for the ionic radius of the eight-coordinated copper (II) and nickel (II) cations were not found, therefore, the six-coordinated ionic radii were used.

$$Volume_1 = (height_{top} - height_{bottom})(- side_{top} * side_{bottom} + 1/3 * (side_{top} - side_{bottom})^2) \quad (14)$$

$$Volume_2 = (Area_{top} * (height_{top} - height_{bottom}) / 3)(1 + side_{bottom}/side_{top} + (side_{bottom}/side_{top})^2) \quad (15a)$$

$$Area_{top} = side_{top}^2 \quad (15b)$$

$$x_{21} = x_2 - x_1;\ y_{21} = y_2 - y_1;\ z_{21} = z_2 - z_1 \quad (16a)$$

$$x_{31} = x_3 - x_1;\ y_{31} = y_3 - y_1;\ z_{31} = z_3 - z_1 \quad (16b)$$

$$x_{41} = x_4 - x_1;\ y_{41} = y_4 - y_1;\ z_{41} = z_4 - z_1 \quad (16c)$$

$$d_{34} = y_{31}*z_{41} - z_{31}*y_{41};\ d_{24} = y_{21}*z_{41} - z_{21}*y_{41};\ d_{23} = y_{21}*z_{31} - z_{21}*y_{31} \quad (16d)$$

$$volume_3 = x_{21}*d_{34} - x_{31}*d_{24} + x_{41}*d_{23} \quad (16e)$$

The values for $height_{top}$ and $height_{bottom}$ are the shortest distances from the z axis to the top and bottom plane, respectively. The values for $side_{top}$ and $side_{bottom}$ are the distances between the vertices for the respective planes. In equation 16, the vertice $(x_1,y_1,z_1)$ links the three remaining vertices $(x_2,y_2,z_2)$, $(x_3,y_3,z_3)$ and $(x_4,y_4,z_4)$ to form a polyhedron. An average volume is calculated using each of the eight vertices as $(x_1,y_1,z_1)$.

| Complex | $Volume_{14}$ [h] ($Å^3$) | $Volume_{15}$ [i] ($Å^3$) | $Volume_R$ [j] ($Å^3$) | $Volume_{16}$ [k] ($Å^3$) |
|---|---|---|---|---|
| (Na,1),$B(Ph)_4$ [a] | 23.42 | 23.43 | 22.53 | 23.32 |
| (Na,1,MeCN),$B(Ph)_4$ [a] | 22.79 | 22.82 | 21.43 | 22.30 |
| (Na,2,MeCN),$ClO_4$ [b] | 24.52 | 24.52 | 23.55 | 24.14 |
| (K,1,MeOH),I [c] | 26.46 | 26.59 | 25.03 | 25.74 |
| (K,1,MeOH),SCN [c] | 27.05 | 27.22 | 25.82 | 26.36 |
| (K,1),$B(p\text{-}PhCl)_4$ [a] | 27.18 | 27.23 | 25.95 | 26.57 |
| (K,1,MeCN),$B(p\text{-}PhCl)_4$ [a] | 26.39 | 26.40 | 24.80 | 25.71 |
| (Ni,1,MeCN),$(ClO_4)_2$ [d] | | | 17.13 | 16.60 |
| (Cu,1,MeCN),$(ClO_4)_2$ [d] | | | 17.78 | 18.07 |
| (Zn,1,MeCN),$(ClO_4)_2$ [d] | | | 17.84 | 18.11 |
| (Fe,1,MeCN),$(ClO_4)_2$ [d] | | | 17.37 | 17.72 |
| (Pb,1,MeCN),$(ClO_4)_2$ [d] | | | 23.02 | 23.45 |
| (Sr,1),$(Pic)_2$ [e] | | | 22.58 | 23.00 |
| (Ag,2,MeCN),$ClO_4$ [f] | | | 27.75 | 28.15 |
| (Pb,3),$ClO_{42}$ [g] | | | 29.63 | 30.70 |

[a] this work. [b] compound 2 refers to *p-tert*-butylcalix[4]arene tetra-oxy(2-pyridylmethyl), see reference 2. [c] see reference 3. [d] see reference 4. [e] see reference 5. [f] see reference 6. [g] compound 3 refers to *p-tert*-butylcalix[4]arene tetra-thioamide, see reference 7. [h] volume calculated using equation 14, errors correspond to ± 0.10 $Å^3$. [i] volume calculated using equation 15, errors correspond to ± 0.10 $Å^3$. [j] volume calculated using Rhinoceros®, errors correspond to ± 0.35 $Å^3$. [k] volume calculated using equation 16, errors correspond to ± 0.20 $Å^3$.

**Table 6.** Comparison of volumes calculated using equations 14, 15 and 16, and Rhinoceros®.

## 5.2 Volume Analysis

In Figure 33a and 33b, the area of the plane formed by the phenolic oxygens and the amide oxygens plotted against the ionic radius of the metals exhibit correlation coefficients of 0.84 and 0.78, respectively. Figure 33c illustrates a moderate relationship between the surface area of the pseudo-cavity and the ionic radius of the respective guests ($r^2 = 0.85$). The cationic guests do not interact uniformly with the four phenol and amide oxygens and thus a complete description of the host/guest interaction is not addressed in the plots.

In Figure 34, there is an improved linear fit ($r^2 = 0.93$) between the volume of the hydrophilic pseudo-cavity of 1 with the ionic radius of the respective metals. The volume increases regularly with the size of the cation though the metal-oxygen distances generally do not show the same trend (for example, $Na^+$-$O_{amide}$ and $Na^+$-$O_{phenolic}$ distances are 2.464(5) and 2.584(5) Å, respectively). The linear trend may be used to predict the volume of the hydrophilic pseudo-cavity of 1 encapsulating a cationic guest not yet crystallized. Deviations from the linear trend for some of the transition metals may be attributed to a preference for square planar complexation over octahedral complexation.[4] Table 6 shows complexes of 1 with and without a neutral guest in the hydrophobic pseudo-cavity (e.g. methanol for acetonitrile) and/or containing a different counteranion (e.g. replacing tetraphenylborate with iodide or isothiocyanate). The volume difference between a sodium complex with and without the co-complexation of an acetonitrile molecule is 1.10 $Å^3$. The neutral guest acetonitrile appears to transmit a minimal long-distance effect on the volume of the pseudo-cavity of 1.[9] The volume

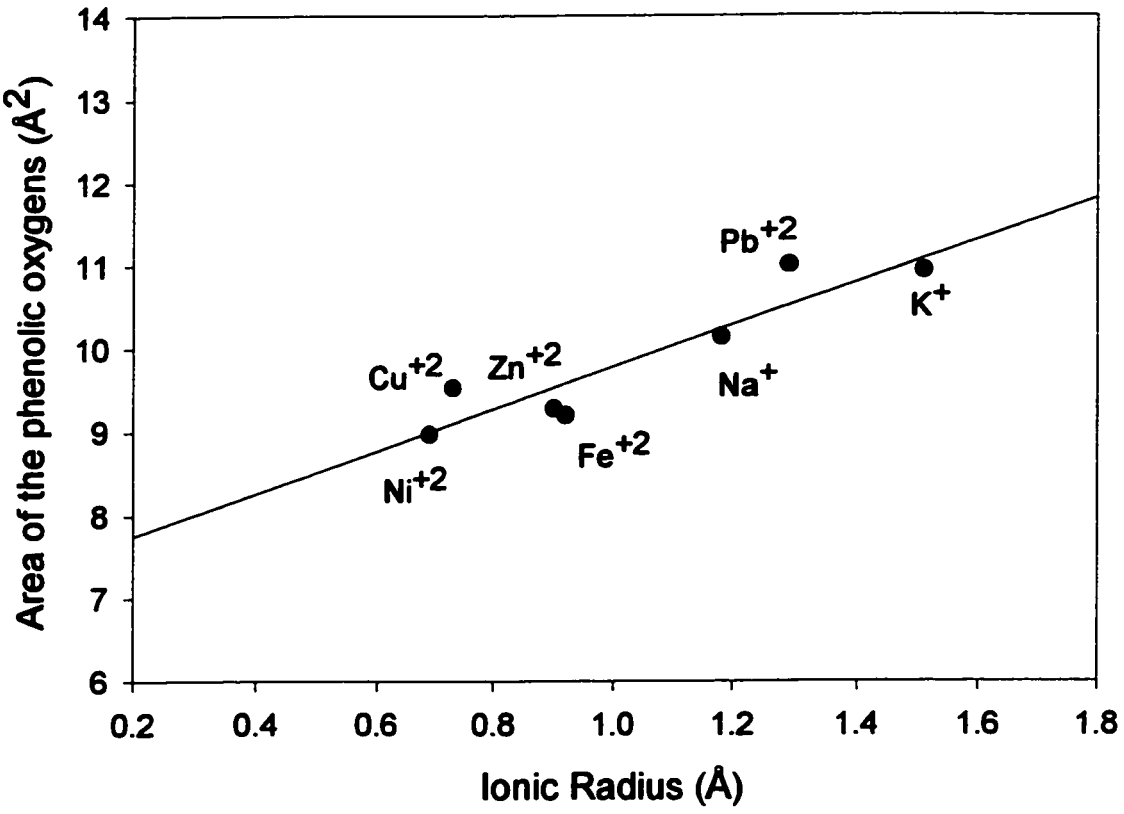


**Figure 33a.** Area (Å$^2$) of the plane formed by the phenolic oxygens of 1 plotted against the ionic radii (Å) of the corresponding metals.

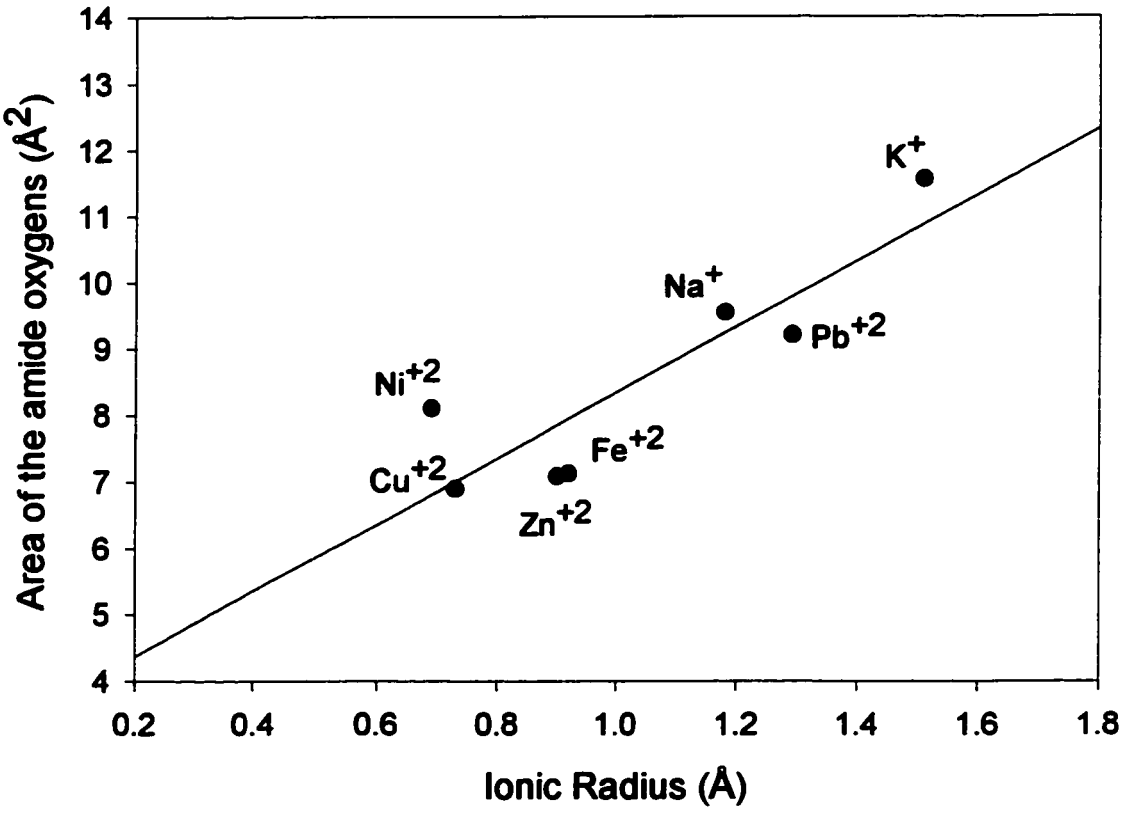


**Figure 33b.** Area (Å$^2$) of the plane formed by the amide oxygens of **1** plotted against the ionic radii (Å) of the corresponding metals.

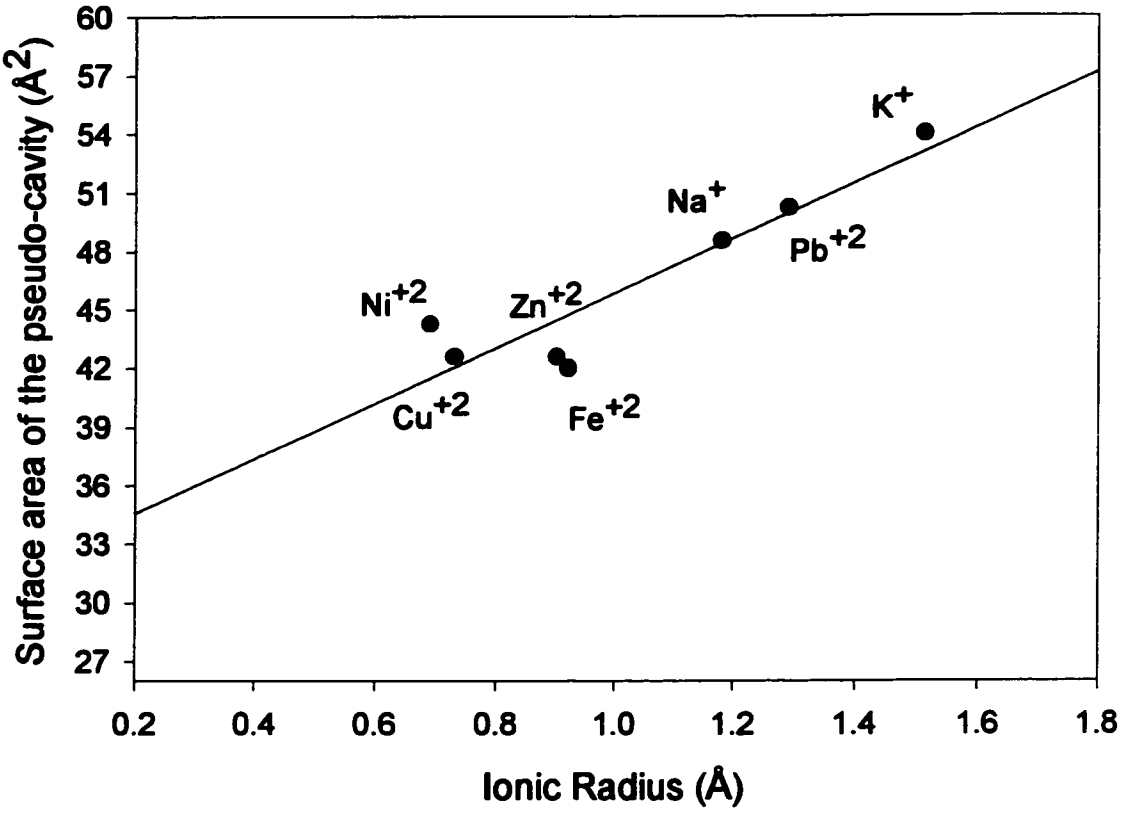


**Figure 33c.** Surface area (Å$^2$) of the pseudo-cavity of 1 plotted against the ionic radius (Å) of the corresponding metals.

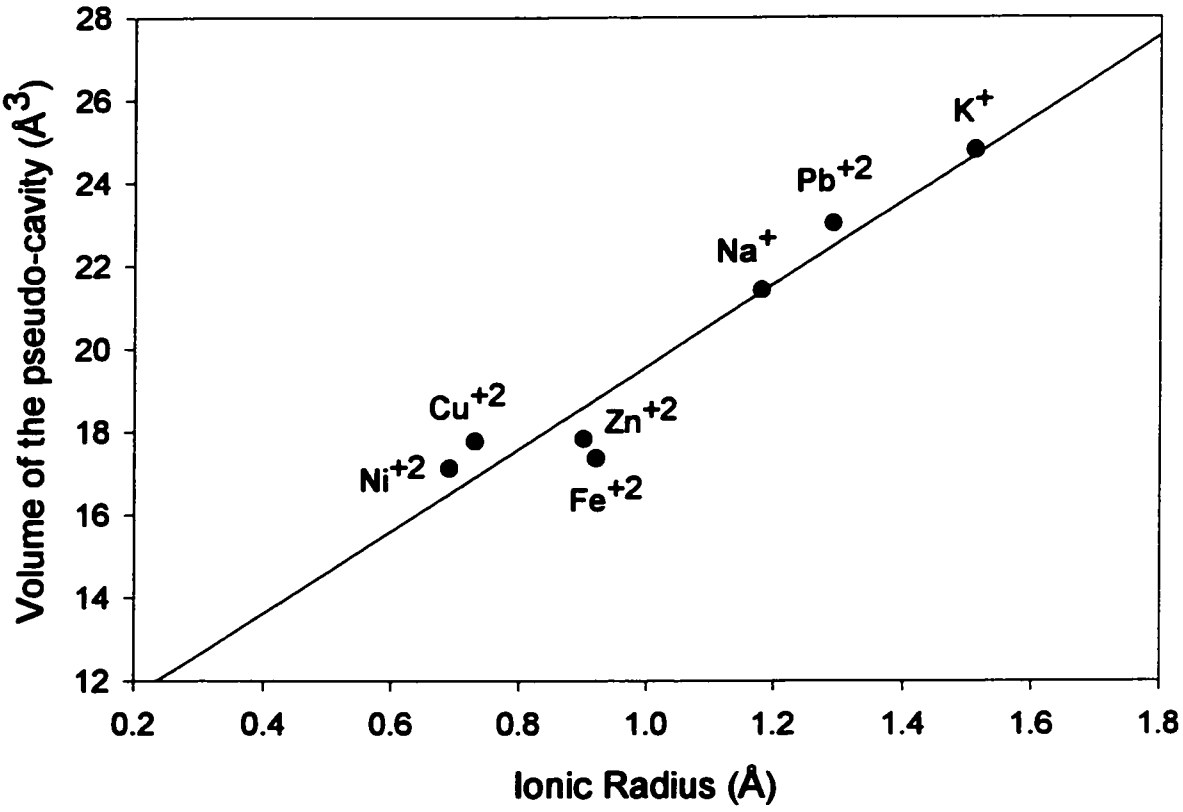


**Figure 34.** Dependence of the volume ($Å^3$) of the pseudo-cavity of **1** on the ionic radius (Å) of the corresponding metals. The plot follows the trend of $y = 9.9\ x + 9.7$ ($r^2 = 0.93$).

difference between a potassium complex with an iodide and an isothiocyanate as a counteranion is 0.79 $Å^3$. The molecular differences in the crystal structures seem to play a minor role in modifying the volume of the hydrophilic pseudo-cavity.

Following the linear relationship, the critical ionic radius for the attainment of the maximum and minimum possible volumes for the encapsulation of a cationic guest can be predicted. The pseudo-cavity of the uncomplexed 1 will produce a maximum volume when the oxygens are directed away from the center of the pseudo-cavity (diverged formation). This is seen with both the crystal structure of uncomplexed 1 reported by Arduini *et al.*[3] and in Chapter 4. The extrapolated volume of the pseudo-cavity is 30.80 $Å^3$ which corresponds to a guest radius of 2.13 Å. Similarly, X-ray data showing an acetonitrile molecule inside the hydrophilic pseudo-cavity of 1 give a volume of 32.17 $Å^3$ which corresponds to a radius of 2.27 Å. Therefore, the hydrophilic pseudo-cavity is capable of accommodating a cation of approximately 2.2 Å or less, and that a larger cation would most likely not be "completely" shielded from its environment by the amide oxygens, and thus not follow the linear trend. Subsequently, the host/guest complex would be less stable to its environment due to an opening of the pseudo-cavity.[9] A proton (ionic radius of < 0.30 Å [8]) would produce a cavity volume of approximately 13.0 $Å^3$. Whether the pseudo-cavity can accommodate such a small guest remains to be seen.

The calculated value of the volume of the hydrophilic pseudo-cavity of 1 for the $(Sr,1)^{+2}$ complex[5] falls within the 95 % confidence interval for the trend shown in Figure 30; the values for the complexes $(Ag,2)^{+}$ [6], $(Pb,3)^{+2}$ [7] and $(Na,2)^{+}$ [2] do not fall within the 95 % confidence interval (Table 6). The nitrogen atoms in the host 2 (*p-tert*-butylcalix[4]arene tetra-oxy(2-pyridylmethyl)) and the sulfur atoms in the host 3 (*p-tert*-

butylcalix[4]arene tetra-thioamide) are less electronegative than the carbonyl oxygens in the host **1**, and thus a slightly larger volume is expected. For example, the $(Na,2)^+$ complex has a larger volume than the $(Na,1)^+$ complex.

Future work in molecular dynamic simulations can be extended from simple linear atomic interactions into complex three-dimensional interactions.[10] Factors such as bond lengths and volume may determine a "best fit", and thus be involved in the metal-binding selectivity.[11] The challenge lies in using structural data to predict kinetic data on solution complexation processes that may provide insight into dynamic metal-binding complexation. Subsequently, linking the volume size to kinetic and thermodynamic data may provide answers on the mechanism of complexation for solution processes.

## References

(1) Robert McNeel & Associates, Rhinoceros®: NURBS modeling for Windows Vers. 1.1, (1993-1999).

(2) Danil de Namor, A. F.; Castellano, E. E.; Pulcha Salazar, L. E.; Piro, O. E.; Jafou, O. *Phys. Chem. Chem. Phys.*, **1999**, *1*, 285.

(3) Arduini, A.; Ghidini, E.; Pochini, A.; Ungaro, R.; Andretti, G. D.; Calestani, G.; Ugozzoli, F. *J. Incl. Phen.*, **1988**, *6*, 119.

(4) Beer, P. D.; Drew, M. G. B.; Leeson, P. B.; Ogden, M. I. *J. Chem. Soc., Dalton Trans.*, **1995**, 1273.

(5) Muzet, N.; Wipff, G.; Casnati, A.; Domiano, L.; Ungaro, R.; Ugozzoli, F. *J. Chem. Soc., Perkin Trans. 2*, **1996**, 1065.

(6) Danil de Namor, A. F.; Piro, O. E.; Pulcha Salazar, L. E.; Aguilar-Cornejo, A. F.; Al-Rawi, N.; Castellano, E. E.; Sueros Velarde, F. J. *J. Chem. Soc., Faraday Trans.*, **1998**, *94*, 3097.

(7) Arnaud-Neu, F.; Barrett, G.; Corry, D.; Cremin, S.; Ferguson, G.; Gallagher, J. F.; Harris, S. J.; McKervey, M. A.; Schwing-Weill, M. J. *J. Chem. Soc., Perkin Trans. 2*, **1997**, 575.

(8) *CRC Handbook of Chemistry and Physics*, D.R. Lide. Ed.; CRC Press LLC, Boca Raton, 1998; pp. 14-16.

(9) Varnek, A.; Wipff, G. *J. Phys. Chem.*, **1993**, *97*, 10840.

(10) Connolly, M. L. *J. Am. Chem. Soc.*, **1985**, *107*, 1118.

(11) Varnek, A.; Helissen, S.; Wipff, G.; Collet, A. *J. Comp. Chem.*, **1998**, *19*, 820.

## Conclusion and Suggestions for Future Work

The complexation process of 1 with the sodium and potassium cations is quantitative ($K_f > 10^4$ $M^{-1}$) on the $^1H$ NMR time scale. The NMR data show the encapsulation of one alkali metal per molecule of 1. The host 1 slowly exchanges sodium and potassium cations on the respective NMR time scales. Cation solvation may not play a crucial role in the complexation process due to the quantitative complexation and the slow exchange observed.

The 1:1 complexation is corroborated by X-ray crystallography. X-ray data revealed the presence of two diastereomorphs complexes in the lattice for both the crystals of the sodium and potassium complexes. This is not observed in the $^1H$ NMR spectra due to the fast averaging motion of the ethyl groups between the diastereomorphs. Crystallographic data show the presence of an acetonitrile molecule inside the hydrophobic pseudo-cavity of 1 such that the organization of the *tert*-butyl carbons in the sodium and potassium complexes are identical to that of (MeCN,1). In retrospect to the NMR data, the sodium and potassium cations are competing with the acetonitrile for the hydrophilic pseudo-cavity. The high formation constant for both the sodium and potassium complexes demonstrates no significant competition from the acetonitrile molecules. The host 1 would highly unlikely be able to selectively discriminate between sodium and potassium. Moreover, upon the formation of the complex, slight variations of the structure of the host to accommodate the guest and/or solvent molecules can result in dramatic changes in the nature of the supramolecular structures being formed.

Based solely on single-crystal X-ray data sets, there exists a linear trend between the volume of the hydrophilic pseudo-cavity of the host **1** and the ionic radius of the guests $Ni^{+2}$, $Cu^{+2}$, $Zn^{+2}$, $Fe^{+2}$, $Pb^{+2}$, $Na^{+}$ and $K^{+}$. The co-presence of an acetonitrile molecule in the hydrophobic pseudo-cavity of **1** demonstrates no significant effect on the hydrophilic pseudo-cavity. Finally, the predicted maximum cationic size of a guest is ~2.2 Å for encapsulation by the host **1**. Future work would include kinetic studies with the metals to link the X-ray data to kinetic data. Different guests with ionic radii would be expected to show different rates of exchange and pseudo-cavity volumes. Subsequently, to determine the relative binding affinities for cesium, potassium, lithium, rubidium and sodium in terms of pseudo-cavity volumes.

The efficiency of inclusions can be controlled by modifications in the lower rim of calixarenes. For example, future templates for calixarenes would possess a fixed volume for the pseudo-cavity to ensure selectivity of guests of varying sizes. This is under the premise that the ionic radius of a guest dictates complexation. I propose a fence-gate model for selectivity to occur by the host **1**. One fence method would be the incorporation of substituents that would link the methylene groups of $OCH_2CO$. Similarly, the ethyl groups can be linked as $NCH_2CH_2N$ to fix the pseudo-cavity's opening. The fence can then be opened through a gate by displacing a link between two nitrogen atoms.

Additional work into whether different counteranions would crystallize with the host and its guest. The possibility then lies in creating new salts of the alkali metals with different counteranions. For example, a solution containing (Cs,**1**),X and NaY where X and Y represent two different counteranions. The new salt CsY can be extracted using

water leaving behind (Na,1),X. The idea lies in the notion that the cesium exchange rate is faster than that for sodium and potassium.

The development of calixarene templates capable of selectively binding metal ions, salts, amino acids, and organic substrates enables a deeper understanding into the interactions of the host/guest system. Modifying the appendages on this special class of ligands has led and will continue to lead to encouraging research into the further design of sophisticated calixarenes. Conformational flexibility of the host affords a deeper understanding the complexation processes. It is through the analysis of different shapes and sizes of the guest that the role of the host size and rigidity may be fully understood.

# Appendix

13C CPMAS spin rate = 4kHz am102

*p-tert*-butylcalix[4]arene tetra-acetamide

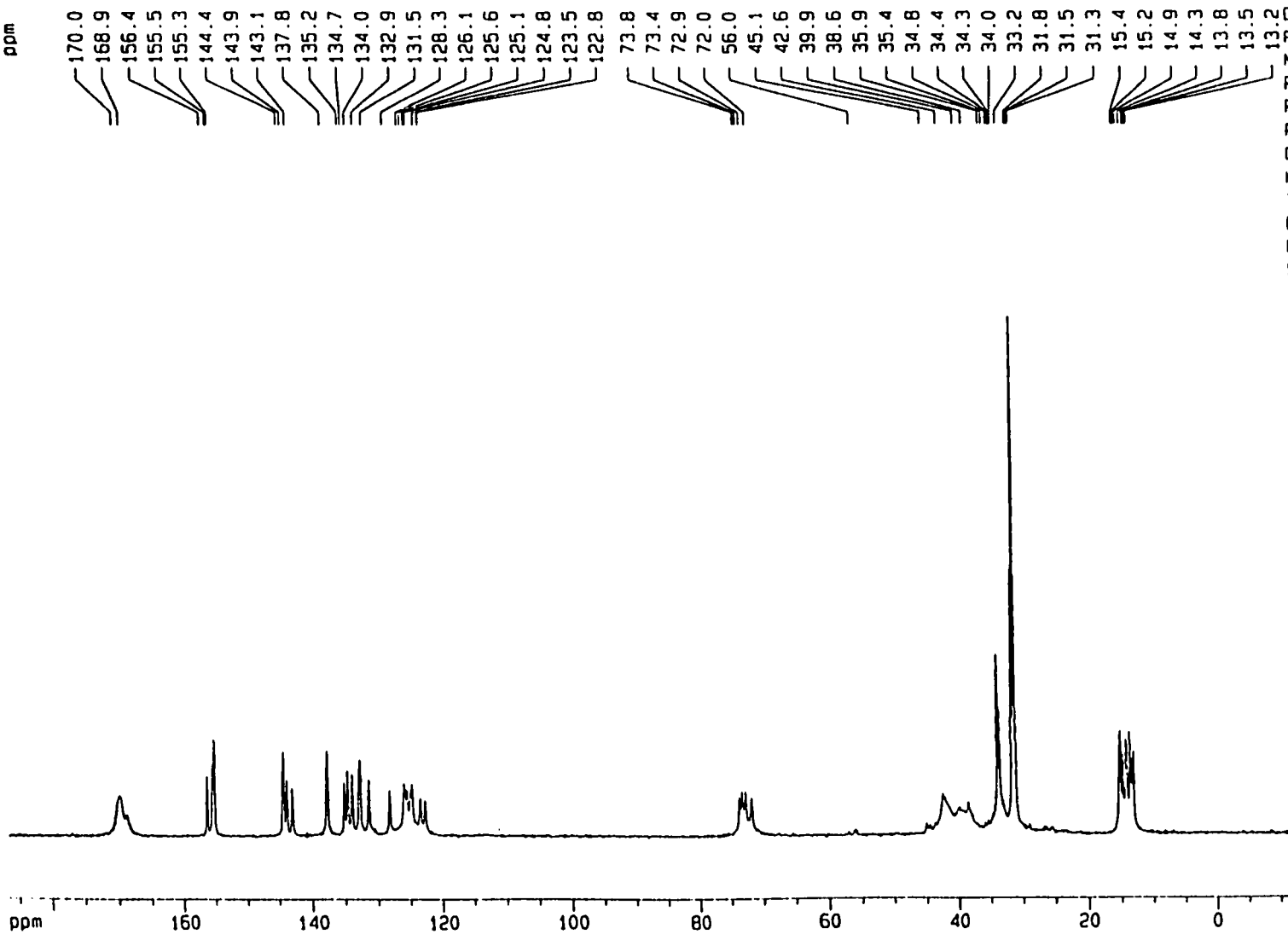


Current Data Parameters

| | |
|---|---|
| NAME | arvin |
| EXPNO | 1 |
| PROCNO | 1 |

F2 - Acquisition Parameters

| | |
|---|---|
| Date | 991112 |
| Time | 12.41 |
| PULPROG | cpramp.gf |
| SOLVENT | CDCl3 |
| AQ | 0.1198560 sec |
| FIDRES | 4 173710 Hz |
| DW | 29.2 usec |
| RG | 16384 |
| NUCLEUS | 13C |
| P3 | 4.3 usec |
| P17 | 0.8 usec |
| P15 | 2000.0 usec |
| D1 | 4.0000000 sec |
| HL1 | 1 dB |
| TL0 | 14.00 dB |
| DL0 | 18.00 dB |
| P90 | 5.1 usec |
| SFO2 | 200.0960500 MHz |
| TP1 | 14.00 dB |
| TPOFFS1 | 0.00 Hz |
| TPNAME1 | hgramp |
| DL1 | 18.00 dB |
| DE | 36.6 usec |
| SFO1 | 50.3189398 MHz |
| SWH | 17095.52 Hz |
| TD | 4096 |
| NS | 512 |
| DS | 0 |

F2 - Processing parameters

| | |
|---|---|
| SI | 65536 |
| SF | 50.3137293 MHz |
| WDW | EM |
| SSB | 0 |
| LB | 0.00 Hz |
| GB | 0 |
| PC | 1.00 |

1D NMR plot parameters

| | |
|---|---|
| CX | 20.00 cm |
| F1P | 186.846 ppm |
| F1 | 9400.90 Hz |
| F2P | -12.243 ppm |
| F2 | -616.00 Hz |
| PPMCM | 9.95444 ppm/cm |
| HZCM | 500.84518 Hz/cm |

dipolar dephasing 13C CPMAS spin rate = 4kHz am102

*p-tert*-butylcalix[4]arene tetra-acetamide

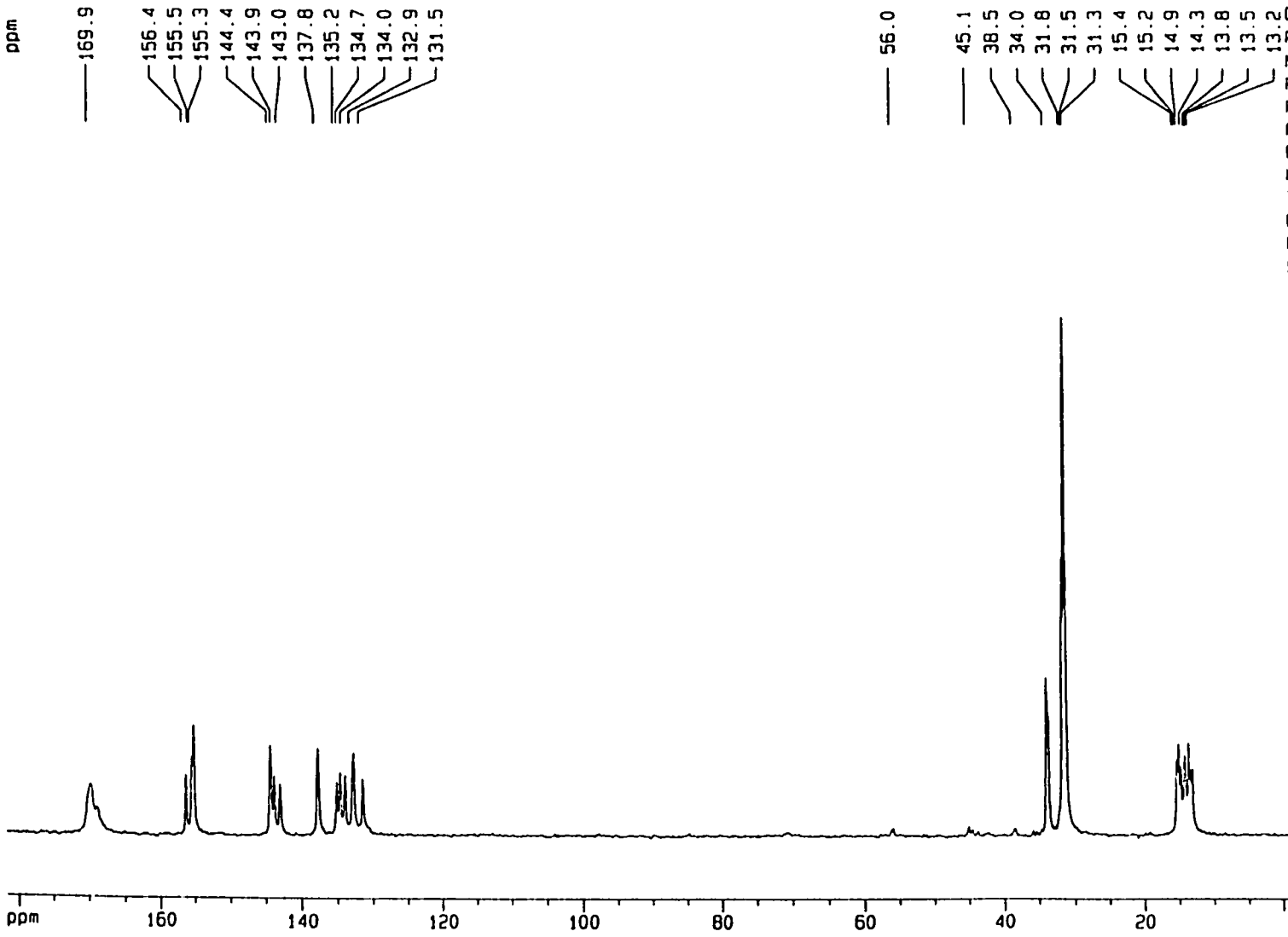


Current Data Parameters

| | |
|---|---|
| NAME | arvin |
| EXPNO | 2 |
| PROCNO | 1 |

F2 - Acquisition Parameters

| | |
|---|---|
| Date | 991112 |
| Time | 13.28 |
| PULPROG | cprampdd.gf |
| SOLVENT | CDCl3 |
| AQ | 0.1198560 sec |
| FIDRES | 4.173710 Hz |
| DW | 29.2 usec |
| RG | 16384 |
| NUCLEUS | 13C |
| P3 | 4.3 usec |
| P17 | 0.8 usec |
| P15 | 2000.0 usec |
| D1 | 4.0000000 sec |
| HL1 | 1 dB |
| TL0 | 14.00 dB |
| DL0 | 18.00 dB |
| P90 | 5.1 usec |
| SFO2 | 200.0960500 MHz |
| TP1 | 14.00 dB |
| TPOFFS1 | 0.00 Hz |
| TPNAME1 | hgramp |
| D10 | 0.0000400 sec |
| DL1 | 18.00 dB |
| DE | 36.6 usec |
| SFO1 | 50.3189398 MHz |
| SWH | 17095.52 Hz |
| TD | 4096 |
| NS | 433 |
| DS | 0 |

F2 - Processing parameters

| | |
|---|---|
| SI | 65536 |
| SF | 50.3137293 MHz |
| WDW | EM |
| SSB | 0 |
| LB | 3.00 Hz |
| GB | 0 |
| PC | 1.00 |

1D NMR plot parameters

| | |
|---|---|
| CX | 20.00 cm |
| F1P | 181.868 ppm |
| F1 | 9150.48 Hz |
| F2P | -1.293 ppm |
| F2 | -65.07 Hz |
| PPMCM | 9.15809 ppm/cm |
| HZCM | 460.77759 Hz/cm |